Optimal Integration of Intermittent Renewable Energy Sources in Power Distribution Systems

Akanit KWANGKAEW

Japan Advanced Institute of Science and Technology

Doctoral Dissertation

Optimal Integration of Intermittent Renewable Energy Sources in Power Distribution Systems

Akanit KWANGKAEW

Supervisor: Mineo KANEKO

Graduate School of Advanced Science and Technology
Japan Advanced Institute of Science and Technology
[Information Science]

September 2023

Abstract

The significance of renewable energy sources, such as solar and wind power, has experienced a remarkable surge in the modern world. Advancements in solar panel technology, along with decreasing costs and the integration of solar power and energy storage, have significantly enhanced the efficiency and cost-effectiveness of solar energy. Similarly, wind energy has made notable strides through the development of larger and more efficient wind turbines, including offshore and floating wind farms. As a result, renewable energy has become an increasingly vital component of power systems.

However, the integration of renewable energy sources presents challenges concerning voltage stability, power loss, and unpredictable reactive power consumption. Voltage instability and power loss in power distribution networks are influenced by the reactive power compensation of renewable distributed generators (RDGs). Consequently, it is important to allocate and determine the optimal placement of RDGs while considering their unpredictable reactive power consumption and the system's capacity for reactive support. This dissertation presents novel methods for the location, sizing, and allocation of RDGs, considering the uncontrolled and reactive power consumption of the generators.

The study begins by addressing voltage instability caused by uncontrolled loads, generators, and the reactive power compensation of RDGs. A methodology is proposed to quantify the system's reactive support capacity and improve voltage stability through the Reactive Power Compensation Support Margin for Voltage Stability Improvement (QSVS). Key functions derived from the complex power formula are utilized to calculate voltage stability and identify the bus most susceptible to voltage collapse. Consequently, the Load-Disabling Nodal Analysis (LDNA) method is introduced for identifying the optimal location and size of RDGs. A methodology is then presented that determines the placement of RDGs using LDNA, which consists of two parts that leverage the QSVS concept. The first part utilizes QSVS as the objective function to maximize the reactive support capacity and determine the optimal location for RDGs. This process of locating RDGs using the QSVS as the objective function to be maximized is called LDNA-QSVS. Subsequently, the loss minimization is conducted to determine the optimal sizing of RDGs. By considering reactive compensation and incorporating safety margins using LDNA-QSVS, the proposed methodology of achieves improved power loss reduction and enhances voltage stability. This emphasizes the significance of compensating reactive power in achieving improved reduction in power losses and ensuring resilient voltage stability.

Next, the Normalized Voltage Stability index (Λ) is introduced for identifying RDG locations that address both voltage stability and power loss. Then, the LDNA for Robust Voltage Stability (LDNA-RVS) method is employed to locate RDGs by maximizing Λ as the objective function. This approach improves robust voltage stability and efficiency in reducing power losses during the integration of RDGs. Consequently, the LDNA-RVS method effectively enhances voltage stability and optimizes power loss reduction in RDG allocation. Comparative analyses conducted on the IEEE 33-bus and IEEE 69-bus test distribution systems demonstrate the superior performance of LDNA-RVS over other techniques, particularly in terms of robust voltage stability and power loss reduction.

Lastly, this dissertation presents an innovative allocation approach that addresses the system's robustness against power fluctuations. By incorporating lower and upper power level bounds, the approach ensures a balanced and stable system operation. The

robustness conditions, inspired by the perfect matching concept from Graph Theory, are employed to establish a solid theoretical framework for the proposed approach. To further validate its effectiveness, simulations are conducted using a simplified model of a real power system, demonstrating the successful application of the proposed approach in maintaining system stability and optimizing power allocation under various operating conditions.

This dissertation investigates novel methods for the precise placement, optimal sizing, and efficient allocation of RDGs within power distribution networks. The research addresses the challenges related to power delivery efficiency, particularly in weather-dependent reactance fluctuations. By introducing innovative approaches, this study contributes significantly to various aspects of power distribution networks, including the seamless integration of renewable energy sources, enhancement of voltage stability, reduction of power losses, improvement of safety measures, reinforcement of system resilience, and the facilitation of practical implementation. These contributions collectively advance the field and pave the way for more sustainable and reliable power infrastructure.

Keywords: renewable energy, voltage stability, reactive compensation, system robustness, loss reduction efficiency

Acknowledgements

I would like to express my deepest appreciation to my supervisor, Prof. Mineo Kaneko, for his unyielding support and invaluable guidance throughout my research journey. The pursuit of a Ph.D. is an arduous and lengthy endeavor, and I am immeasurably grateful for Prof. Kaneko's persistent supervision and encouragement at each stage. As a member of the Kaneko-lab, I have encountered numerous challenges, but never once contemplated surrender. Prof. Kaneko's enduring motivation has fostered my growth into a true researcher, and it is a privilege to have him as my mentor. His profound knowledge and expertise across diverse research fields have been priceless, and his advice has been pivotal in helping me surmount many hurdles. The lessons I have learned from him are numerous, and I am sincerely appreciative of his teachings, which will indubitably leave a lasting imprint on my academic and professional career.

I wish to extend my deepest gratitude to Assoc. Prof. Yuto Lim, my co-supervisor, and Prof. Yasuo Tan, my minor research supervisor, for their unwavering support, insightful advice, and relentless dedication throughout my academic journey. Their invaluable guidance and mentorship have significantly shaped my research and aided in overcoming numerous obstacles. I am profoundly thankful for their considerate and encouraging demeanor. Additionally, I extend my heartfelt thanks to Asst. Prof. Saher Javaid, whose assistance has proven invaluable to me on multiple occasions.

I wish to express my earnest gratitude to my two co-supervisors from Thailand, who have been indispensable to my success. Firstly, I extend my deepest appreciation to Assoc. Prof. Dr. Chalie Charoenlarpnopparut from the Sirindhorn International Institute of Technology (SIIT), Thammasat University. Dr. Charoenlarpnopparut has been akin to a mother to me throughout my doctoral studies, consistently providing generous and compassionate support that enabled me to conquer many difficulties. My second co-supervisor, Dr. Siriya Skolthanarat, who granted me the wonderful opportunity to pursue a Ph.D. Dr. Skolthanarat is not only a respected teacher at NECTEC but also a valued mentor in academia. I am thankful for her efforts and suggestions, which have significantly enhanced my research. I express my heartfelt thanks to both of you.

I am humbly and deeply grateful to all members and friends of JAIST and SIIT, as well as those from around the globe, who have offered their unwavering encouragement and priceless motivation throughout my academic journey.

Finally, I owe an immeasurable debt of gratitude to my parents and family for their ceaseless love and support over the years. To my beloved wife, her family, and our son 'Journal', who have been a consistent source of encouragement and inspiration, I dedicate any and all successes that I may achieve in the future.

Contents

This dissertation was prepared according to the curriculum for the Collaborative Education Program organized by Japan Advanced Institute of Science and Technology and Sirindhron International Institute of Science and Technology, Thammasat University.

List of Figures

List of Tables

Notations

$\overline{I}_k$	the complex current of the kth bus
δ_k	the voltage angle of the kth bus
N	the number of buses
$Nsum$	the sum of individually normalized
$Q_{C.k}$	the reactive power compensation support of the kth bus
V_k	the voltage magnitude of the kth bus
Γ	the voltage-reactive power margin with respect to voltage collapse
Λ	the normalized voltage stability index
$\overline{\psi}_k$	the complex voltage product (v-p) function of the kth bus
$\overline{S}_k$	the complex power injection of the kth bus
$\overline{V}_k$	the complex voltage of the kth bus
$\overline{Y}_{mn}$	the mth row, the nth column complex element of the admittance matrix $\mathbf{Y}_{bus}$
RCR	reactive power compensation rate
$\mathcal{PL}$	the sets of power loads
$\mathcal{PS}$	the sets of power sources
$\mathcal{X}$	the set of connections between elements in $\mathcal{PS}$ and $\mathcal{PL}$
ψ_k	the voltage product (v-p) magnitude function of the kth bus
ζ_k	the voltage product (v-p) angle function of the kth bus
$\mathbf{Y}_{bus}$	the admittance matrix
pl_n	the actual consuming power level of the nth bus
ps_m	the actual generating power level of the mth bus

Abbreviations

QSVS	Reactive Power Compensation Support Margin for Voltage Stability Improvement
ALGA	Augmented Lagrangian Genetic Algorithm
ALOA	Ant Lion Optimization Algorithm
BB-BC	Supervised Big Bang-Big Crunch
BBPSO	Bones Particle Swarm Optimization
BSOA	Backtracking Search Optimization Algorithm
DE	Differential Evolution
DG	Distributed Generator
DP-RDG	Dispatchable-RDG
GA	Genetic Algorithm
LDNA	Load-Disabling Nodal Analysis
LDNA-QSVS	Load-Disabling Nodal Analysis for Reactive Power Compensation Support Margin for Voltage Stability Improvement
LDNA-RVS	Load-Disabling Nodal Analysis for Robust Voltage Stability
LRE	Power Loss Reduction
MMNRES	Multi-Membered Non-Recombinative Evolution Strategy
MTLBO	Modified Teaching-Learning Based Optimization
NDP-RDG	Non-dispatchable-RDG
PV	Photovoltaic
RDG	Renewable Distributed Generator
RES	Renewable Energy Source
SNB	Saddle nodal bifurcation
v-p	Voltage product
WT	Wind turbine

Chapter 1

Introduction

The demand for clean and sustainable energy is on the rise, the significance of this research study becomes evident. By addressing this pressing need, the study aims to make a meaningful contribution to the advancement of renewable energy systems. This research, therefore, delves into these technological advancements with the goal of amplifying the potential of these clean energy sources. The overarching aim is to foster the proliferation of sustainable power sources, thereby contributing to a greener and more sustainable future. However, the path pursued encounters challenges that must be addressed. To overcome these obstacles, the research aims to determine the optimal location and size of Renewable Distributed Generator (RDG), considering the unpredictable nature of reactive power utilization, taking into account the unpredictable use of reactive power. The suggested approach incorporates the potential for reactive support, indicative of the system's capacity to provide compensation for reactive power. By giving importance to these factors, the investigation is aimed at bolstering voltage stability and facilitating the seamless integration of RDG.

1.1 Background

The urgent need for green energy sources, particularly solar and wind power, has emerged as a key solution to mitigate environmental impacts and promote sustainable development in various social and industrial situations. In the social context, the increasing awareness of climate change and its detrimental effects on the planet has prompted governments, organizations, and individuals to prioritize the adoption of renewable energy sources. Transitioning to solar and wind power offers an opportunity to reduce greenhouse gas emissions, improves air quality, and addresses energy security concerns.

In the industrial sector, the integration of green energy sources has become crucial for achieving sustainable production processes. Industries are recognizing the benefits of renewable energy in reducing operational costs, enhancing energy efficiency, and complying with environmental regulations. Solar and wind power are being leveraged to power manufacturing facilities, support renewable-based heating and cooling systems, and enable the electrification of transportation.

However, the widespread adoption of solar and wind power also presents certain challenges and problems. One of the key challenges is the intermittent nature of these energy sources, as they are dependent on weather conditions and daylight availability. This intermittency requires the development of efficient energy storage systems and smart grid technologies to ensure a reliable and stable power supply. Additionally, the integration

of solar and wind power into existing energy grids requires infrastructure upgrades, grid management strategies, and policies to facilitate the smooth transition.

In terms of research trends, there is a growing focus on advancing the efficiency, reliability, and cost-effectiveness of solar and wind power technologies. Researchers are exploring innovative approaches for increasing the conversion efficiency of solar panels, improving wind turbine designs, and optimizing energy storage solutions. Additionally, there is a strong emphasis on grid integration studies, demand-side management techniques, and forecasting models to enable better utilization and integration of renewable energy sources.

Overall, the urgent need for green energy sources, such as solar and wind power, arises from the pressing social and industrial concerns related to climate change, environmental impact, and sustainable development. Ongoing research and technological advancements are essential to address the challenges, maximize the potential benefits, and accelerate the transition towards a greener and more sustainable energy future.

The issues of voltage instability and escalating power loss are significant impediments to incorporating renewable energy into power distribution grids. The compensation of reactive power, alongside uncontrolled loads and generators, significantly influences voltage regulation.

1.2 Intermittent Nature of Renewable Energy Integration

The integration of renewable energy sources, such as solar and wind power, presents unique challenges due to their intermittent nature. The availability of renewable energy is subject to variations caused by weather conditions and daylight availability. Solar power, for instance, is highly susceptible to diurnal intermittency, meaning it relies on daylight hours and is unavailable during nighttime. In addition, weather-related intermittency can occur due to cloud cover, reducing the solar irradiance and affecting energy generation, especially in regions with variable weather patterns. Similarly, wind power experiences intermittent fluctuations in energy production. Wind turbines require consistent wind speeds within a specific range to generate electricity efficiently. Variations in wind speed, commonly caused by atmospheric conditions and geographic factors, can lead to intermittent energy output, as gusts and lulls in wind can affect the turbines' ability to generate power consistently. Hydropower, another renewable energy source, can also be subject to intermittent availability. Seasonal changes in precipitation levels and the upstream water flow can lead to fluctuations in the water reservoirs, impacting the consistent generation of electricity from hydropower plants. Geothermal energy, although relatively stable compared to solar and wind, may still face intermittency if the underground heat source weakens or depletes over time, affecting the continuous availability of this renewable resource. These examples underscore the need for sophisticated grid design and management to mitigate the intermittency challenges associated with renewable energy sources and ensure a reliable and consistent power supply.

1.3 Motivation, Challenges and Research Goal

The intermittency of renewable energy sources leads to fluctuations in power generation, making it complex to maintain a stable voltage profile in power distribution

networks. The balance between supply and demand becomes intricate when dealing with these intermittent sources, necessitating advanced control and management strategies. Addressing these challenges is vital for the reliable and efficient integration of renewable energy into existing power grids. Additionally, determining the optimal placement and size of Renewable Distributed Generators (RDGs) introduces complexities, considering the interactions between reactive power compensation, uncontrolled loads, generators, and system constraints. Unpredictable reactive power consumption from RDGs can impact voltage stability, posing further obstacles in the decision-making process. Overcoming technical, logistical, and modeling challenges is essential for achieving successful and practical integration.

Determining suitable locations and sizes for RDGs is a critical task in power system management. As summarized earlier, there is potential for improvement in the location algorithm. This study addresses the following major concerns:

- The increasing need for green energy, specifically uncontrollable renewable energy sources, due to environmental concerns and the need for sustainable energy sources.
- Uncontrollable RDG can contribute to increased power losses as a result of uncontrollable reactive power compensation.
- Employing total power losses as the exclusive objective function might not guarantee effective loss reduction.
- Consequently, a methodology for ascertaining the optimal placement of RDGs should consider voltage stability robustness in the face of uncontrollable reactive compensation.

One of the primary challenges is addressing voltage instability caused by the variability and intermittency of renewable energy generation. Solar and wind power are subject to fluctuations due to weather conditions, making it challenging to maintain a stable voltage profile in the distribution network. Balancing supply and demand becomes more intricate when incorporating these intermittent sources, requiring advanced control and management strategies.

Another significant challenge lies in determining the optimal placement and size of RDG considering the interactions between reactive power compensation, uncontrolled loads and generators, and system constraints. Unpredictable reactive power consumption from RDGs can impact voltage stability, complicating the placement decision-making process. Additionally, ensuring the compatibility and seamless integration of renewable energy systems with existing power infrastructure requires overcoming technical and logistical challenges. Deploying and maintaining solar panels and wind turbines, especially in offshore or remote areas, can pose significant difficulties in terms of installation, maintenance, and grid connection.

Accurately modeling and simulating the proposed methodologies is another critical challenge. Developing realistic models that capture the complexity of real power systems and validating the effectiveness of the proposed methods using real-world data can be intricate tasks. The scalability and applicability of the proposed approaches to different power system configurations and sizes also need to be carefully considered to ensure their practical implementation.

These insights inspire the development of a more comprehensive and sophisticated approach that simultaneously addresses power loss reduction and voltage stability enhancement when determining the optimal location and size of RDG. It is crucial for

the methodologies to thoroughly consider the allocation, location, and sizing of RDGs while taking into account the impact of uncontrollable reactive power compensation. The proposed methodology aims to provide effective solutions to optimize the allocation, determine the ideal locations, and sizes of RDGs, while mitigating the adverse effects of uncontrollable reactive power compensation, such as increased power losses and voltage instability.

In order to implement the proposed methodologies and drive their adoption, it is essential to navigate regulatory requirements and industry standards in the power sector. Aligning the methodologies with existing regulations, standards, and policies ensures their acceptance and facilitates their integration into power system planning and operation.

This research proposes advanced methodologies that comprehensively address the design, distribution, location, and sizing of power devices, focusing specifically on uncontrolled generators.

First, the focus is on the approach for determining the location and size of RDG with the objective of improving voltage stability and mitigating power losses.

Next, a novel method is developed, integrating a sophisticated mathematical approach within the methodologies to precisely ascertain the optimal location and size of RDG. These advanced tools play a pivotal role in identifying optimal solutions, thereby reinforcing the robustness of voltage stability in scenarios involving unpredictable reactive power compensation. Consequently, the research places emphasis not only on achieving voltage stability but also on maximizing the efficiency of Power Loss Reduction (LRE).

Further, the approaches consider the lower and upper limits of power levels in sizing calculations, employing an allocation approach that significantly enhances the precision of device measurements. To reinforce the robustness and effectiveness of the proposed strategies, principles from Graph Theory, specifically maximum matching, are incorporated. This application serves to augment the resilience and efficiency of the methodologies. Innovative guidelines are introduced to regulate uncontrolled generators, aiming to enhance the resilience of power delivery to loads using controllability conditions. Consequently, this allocation approach contributes to the overall improvement of power delivery resilience.

In conclusion, the significance of this research lies in its potential to revolutionize the integration of green energy sources, specifically solar and wind power, into power distribution networks. By addressing voltage instability and optimizing the placement and size of power devices, this study contributes to the advancement of renewable energy systems. While challenges exist, this research remains committed to overcoming them and ensuring the compatibility, reliability, and scalability of the proposed methodologies. The objective is to establish a pathway towards a sustainable and environmentally conscious future driven by clean and efficient energy sources.

1.4 Research Philosophy

The philosophy underlying this research is based on recognizing that power delivery efficiency is influenced by the interaction between power sources and loads within the distribution system. It acknowledges that in the absence of power demand, power sources remain idle and energy cannot be dispatched. Additionally, it acknowledges that as the power demand increases, the power delivery efficiency tends to decrease. However, when there is a requirement for power load, the power flow is initiated, facilitating the transfer of energy from the sources to the load.

While it is essential for the power load to fall within the acceptable generating capacity to ensure sufficient power delivery, it does not guarantee efficiency. To achieve efficient power delivery, the research philosophy emphasizes the significance of managing voltage stability and minimizing power loss. It particularly focuses on employing power load disabling analysis as a key approach in achieving these goals. By analyzing the power load disabling scenarios, crucial insights can be gained into managing voltage stability and minimizing power loss, thereby enhancing power delivery efficiency.

The research philosophy also recognizes the complexity of determining the optimal location and size and suggests breaking down this problem into smaller, manageable parts and treating them while considering their sensitivity to the overall problem. By focusing on power load analysis as a guiding principle, the research aims to address these smaller parts and ultimately find a comprehensive solution for the larger problem

Adopting this philosophy, the research endeavors to develop strategies and methodologies that leverage the characteristics of the power load to enhance the efficiency and reliability of power delivery. The research solutions involve considering the utilization of this concept to optimize the overall performance of power systems and make significant contributions to the advancement of the field.

1.5 Dissertation Outline

The dissertation is arranged systematically as follows:

Chapter 2 initiates with a preliminary study that is vital for the development of mathematical expressions. These expressions will be later utilized in the methodologies for determining the optimal location and size of RDG.

Chapter 3 sets the stage with a comprehensive literature review, incorporating the problem statement, existing methodologies, and their respective limitations in the domain.

In Chapter 4, an innovative methodology is put forth for determining the location and size of RDGs, with reactive power compensation taken into account. This chapter emphasizes the significance of this methodology to the research, and introduces a novel technique called Load-Disabling Nodal Analysis, which plays a crucial role in the proposed methodology for optimal RDG location in the following chapters.

Chapter 5 builds upon the methodology proposed in Chapter 4, offering a more advanced methodology and proposing a novel indicator for determining the location and size of RDGs. This enhanced approach, with a focus on reactive power compensation, aims to improve robust voltage stability and reduce power loss. This chapter also contrasts the results with those derived from other methodologies, emphasizing the superior performance of the proposed approach.

Chapter 6 introduces a method for allocating RDGs while considering system robustness against power fluctuations. The importance of this allocation procedure is to guarantee power delivery from fluctuating sources to load demands, taking advantage of the controllability conditions.

Finally, Chapter 7 wraps up the dissertation by summarizing the key insights, highlighting the contributions made, and suggesting potential avenues for future research in the area.

Each chapter is an integral part of this research journey, contributing to a holistic exploration of the topic.

Chapter 2

Preliminaries

2.1 System Model

A power distribution system, also known as a distribution system, is a network that comprises buses, connections, generators, and loads. This system can be depicted visually through a single-line diagram, illustrating the interconnections between the buses. In this model, generators have a maximum power generation capacity, and loads represent the power consumption at specific buses. The connections between buses are described by their electrical properties, such as admittance. Each bus is associated with a steady-state voltage. In a power distribution system, the slack bus refers to a specific bus that acts as a reference point for voltage and power. It is usually connected to a large power source or a generator that maintains a constant voltage level. The power flows from this slack bus to the loads connected to the system through power lines or transmission lines. It is important to note that this model focuses on steady-state analysis and does not consider transient or dynamic behavior. By understanding these components and their relationships, the mathematical model of a distribution system helps analyze and optimize its performance.

Reactive support and reactive compensation are terms used in power systems to manage the reactive power requirements and voltage stability. Reactive support involves providing reactive power to the electrical system to maintain stable voltages and support inductive loads. Reactive power, which doesn't contribute to actual work, is crucial for establishing and maintaining desired voltage levels throughout the network. On the other hand, reactive compensation focuses on actively controlling and adjusting reactive power flow in the system. It aims to improve power system performance by regulating voltage, correcting power factors, and reducing system losses. Reactive compensation is achieved using devices like capacitors and reactors. Capacitors inject reactive power to support voltage levels, especially when there is excessive reactive power consumption. Reactors absorb excess reactive power, ensuring stable voltages, particularly when there is excessive reactive power generation. By effectively managing reactive power, power system operators optimize performance, minimize losses, and ensure reliable power supply.

Efficient and reliable operation of distribution systems is crucial for meeting the increasing demand for electricity while minimizing environmental impacts. The integration of renewable distributed generators (RDGs) into distribution systems has emerged as a promising solution to achieve cleaner energy without compromising on the efficiency and reliability of the operation. Optimal placement of RDGs in a distribution system is an essential task to ensure maximum power generation and consumption in a steady state.

The model for determining the optimal placement of RDGs in distribution systems takes into consideration the crucial role of reactive compensation in maintaining a nominal voltage level in a steady state. Reactive compensation is determined by multiplying the generated active power by the reactive power compensation ratio (RCR). The evaluation of the impact of uncontrollable reactive compensation from RDGs, which is directly linked to their generated power, is carried out using RCR. It is important to note, however, that this study only focuses on maximum power generation and consumption in a steady state. Therefore, it is essential to acknowledge the limitations of the mathematical formulation and simulation for determining the optimal placement of RDGs in a distribution system based on predetermined installation quantity.

Further, to evaluate the effectiveness of the proposed model, the IEEE test distribution system is used, providing essential information such as the single-line diagram, line impedance, and power consumption levels. Knowledge of the maximum power consumption levels of loads is necessary when examining voltage stability and maximum power losses. The impacts of unbalanced load and compensation of both active and reactive power are neglected in the model. The installation quantity of RDGs is predetermined.

2.2 Reactive Power Compensation of RDGs

Different types of generators convert natural energy into electricity resulting in non-uniform reactive power compensation. Basically, the reactive compensation of generators is described using the Power factor, which is the cosine of the difference between voltage and current phase angles. For simplification, reactive power compensation and active generated power of a RDG are represented using a ratio named reactive power compensation rate (RCR), as follows.

$$\mathrm{RCR} = \frac{Q_{comp}^{RDG}}{P^{RDG}} \tag{2.1}$$

where Q_{comp}^{RDG} and P^{RDG} are reactive power compensation of generators and the active power generated by a generator, respectively.

In this paper, the RCR is used for distinguishing the type of RDGs. It can be assumed that, for Dispatchable-RDG (DP-RDG), the generator is not compensated any reactive power from the system, and RCR is zero. On the other hand, for Non-dispatchable-RDG (NDP-RDG), the generator's level of compensated reactive power is assumed to be equal to the generated active power times RCR.

2.3 Voltage Stability Index

In order to determine the ideal location of RDGs, the main priority is to identify the voltage stability limit dominated by generator reactive consumption. One of the measures used to evaluate the system is the L-index, proposed by Kessel et al. [1], which quantitatively measures a weak bus and forecasts voltage collapse. The L-index is formulated in Equation (2.2)

$$L = \max_{j \in \mathcal{T}} \left| 1 - \frac{\sum_{i \in \mathcal{S}} \bar{F}_{ji} \bar{V}_i}{\bar{V}_j} \right| \tag{2.2}$$

where $\bar{V}_i$,$\bar{V}_j$ are complex voltages of the ith and jth buses, respectively, $\mathcal{T}$ is a set of loads,

$\mathcal{S}$ is a set of generators, $\bar{F}_{ji}$ is the jth row, ith column element of the hybrid matrix, which is generated from the matrix $\mathbf{Y}$ by a partial inversion, described in [1].

Under stable operation, the value of the L-index should be less than 1, and the smaller the value of the L-index from 1, the more stable the system.

2.4 Total Power Loss

Power losses are caused by various factors such as resistance, leakage, and inefficiencies. Studies have shown that the size and location of Distributed Generator (DG) can significantly reduce total power losses. The mathematical expression for power losses is given by Equation (2.3) [2].

$$P_{loss} = \sum_{m=1}^{N} \sum_{n=1}^{N} (a_{mn}(P_m P_n + Q_m Q_n) + b_{mn}(Q_m P_n - P_m Q_n)) \tag{2.3}$$

where

$$a_{mn} = \frac{r_{mn}}{V_m V_n} \cos(\delta_m - \delta_n),$$

$$b_{mn} = \frac{r_{mn}}{V_m V_n} \sin(\delta_m - \delta_n),$$

V_m,V_n—voltage magnitudes of the mth and nth buses, respectively,

δ_m,δ_n—voltage angles of the mth and nth buses, respectively,

r_{mn}, x_{mn}—resistance and reactance of the mth row, nth column element of the impedance matrix $\mathbf{Z}_{bus}$,

P_m,P_n—active power injections at the mth and nth buses, respectively,

Q_m, Q_n—reactive power injections at the mth and nth buses, respectively,

N—the number of buses.

2.5 Loading Margin

The loading margin is a crucial factor in determining the proximity of a power system to voltage collapse [3], which can lead to blackouts and other severe consequences. It is defined as the difference between the current operating point and the point at which voltage collapse occurs, expressed as a percentage of the distance between the two points. In other words, it represents the remaining capacity of the system to accommodate additional loads or other changes before reaching a critical point.

In this research, the loading margin is used to evaluate the system's stability and its ability to handle potential disturbances. By determining the minimum loading margin required for safe operation, the optimal placement of RDGs can be identified. This is because RDGs can affect the voltage stability of a power system and can lead to instability if not correctly placed and operated.

Therefore, it is essential to consider the loading margin when evaluating the potential impact of RDGs on the system's stability. The loading margin calculation allows us to estimate the remaining margin between the current operating point and the point of voltage collapse, providing insight into the system's stability and ability to handle disturbances. By demonstrating the minimum loading margin required for each optimal RDG placement, it ensures that the system remains safe from voltage collapse and operates efficiently and reliably.

Chapter 3

Related Works

3.1 Introduction and Problem Statement of Renewable Integration Systems

The escalating problem of greenhouse gas emissions, coupled with the inadequacy of conventional power sources to keep pace with the surging global energy demand, has amplified the promotion of renewable distributed generators (RDGs) worldwide [4–6]. Championed as an environmentally friendly alternative, these RDGs, including Photovoltaic (PV) and Wind turbine (WT) systems, are garnering widespread acceptance.

However, the intermittent nature of these renewable energy sources presents significant challenges. Unlike traditional, dispatchable energy sources such as oil, natural gas, and coal, the power generation from RDGs is unpredictable and uncontrollable. This lack of control can result in poor sizing and placement of RDGs, leading to amplified power losses and degraded voltage stability [7–10].

The optimal sizing and siting of RDGs have been the focus of numerous studies, with researchers endeavoring to develop methodologies that minimize total power losses and improve voltage profiles [11–23]. These methodologies apply a wide range of techniques, including analytical expressions, differential evolution, particle swarm optimization, genetic algorithms, and more, to determine the optimal location and size of RDGs

Reactive power compensation is important in modern power systems due to their increasing complexity and the continuous evolution of power conversion technologies [24]. The approach allows for a comprehensive analysis of the relationship between voltage stability margin and reactive power compensation. By applying the method to both the IEEE39-bus system and an actual provincial grid, the study demonstrated its effectiveness and validity. These findings highlight the significance of realizing reactive compensation in enhancing voltage stability and ensuring the reliable and efficient operation of power systems amidst the challenges posed by complex systems and evolving power conversion technologies.

While these studies have made considerable strides in minimizing power loss and improving voltage profiles, they often overlook the robustness of voltage stability and reactive compensation. The neglect of these factors may lead to heightened power loss in situations where reactive compensation is uncontrollable. As society embarks on a future increasingly dependent on renewable energy, addressing these challenges is imperative.

3.2 Existing Methodologies for Optimal Location and Size of RDGs

The methodologies for determining the optimal location and size of RDG can be broadly categorized into the following based on the techniques used and the objectives they aim to achieve:

Analytical Expressions

Some researchers have proposed analytical expressions to estimate the optimal size of DG [11]. They also present methodologies to determine the optimal locations of the DGs.

Differential Evolution (DE)

DE has been used to determine the sizes of DGs considering the minimization of losses [12].

Bones Particle Swarm Optimization (BBPSO) and Multi-Membered Non-Recombinative Evolution Strategy (MMNRES)

These techniques were proposed and proved to yield the best results in terms of minimum losses and voltage profile improvement [12].

Genetic Algorithm (GA)

GA has been widely utilized to determine the locations of DGs, considering the minimization of losses [14, 25]. In one of the studies, energy saving in terms of cost was also considered [25].

Augmented Lagrangian Genetic Algorithm (ALGA)

This is a development of the GA used to determine the locations of RDGs, minimizing both losses and investment cost [26].

Sensitivity Factor Formulation

Some researchers have formulated the sensitivity factor and used it to determine the optimal location and size of DGs, minimizing losses using an analytical method and the classical grid search algorithm [13].

Particle Swarm Optimization (PSO) and Multileader Particle Swarm Optimization (MLPSO)

PSO has been used to solve the optimal placement of DGs while considering loss minimization [27]. It was later developed into MLPSO, which yielded better results [28].

Modified Teaching-Learning Based Optimization (MTLBO)

MTLBO was proposed to determine the optimal location and size of DGs simultaneously in distribution systems [16].

Supervised Big Bang-Big Crunch (BB-BC)

BB-BC was used to determine the optimal placement and size of DGs by minimizing the multi-objective performance index, including active power loss, reactive power loss, voltage profile, and reserve capacity indices [17].

Backtracking Search Optimization Algorithm (BSOA)

BSOA was used to determine locations and sizes of DGs by adapting the weighting factor in the objective function to reduce losses and enhance the voltage profile [29].

Ant Lion Optimization Algorithm (ALOA)

ALOA was utilized to determine the optimal placement of RDGs, resulting in minimum losses [18].

These methodologies have made significant strides in loss minimization and voltage profile improvement. However, they often overlook voltage stability robustness and reactive compensation, leading to potential increased power loss in cases of uncontrollable reactive compensation.

3.3 Limitations of Existing Methodologies

The existing methodologies utilized worldwide for determining the optimal location and size of RDG have demonstrated significant success. However, this research focuses on addressing their two specific limitations that have garnered significant attentions.

Existing methods for optimizing and controlling power systems have made significant progress in reducing power loss and improving voltage profiles. These methods aim to make power systems more efficient and reliable by finding the best ways to use generators, loads, and transmission lines. They use different techniques to decide where to place RDGs for maximum benefit. However, there are still important limitations to consider. One limitation is that these methods often ignore the importance of voltage stability and reactive compensation. This disregard for voltage stability robustness and the need for appropriate reactive compensation may lead to increased power loss, particularly in scenarios involving uncontrollable reactive compensation. Therefore, it is important to do more research and develop new methods that take voltage stability and effective reactive compensation into account for better power system optimization.

Table 3.1 provides an overview of the limitations discussed in the literature review and their impact on the field of optimal RDG location and sizing. Addressing these limitations is paramount to advancing the field and achieving optimal RDG deployment strategies.

Table 3.1: Summary of Literature Review with Limitations

Reference/Year (Citations)	Method	Test System Used	Features					
			Loss Minimization	Voltage Profile	RDG Limitation	Reactive Compensation	Robust Voltage Stability	Computation Time (s)
[11]/2006 (1396)	*Analytical expressions	IEEE69	Yes	No	No	No	No	4.109 [13]
[13] /2009 (784)	Analytical method	IEEE69	Yes	Yes	No	No	No	0.078
[14] /2009 (115)	GA	IEEE69	Yes	No	No	No	No	262.12
[25] /2010 (250)	GA	IEEE33, 69	Yes	No	No	No	No	N/A
[12]/2012 (172)	*DE with BBPSO, MMNRES	IEEE6, 30	Yes	Yes	No	No	No	N/A
[15]/2013 (307)	*EP	IEEE69	Yes	Yes	No	No	No	N/A
[27] /2013 (426)	PSO	IEEE33, 69	Yes	No	No	No	No	N/A
[16] /2013 (332)	MTLBO	IEEE69	Yes	No	No	No	No	0.3
[19]/2014 (218)	*Analytical expressions	IEEE69	Yes	Yes	No	No	No	N/A
[17] /2015 (66)	BB-BC	IEEE69, 119	Yes	Yes	No	No	No	N/A
[30]/2017 (306)	ALOA	IEEE33, 69	Yes	Yes	No	No	No	N/A
[26] /2017 (89)	GA	IEEE33, 69, 123	Yes	Yes	No	No	No	N/A
[31]/2018 (132)	WOA	IEEE15, 33, 69, 85, 118	Yes	Yes	No	No	No	N/A
[20]/2018 (120)	PSO	IEEE31	Yes	Yes	No	No	No	N/A
[28] /2020 (39)	MLPSO	IEEE33, 54	Yes	Yes	No	No	No	N/A

Note: This citation is retrieved on 2023-06-19, ($*$: Exhaustive power flow).

3.4 Summary

Renewable Distributed Generators (RDGs) have become increasingly popular worldwide due to environmental concerns and the growing energy demand. However, due to their intermittent nature, the power generation from RDGs, such as photovoltaics and wind turbines, is uncontrollable compared to conventional energy sources. This uncontrollability can lead to increased power losses and degraded voltage stability if RDGs are not optimally sized and placed. Particularly, the uncontrollable reactive compensation of these energy sources can cause voltage stability degradation.

The optimal location and size of RDGs have been extensively researched. Numerous methodologies have been developed that focus on minimizing total power losses and improving voltage profiles. For instance, methods using genetic algorithms, particle swarm optimization, and the Ant Lion Optimization Algorithm have been employed to

determine optimal RDG locations, sizes, and installation objectives. Some methodologies also consider the cost of energy, investment cost, and multi-objective performance indices, such as active power loss, reactive power loss, voltage profile, and reserve capacity indices.

Despite the successes of these methodologies, most of them often overlook two critical aspects: voltage stability robustness and reactive compensation. Neglecting these aspects can lead to increased power loss in cases of uncontrollable reactive compensation.

Chapter 4

Incorporating Safety Margins using LDNA-QSVS: A Methodology for RDGs Location and Size Determination

4.1 Introduction

Power distribution networks, where reactances dominate voltage control, are susceptible to voltage instability due not only to uncontrollable loads and generators but also to reactive power compensation of renewable distributed generators (RDGs) [32]. As such, it becomes crucial to scrutinize the uncontrollable reactive power consumption when determining optimal RDG placement.

This chapter introduces a methodology for determining the optimal location and size of RDGs. This approach involves considering the capacity for reactive support - the system's ability to handle reactive power compensation. To assist in this, several key functions such as the voltage product (v-p) function, the active v-p function, and the reactive v-p function are derived from the fundamental complex power formula. These functions serve to calculate voltage stability at each bus within the power system.

To estimate the bus most vulnerable to voltage collapse, a safety margin is formulated with these key functions. This safety margin is referred to as the Reactive Power Compensation Support Margin for Voltage Stability Improvement (QSVS).By integrating reactive compensation and the safety margin using QSVS in the optimal location and size determination, the proposed methodology promises enhanced results. Specifically, it offers improvements in reducing power losses and augmenting voltage stability. This chapter delves into the details of these processes and their implications for RDG placement and power system optimization.

4.2 Mathematical Key Functions

In order to generate a voltage stability indicator, the basic complex power equation $\overline{S}^* = \overline{V}^* \overline{I}$ is converted into non-complex functions by employing specific mathematical functions.
For any kth bus,

$$\overline{S}_k^* = \overline{V}_k^* \overline{I}_k$$
$$\overline{S}_k^* = \overline{V}_k^* \sum_{n=1}^{N} \overline{Y}_{nk} \overline{V}_n$$

which can be converted to

$$\frac{\overline{S}_k^*}{\overline{Y}_{kk}} = (\frac{\sum_{n=1,\neq k}^{N} \overline{Y}_{nk} \overline{V}_n}{\overline{Y}_{kk}}) \overline{V}_k^* + V_k^2 \tag{4.1}$$

where $\overline{S}_k$ is the complex power injection, $\overline{V}_k$ is the complex voltage and $\overline{I}_k$ is the complex current at the kth bus.
The complex Voltage product (v-p) function ($\overline{\psi}_k$) at the kth bus is defined as

$$\overline{\psi}_k \triangleq \frac{\sum_{n=1,n\neq k}^{N} \overline{Y}_{nk} \overline{V}_n}{\overline{Y}_{kk}} \tag{4.2}$$

where $\overline{V}_n$ is the complex voltage at the nth bus, $\overline{Y}_{mn}$ is the mth row, the nth column complex element of the admittance matrix $\mathbf{Y}_{bus}$ and N is the number of buses.
Equation (5.3) can be restated as follows by substituting $\overline{\psi}_k$.

$$\frac{\overline{S}_k^*}{\overline{Y}_{kk}} = \overline{\psi}_k \overline{V}_k^* + V_k^2 \tag{4.3}$$

Likewise, Equation (4.3) takes the form

$$\overline{\psi}_k \overline{V}_k^* + V_k^2 = \psi_k V_k \cos(\zeta_k - \delta_k) + j\psi_k V_k \sin(\zeta_k - \delta_k) + V_k^2 \tag{4.4}$$

where V_k, δ_k are voltage magnitude and the voltage angle of the kth bus, respectively and ψ_k, ζ_k are the v-p magnitude, the v-p angle of the kth bus, respectively.
Separating Equation (5.5) into real and imaginary parts, the following can be obtained:

$$\alpha_k(V_k, \Delta_k, \psi_k) \triangleq V_k^2 + \psi_k V_k \cos(\Delta_k) \tag{4.5}$$
$$\beta_k(V_k, \Delta_k, \psi_k) \triangleq \psi_k V_k \sin(\Delta_k) \tag{4.6}$$

where $\Delta_k = \zeta_k - \delta_k$. For simplification, α_k and β_k are used for $\alpha_k(V_k, \Delta_k, \psi_k)$ and $\beta_k(V_k, \Delta_k, \psi_k)$ if the augments are clear from the context. In the following, α_k and β_k are called active v-p function and reactive v-p function, respectively. To calculate the magnitude of the voltage at the kth bus, the substitution of Equations (4.5) and (4.6) into Equation (5.5) yields the bus voltage equation as follows:

$$V_k^4 - V_k^2 \left(\psi_k^2 + 2\alpha_k\right) + \alpha_k^2 + \beta_k^2 = 0 \tag{4.7}$$

Voltage stability and security assessment play an important role in the operation and planning of renewable integrated energy systems. The increasing integration of renewable energy sources exacerbates voltage stability concerns, as these sources often generate power that varies in output and intermittency, which can have an impact on the power system's voltage profile. Voltage stability refers to the ability of the power system to maintain acceptable voltage levels despite changing conditions. Voltage instability could result in voltage collapse, which could lead to severe consequences like blackouts. Therefore, the power system must be able to respond to variations in demand and generation,

maintaining a stable voltage profile throughout the network. Security assessment involves analyzing the power system's security under different operational conditions, such as the presence of faults or the loss of a transmission line, identifying possible issues that could lead to voltage instability or other operational problems.

Incorporating renewable energy sources into integrated energy systems has a significant impact on voltage stability and security. The unpredictability of solar and wind generation can cause voltage profile fluctuations in the power system, leading to system inefficiency and unreliability. This chapter presents a comprehensive method for measuring voltage stability and security assessment in renewable integrated energy systems. These assessments are critical components of the operation and planning of renewable integrated energy systems, and the proposed method utilizes advanced modeling and simulation techniques to evaluate voltage stability and security. By utilizing this method, it can be effectively managed the challenges posed by the integration of renewable energy sources in power systems and ensure reliable and efficient operation.

4.3 Basic Idea of Voltage Stability Assessment

According to [33], voltage stability is the ability to maintain acceptable voltage levels at each bus during normal operation and after any contingency events. The VQ curve is a graphical representation of the relationship between reactive support (Q_c) at a particular bus and the voltage at that bus. The value of Q_c is a measure of the system's need for external reactive power injection to maintain system operability. A positive value of Q_c indicates that the system requires external reactive power injection, while a negative value indicates that the system provides sufficient reactive power margins for compensation at an operating point. Figure 4.1 illustrates an example of reactive support in the VQ curve of the kth bus on a test distribution system. The summation of Q_c and external reactive power must be equal to zero during stable operation. Therefore, the value of Q_c is an important factor controlling voltage stability.

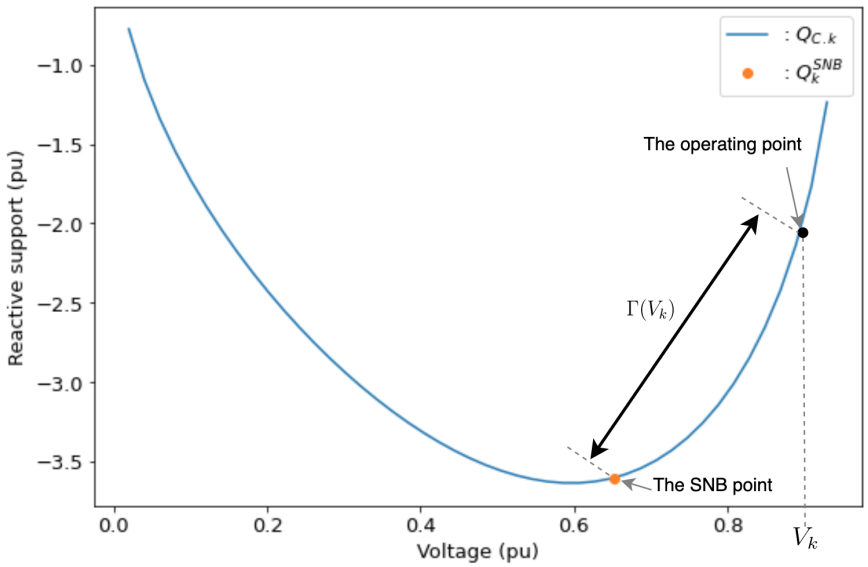

Figure 4.1: An example of reactive support variation at different voltage levels with parameter description for estimating vulnerable buses of voltage collapse.

The VQ curve shows a critical point known as the Saddle nodal bifurcation (SNB), which marks the operating point where voltage collapse may happen [33,34]. Maintaining a safe distance between the operating point and the SNB is necessary to ensure voltage stability. Uncontrolled reactive power compensation from RDG can cause voltage collapse, which is a system instability. Therefore, it is essential to assess voltage stability while considering the possibility of voltage collapse to determine the best RDG placement.

Furthermore, voltage stability in power systems relies on maintaining the operating point of power load and voltage. It is crucial to ensure that this operating point remains distant from the voltage collapse point, which is commonly found at the maximum power or nose point. In addition, operating with voltages below the nose point can result in system instability. Hence, it is vital to conduct thorough assessments and implement effective management strategies to maintain voltage stability, prevent voltage collapses, and guarantee a stable power supply. This relationship is exemplified in the IEEE33-bus test distribution system, as illustrated in Figure 4.2. The research conducted acknowledges the importance of this correlation and integrates it into the proposed methodology. As a result, the solution for voltage will be confined within the established boundaries set by the proposed method. This constraint ensures the preservation of voltage stability and promotes the reliable operation of the power system.

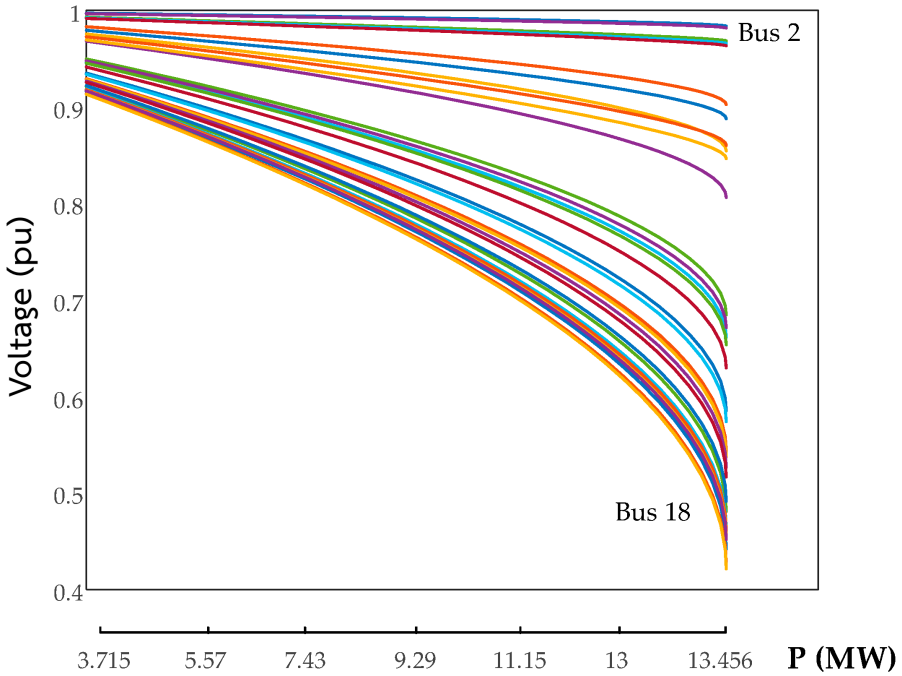

Figure 4.2: Operating Point of Power Load Variation at Different Voltage Levels with Parameter Description for Estimating Vulnerable Buses of Voltage Collapse

Maintaining voltage stability entails ensuring sufficient reactive power compensation provided by Q_c at operating points and increasing the distance between the SNB point and the operating point to avoid voltage collapses.

4.4 Formulation of Mathematical Equations

4.4.1 Reactive support Q_c

Voltage solutions which are obtained from Equation (4.7) are the feasible power flow solution. Once the solution is investigated using the VQ curve, the reactive support Q_C is obtained from Equation (4.7) as

$$Q_{C.k} = -\frac{Y_{kk}\sin(\phi_k)}{\sin(\phi_k + \theta_{kk})} \cdot \psi_{Q.k} \tag{4.8}$$

where Q_k is the magnitude of reactive power injection at the kth bus, $Q_{C.k}$ is the magnitude of reactive support at the kth bus, ϕ_k is the angle of the phasor of complex power injection $\bar{S}_k$ at the kth bus, Y_{kk} is the magnitude of the kth row, the kth column complex element of the admittance matrix $\mathbf{Y}_{bus}$, θ_{kk} is the angle of the kth row and the kth column complex element of the admittance matrix $\mathbf{Y}_{bus}$.

It should be noted that a negative solution for $Q_{C.k}$ indicates that the voltage is stable without requiring external reactive power injection, while a positive solution for $Q_{C.k}$ indicates that external reactive power injection is necessary to maintain the voltage level within an acceptable range. Therefore, Q_c is an essential indicator of voltage stability.

4.4.2 Identification of voltage collapse

As the discussion in [1, 32, 35], the power flow Jacobian matrix becomes singular at the point of voltage collapse or the SNB.
From Equations (4.5) and (4.6), the singularity of Jacobian matrix can be written as

$$\begin{vmatrix} \frac{\partial \alpha_k}{\partial V_k} & \frac{\partial \alpha_k}{\partial \Delta_k} \\ \frac{\partial \beta_k}{\partial V_k} & \frac{\partial \beta_k}{\partial \Delta_k} \end{vmatrix} = 0$$

$$\begin{vmatrix} 2V_k + \psi_k \cos(\Delta_k) & -V_k\psi_k \sin(\Delta_k) \\ \psi_k \sin(\Delta_k) & V_k\psi_k \cos(\Delta_k) \end{vmatrix} = 0$$

$$V_k\psi_k\left(2V_k\cos(\Delta_k) + \psi_k\right) = 0 \tag{4.9}$$

The SNB condition using Equation (4.9) can be written as

$$\psi_k = -2V_k\cos(\Delta_k) \tag{4.10}$$

By taking into account the possible solutions for the voltage obtained from Equation (4.7) and substituting Equations (4.5) and (4.6), as well as the SNB condition given in Equation (4.10), the voltage V_k^{SNB} at the SNB point can be determined as

$$V_k^{SNB} = \sqrt{V_k^2 - \sqrt{V_k^2\sin^2(\Delta_k)\cdot|4V_k^2\cos^2(\Delta_k) - \psi_k^2|}} \tag{4.11}$$

Similarly, the solution for the reactive v-p function β_k^{SNB} at the SNB point can be obtained by solving Equation (4.7) with the SNB condition given in Equation (4.10).

$$\beta_k^{SNB} = \begin{cases} \sqrt{(V_k^{SNB})^2\psi_k^2 - ((V_k^{SNB})^2 - \alpha_k)^2} & \text{if } \cos^{-1}(\frac{0.5\psi_k}{V_k}) \in [0, \pi] \\ -\sqrt{(V_k^{SNB})^2\psi_k^2 - ((V_k^{SNB})^2 - \alpha_k)^2} & \text{if } \cos^{-1}(\frac{0.5\psi_k}{V_k}) \in [\pi, 2\pi] \end{cases} \tag{4.12}$$

Eventually, by substituting $\psi_{Q.k}^{SNB}$ into Equation (4.8), the reactive power at the SNB point ($Q_{C.k}^{SNB}$) is obtained as

$$Q_{C.k}^{SNB} = -\frac{Y_{kk}\sin(\phi_k)}{\sin(\phi_k + \theta_{kk})}\beta_k^{SNB} \tag{4.13}$$

4.5 Voltage-Reactive Power Margin

Voltage stability is a critical consideration in power system operation and planning. To estimate the risk of voltage collapse, identifying the most vulnerable bus is crucial. A useful indicator for this is the voltage-reactive power margin with respect to voltage collapse, denoted by Γ. By calculating Γ for each bus, the most vulnerable bus can be identified, allowing measures to be taken to prevent voltage collapse and maintain system stability.

Maintaining voltage stability is a critical aspect of power system operation and planning. To assess the risk of voltage collapse, it is essential to estimate the most vulnerable bus, i.e., the highest risk of voltage collapse. In this regard, the distance between the coordinates of the operating point (V_k, $Q_{C.k}(V_k)$) and the saddle nodal bifurcation (SNB) point ($V_{C.k}^{SNB}, Q_{C.k}^{SNB}$) in the voltage-reactive power (VQ) curve of the kth bus is used. This distance is called "the voltage-reactive power margin with respect to voltage collapse" and is denoted by Γ. At the kth bus, the voltage-reactive power margin with respect to voltage collapse $\Gamma(V_k)$ is obtained by computing the distance between the operating point and the SNB point in the VQ curve. By estimating the voltage-reactive power margin with respect to voltage collapse at each bus, the most vulnerable bus can be identified, and appropriate measures can be taken to maintain voltage stability and prevent voltage collapse.

$$\Gamma(V_k) \triangleq \left| \sqrt{(Q_{C.k}(V_k) - Q_{C.k}^{SNB})^2 + (V_k - V_k^{SNB})^2} \right| \tag{4.14}$$

For simplification, Γ is used for $\Gamma(V_k)$ if the augments are clear from the context. Under security operation, the value of Γ should be greater than 0. The voltage collapse occurs if Γ is equal to 0. Therefore, the greater than 0 the value of Γ, the more safe the system.

To demonstrate the voltage collapse risk assessment of systems, IEEE5-bus and IEEE33-bus test distribution systems where the information of them are given in Table B.2–B.4, are used. Then, the most vulnerable bus of voltage collapse is investigated on these test distribution systems using the minimum Γ and the loading margin, as in Tables 4.1.

Table 4.1: The most vulnerable bus of voltage collapse detection on IEEE5-bus and 33-bus distribution test systems

The most vulnerable bus of voltage collapse	**Distribution system**	
	IEEE5-bus	**IEEE33-bus**
minimum Γ	Bus 5	Bus 15, 17, 18, 22
loading margin	Bus 5	Bus 17, 18

By comparing the minimum Γ to the loading margin, these results show that the minimum of Γ include the bus with the highest possibility of voltage collapse of IEEE5-bus and IEEE33-bus systems, as shown in Figures 4.3 and 4.4 .

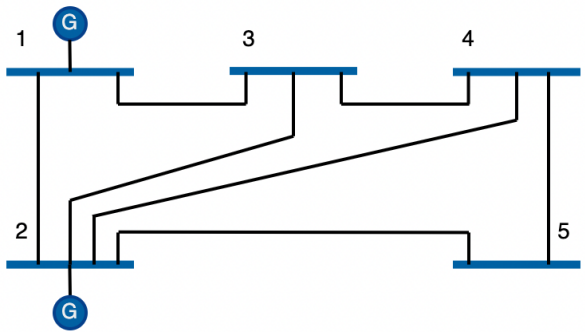

Figure 4.3: Single line diagram of the 5-bus test distribution system

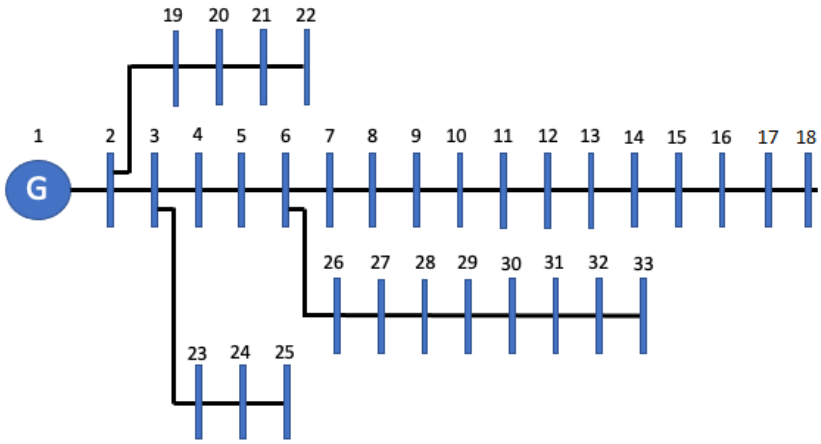

Figure 4.4: Single line diagram of the 33-bus test distribution system

4.5.1 Effect of reactive power compensation

The integration of RDGs into distribution systems has the potential to provide many benefits, including reduced greenhouse gas emissions, increased energy efficiency, and improved power quality. However, the integration of RDGs can also create significant challenges, such as voltage stability issues that can cause voltage collapse. Reactive compensation of RDGs can be uncontrollable, leading to voltage instability, and as a result, it is crucial to investigate the impact of reactive compensation on voltage stability.

Voltage collapse can occur due to uncontrollable reactive compensation of RDGs. To investigate this phenomenon, the impact of reactive compensation is demonstrated on voltage stability using the IEEE5-bus and IEEE33-bus test distribution systems, where the generators' reactive compensation is assumed to be uncontrollable. Subsequently, the most vulnerable bus susceptible to voltage collapse is investigated.

In order to demonstrate the impact of reactive compensation on voltage stability, varying levels of negative reactive compensation are applied to the RDGs in the IEEE5-bus and IEEE33-bus test distribution systems. Specifically, reactive compensation levels of -0.10 pu and -0.20 pu are applied to the IEEE5-bus system, while the IEEE33-bus system is subjected to -0.0001 pu and -0.0002 pu of reactive compensation. The voltage stability of the test systems is analyzed using the L-index voltage stability indicator proposed by Kessel. The analysis results indicate that the 5th and 22nd buses of the IEEE5-bus and IEEE33-bus systems, respectively, exhibit the weakest voltage stability.

Further, in order to identify the most vulnerable buses susceptible to voltage collapse, the loading margins of the test systems are analyzed. The analysis reveals that the 5th bus of the IEEE5-bus system and the 17th and 18th buses of the IEEE33-bus system are the most vulnerable to voltage collapse, as indicated in Tables 4.2 and 4.3. The first two weakest buses with the highest probability of voltage collapse, determined using the minimum value of Γ and the loading margin, are found to be almost the same. Remarkably, for the IEEE5-bus system, the weakest bus in voltage stability is the same as the most vulnerable bus of voltage collapse, as shown in Table 4.2.

Table 4.2: Comparisons of first two weakest buses of voltage stability and the most vulnerable bus of voltage collapse on IEEE5-bus distribution test system

	Reactive compensate		
	0.00 pu	**−0.10 pu**	**−0.20 pu**
The weakest two buses of voltage stability (L-index)	Bus 5, 1 (0.0029, 0.0017)	Bus 5, 1 (0.0029, 0.0017)	Bus 5, 1 (0.0029, 0.0017)
The weakest two buses of Γ: (Γ)	Bus 5, 4 (98.58, 228.76)	Bus 5, 1 (233.62, 270.26)	Bus 1, 5 (270.25, 353.36)
The lowest loading margin:	Bus 5 (248 pu)	Bus 5 (248 pu)	Bus 5 (248 pu)

However, by comparing the results from the loading margin and L-index as given in Table 4.3, the weakest bus of voltage stability using L-index is not the same with the most vulnerable bus of voltage collapse by the loading margin for the IEEE33-bus system.

Table 4.3: Comparisons of first two weakest buses of voltage stability and the most vulnerable bus of voltage collapse on IEEE33-bus distribution test system

	Reactive compensate		
	0.0000 pu	**−0.0001 pu**	**−0.0002 pu**
The weakest two buses of voltage stability: (L-index)	Bus 22, 25 (0.0698, 0.0691)	Bus 22, 25 (0.0699, 0.0692)	Bus 22, 25 (0.0700, 0.0693)
The weakest two buses of Γ: (Γ)	Bus 15, 17 (0.3174, 0.578)	Bus 18, 22 (0.8216, 0.8567)	Bus 18, 22 (0.9913, 1.0936)
The lowest loading margin:	Bus 18 (0.03 pu)	Bus 17,18 (0.03 pu)	Bus 17 (0.03 pu)

The validity of Γ in approximating the most vulnerable bus of voltage collapse is verified by determining one of the first two weakest buses based on loading margin levels of the IEEE5-bus and 33-bus systems, as shown in Tables 4.2 and 4.3, respectively. The results demonstrate that Γ can effectively consider the different levels of reactive compensation and be used to improve voltage stability and safety by formulating the objective function for determining the optimal placement while also considering the reactive power compensated by generators.

In addition, it was observed that the voltage collapse risk increases with reactive compensation when using Γ, as indicated by Figures 4.5 and 4.6. This implies that uncontrolled reactive compensation from RDGs can lead to a reduction in system operational reliability and potential voltage collapse.

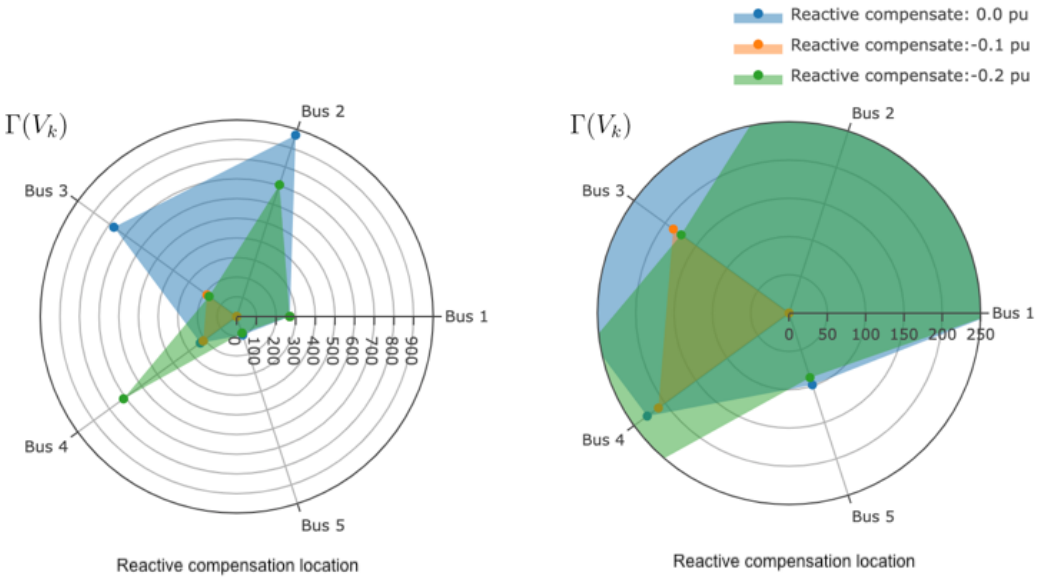

Figure 4.5: The variation of Γ indicating voltage collapse risk on IEEE5-bus test distribution system

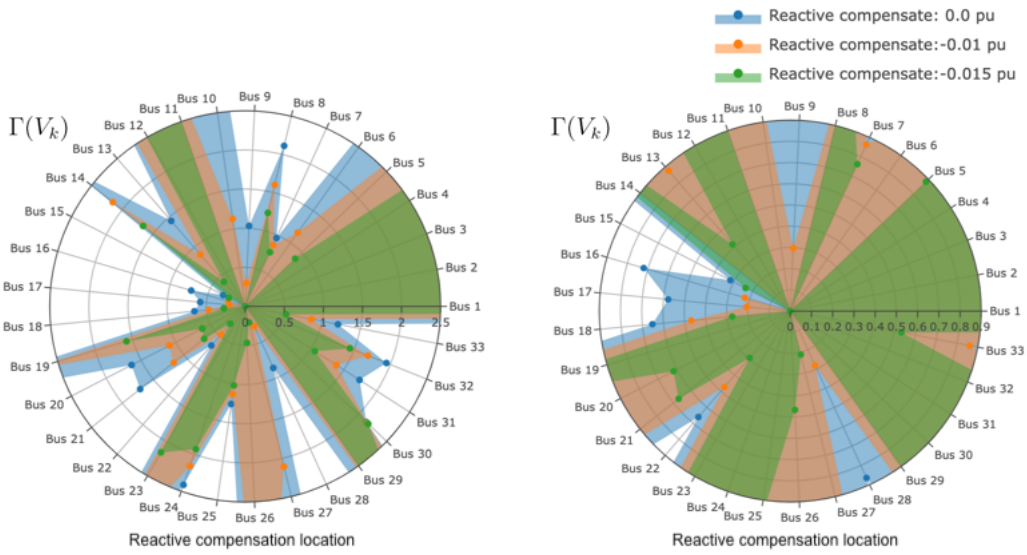

Figure 4.6: The variation of Γ indicating voltage collapse risk on IEEE33-bus test distribution system

4.6 Load-Disabling Nodal Analysis

Maintaining power system stability is a crucial aspect of the design and operation of power systems, and the power consumption of loads at each bus is a critical factor that can impact the stability of the system. Typically, the worst degrading factor for system stability is the power consumption of the bus with the highest load. To reduce the power consumption at this bus and improve the system's stability, electrical power must be supplied to it. Based on this observation, a methodology has been proposed for determining the location of RDGs in power systems. In addition to determining the location of RDGs, the size of the RDGs is also a critical consideration. Therefore, a loss minimization strategy is employed to determine the optimal size of RDGs. By integrating both location and size considerations, this methodology provides a comprehensive approach to enhance the stability and efficiency of power systems. The proposed methodology represents a significant contribution to the field of power systems engineering, offering a valuable tool for power system planning and design.

In this chapter, the proposed methodology is presented for identifying the optimal placement and dimensions of RDGs that can accommodate any given objective function for maximization. This approach, named "Load-Disabling Nodal Analysis (LDNA)," includes two essential design phases: (1) identification of optimal location and (2) determination of optimal size. The suggested approach offers a viable solution to the challenges encountered by conventional optimization techniques and delivers a more comprehensive and robust framework for RDG design.

RDG location determination

The primary responsibility of a power distribution system is transferring power from sources to loads with maintaining voltage levels within an acceptable range and keeping power losses as low as possible. Hence the RDG location problem is to find RDG

installation locations so that the voltage levels are maintained and power losses are decreased effectively. When a RDG is installed at kth bus, it may raise a naive behavioral assumption that the load at kth bus may receive a sufficient power from the newly installed RDG, and is hidden from the rest of the power distribution system. It motivates us to observe the system behavior after disconnecting the load from kth bus for evaluating the effect of installing a RDG at kth bus.

A vector $(c_1, c_2, ..., c_N)$, which $c_k = 0$ means that the load of kth bus is disconnected and $c_k = 1$ means otherwise, is introduced. Note that the number of 0s is no larger than N_{RDG} which is the maximum number of RDGs to be installed. The vector is called the "location vector" hereinafter. Now let $\mathcal{C}$ be the set of all possible location vectors, and the best location(s) of RDG installation ($\mathcal{X}$) is determined by the location vector which maximizes a given objective function f_o over the set $\mathcal{C}$.

$$(c_1^*, c_2^*, \cdots, c_N^*) = \underset{(c_1,c_2,...,c_N)\in\mathcal{C}}{\arg\max} \{f_o((c_1, c_2, ..., c_N), lf, \mathrm{RCR})\} \tag{4.15}$$

and

$$\mathcal{X} = \{k | c_k^* = 0\} \tag{4.16}$$

(4.15) should be solved with being subjected to the following constraints.

Constraints

1. Voltage constraint

The minimum and the maximum voltage constraints of each bus are expressed as follows.

$$V^{min} \leq V_k \leq V^{max}, \quad k \in \mathcal{N} \tag{4.17}$$

where V^{min} and V^{max} are taken as 0.95 and 1.05 p.u respectively as given in Refs [26,30].

2. Voltage collapse constraint

The voltage magnitude at each bus must be greater than its voltage stability limit (V_k^{SNB}), since the violation of the constraint results in voltage collapse and system blackout. This constraint is expressed as follows.

$$V_k^{SNB} < V_k, \quad k \in \mathcal{N} \tag{4.18}$$

3. Feasibility constraint

From the voltage equation of (4.7), V_k^2 can be expressed,

$$V_k^2 = \frac{\psi_k^2 + 2\alpha_k \pm \sqrt{(\psi_k^2 + 2\alpha_k - 2V_k^2)^2}}{2} \tag{4.19}$$

Thus, V_k is a feasible solution only if the following equation is satisfied,

$$\psi_k^2 + 2\alpha_k \pm \sqrt{(\psi_k^2 + 2\alpha_k - 2V_k^2)^2} \geq 0 \tag{4.20}$$

$$V_k^2 - \psi_k^2 - 2\alpha_k \leq 0, \quad k \in \mathcal{N} \tag{4.21}$$

Further, the algorithm of the RDGs optimal location is given as Algorithm 1.

Algorithm 1 Optimal location for RDGs

Input:
f_o – a given objective function to be maximized
N^{RDG} – number of RDGs
lf – a peak load factor
RCR – a common RCR for all RDGs
Data: a power distribution system
Initialize:
$X \leftarrow \{\}$,
$\mathcal{C} \leftarrow$ 0-1 vectors of length $N-1$, where the number of zeros is no larger than N^{RDG}
(0) $f_o^{max} \leftarrow -\infty$
forall $t = (c_2, \ldots, c_N) \in \mathcal{C}$ **do**
  (1) Recall the original system
  forall $c_i = 0$ **do**
    (2) Disconnect the i-th bus(s)
  end
  (3) Run the power flow solver
  (4) Determine f_o^{max} with lf and RCR

  (5) **if** $f_o^{max} < f_o$ **then**
    $f_o^{max} \leftarrow f_o$
    $X \leftarrow \{i | c_i = 0, i \in \{2, 3, \ldots, N\}\}$
  end

end
Output: X – a set of bus number(s) of integrating RDG(s) for given lf and RCR

RDG size determination

Once the optimal locations of the buses for RDGs are identified using Algorithm 1, the subsequent step involves determining the optimal sizes of the RDGs. This optimization process for determining the RDG sizes involves minimizing the power losses (P_{loss}) that are associated with the RDGs. The power loss can be calculated using Equation (2.3) and is expressed as follows.

$$\min_{\{P_k^{RDG} \in \mathbb{R}, k \in X\}} P_{loss}(P_k^{RDG}, Q_k^{RDG}) \tag{4.22}$$

The determination of the optimal sizes of RDGs after identifying their optimal locations using Algorithm 2 is a critical step in the RDG design process, as it significantly impacts the overall performance and reliability of the power system.

Algorithm 2 Optimal size of RDGs

Input:
X – $\{k_1, k_2, ..., k_{N^{RDG}}\}$ location(s) of RDG(s),
RCR – a common RCR for all RDGs,
P^t – the limitation of RDGs' generating capacity design, Equation (4.23),
N_s– number of samples
Data: A distribution system
Initialize:
$P_k^{RDG} \leftarrow 0$ for $k \in X$
$\mathcal{P}^{tmp} \leftarrow \{0, P^t \cdot (\frac{1}{N_s}), P^t \cdot (\frac{2}{N_s}), ..., P^t \cdot (\frac{N_s}{N_s})\}$
$P_{loss}^{min} \leftarrow \infty$
forall $(P_{k_1}^{tmp}, P_{k_2}^{tmp}, ..., P_{k_{N^{RDG}}}^{tmp}) \in (\mathcal{P}^{tmp})^{N^{RDG}}$ **do**
(0) Recall the original system
(1) Set $Q_k^{tmp} = -P_k^{tmp} \times RCR$ for $k \in X$
(2) Integrate RDG(s) with the sizes of active power P_k^{tmp} and reactive power Q_k^{tmp} to the kth bus of the system for all $k \in X$
(3) Run the power flow solver and compute total power loss P_{loss}^{tmp} using Equation 4.22
(4) Check the conditions Equations (4.17) and (4.18) and if fails, then skip (5)
(5) P_{loss}^{tmp} is compared with P_{loss}^{min}, and if P_{loss}^{tmp} is smaller than P_{loss}^{min}, then the temporary best size and P_{loss}^{min} are updated as;
$P_k^{RDG} \leftarrow P_k^{tmp}$ for $k \in X$
$P_{loss}^{min} \leftarrow P_{loss}^{tmp}$
end
Output: P_k^{RDG} for $k \in X$

The minimization is given in Equation (4.22) should be solved with being subjected to the following inequality and equality constraints.

The total active power produced by RDGs should be no larger than the system's total active power demand because the violation of this constraint results in a reverse power flow in the system. This constraint is expressed as follows.

$$0 \leq \sum_{k \in \mathcal{X}} P_k^{RE} \leq \sum_{k=1}^{N} P_k \tag{4.23}$$

After finding the locations $\mathcal{X} = \{G_1, \cdots, G_{|\mathcal{X}|}\}$ of RDGs, the optimal sizes of RDGs are determined so as to minimize the power losses ($P_{loss}^{\mathcal{X}}$), which can be calculated using (2.3).

$$(P_{G_1}^{RE}, \ldots, P_{G_{|\mathcal{X}|}}^{RE}) = \underset{(x_{G_1}, \ldots, x_{G_{|\mathcal{X}|}}) \in \mathbb{R}^{|\mathcal{X}|}}{\arg\min} \left\{ P_{loss}^{\mathcal{X}}((x_{G_1}, \ldots, x_{G_{|\mathcal{X}|}}), \mathrm{RCR}) \right\} \tag{4.24}$$

(5.48) should be solved with being subjected to (4.17), (4.18), (4.19) and (4.23).

In summary, the proposed system design process is described using the flowchart of LDNA which is shown in Figure 4.7. First, the information of a power distribution system, i.e., load and line data, a peak load factor, a value of RCR, and the number of RDG(s) to be installed are given. Next, the optimal locations are chosen by maximizing a given objective function which is explained in the next sub-section.

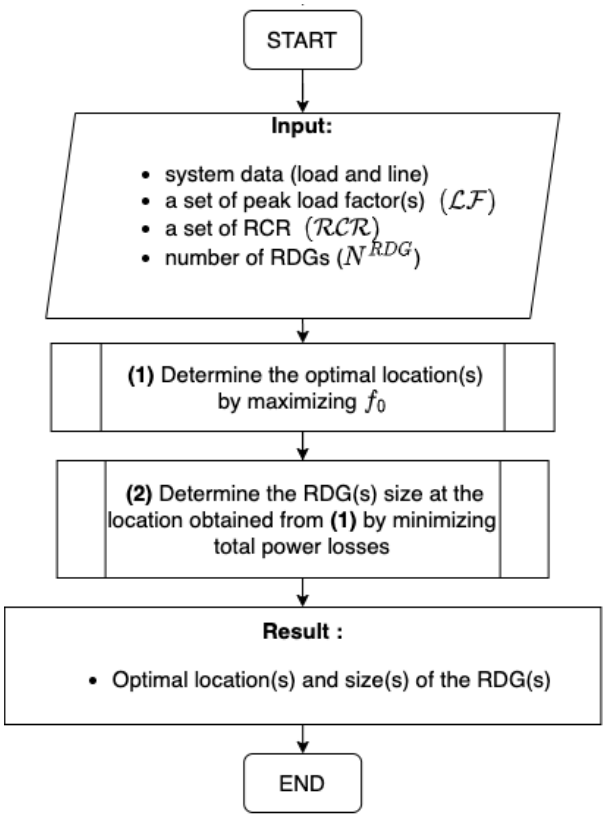

Figure 4.7: The overall procedure of Load-disabling Nodal Analysis (LDNA).

4.7 Voltage Stability and Security System Indicator

Based on the previous findings, it has been determined that the potential for voltage collapse of each bus is influenced by the amount of available reactive support, Q_C. The proposed Γ formulation can be used to estimate Q_C, and the minimum value of Γ can be used to identify the bus with the highest risk of voltage collapse. As a result, the proposed objective function is named Reactive Power Compensation Support Margin for Voltage Stability Improvement (QSVS), which is subject to the condition of $V_k > V_k^{SNB}$.

$$\mathrm{QSVS}_k = \min_{\substack{V^{min} \le V_k \le V^{max}, \\ V_k^{SNB} < V_k}} \{\Gamma(V_k)\} \tag{4.25}$$

The value of QSVS_k at the kth bus represents the limit of voltage stability in relation to voltage collapse. A value of $\mathrm{QSVS}_k > 0$ indicates that there is no risk of voltage collapse, while $\mathrm{QSVS}_k = 0$ indicates an imminent voltage collapse.

In order to estimate the voltage stability limit of the overall system, the objective is to find the minimum value of QSVS_k over all buses. This value represents the highest possibility of voltage collapse, indicating the weakest bus in the system.

$$\mathrm{QSVS} = \min\{\mathrm{QSVS}_2, \mathrm{QSVS}_3, \ldots, \mathrm{QSVS}_N\} \tag{4.26}$$

To ensure stable operation of a power system, the value of the QSVS should be greater than 0. The higher the value of QSVS, the more stable and safe the system will be from

voltage collapse. Conversely, if the value of QSVS is equal to 0, it indicates that voltage collapse will occur, which should be avoided for safety in operating the system.

4.8 LDNA-QSVS: The Methodology for Optimal Location and Size of RDGs

Since power consumption at each bus affects the voltage stability limit and the risk of voltage collapse differently, there is a bus that poses the highest risk of voltage collapse. The bus with the highest risk of voltage collapse needs to be mitigated by additional power injection. Therefore, when integrating RDGs, it is crucial to identify the bus with the highest risk. To achieve this goal, the load transfer approach is adopted, which involves disconnecting loads from certain buses in the system and transferring them to other buses. The vector $(c_2, c_3, \cdots, c_N)$ is used to specify the buses with disconnected loads, where $c_k = 0$ indicates that the load of the k-th bus is disconnected, and $c_k = 1$ indicates otherwise. In addition, the peak load factor (lf) and the reactive power compensation ratio (RCR) are considered as parameters, with the voltage stability index QSVS being a function of these parameters. Finally, the optimal locations of RDGs by maximizing $\text{QSVS}((c_2, c_3, \cdots, c_N), lf, \text{RCR})$ over all possible vectors $(c_2, c_3, \cdots, c_N)$ are obtained.

4.8.1 Optimal location determination

LDNA that uses the QSVS objective function is called Load-Disabling Nodal Analysis for Reactive Power Compensation Support Margin for Voltage Stability Improvement (LDNA-QSVS). The QSVS objective function has been formulated with the aim of maximizing the reactive power support margin of the system, which in turn, enhances the voltage stability of the power system. Through the maximization of the QSVS function, the optimal location for RDGs can be determined. It is important to note that the QSVS objective function is a key element of the LDNA approach utilized for locating RDGs. Its significance lies in the improvement of the stability and efficiency of power systems. The formulation of the QSVS objective function can be expressed as follows.

$$\underset{(c_1,c_2,\cdots,c_N)\in\mathcal{C}}{\arg\max} \{\text{QSVS}((c_1, c_2, \cdots, c_N), lf, RCR)\} \tag{4.27}$$

The optimization problem given in (4.27) should be solved with being subjected to (4.17), (4.18) and (4.21).

4.8.2 Optimal size determination

Once the optimal location of RDGs is determined using the LDNA-QSVS approach, the next step is to determine the appropriate size of the RDGs. To accomplish this, the total power loss of the system is taken into consideration. By considering the total power loss, the size of the RDGs can be optimized to minimize the power losses and improve the overall efficiency of the system. This step is crucial in ensuring that the RDGs are not only optimally located but are also appropriately sized for the given system. Therefore, determining the size of the RDGs after the optimal location is found using LDNA-QSVS is a critical aspect of the design process that significantly impacts the overall performance and efficiency of the power system.

After finding the locations $\mathcal{X} = \{G_1, \cdots, G_{|\mathcal{X}|}\}$ of RDGs, the optimal sizes of RDGs are determined so as to minimize the power losses ($P_{loss}^{\mathcal{X}}$), which can be calculated using (2.3).

$$(P_{G_1}^{RE}, \ldots, P_{G_{|\mathcal{X}|}}^{RE}) = \underset{(x_{G_1}, \ldots, x_{G_{|\mathcal{X}|}}) \in \mathbb{R}^{|\mathcal{X}|}}{\arg\min} \left\{ P_{loss}^{\mathcal{X}}((x_{G_1}, \ldots, x_{G_{|\mathcal{X}|}}), \mathrm{RCR}) \right\} \tag{4.28}$$

(5.48) should be solved with being subjected to (4.17), (4.18), (4.19) and (4.23).

4.9 LDNA-QSVS: Simulations

The proposed methodology has been implemented utilizing the Python programming language and a library called PYPSA [36]. A series of simulations were conducted to evaluate the methodology, which comprised of two simulation scenarios. In Simulation 1, the optimal location and size of one and two RDGs were determined without reactive compensation. In Simulation 2, a reactive power compensation test was conducted to further validate the methodology. This approach provided a rigorous method for testing the effectiveness and reliability of the proposed methodology.

In this study, the proposed methodology was applied to the IEEE33-bus test distribution system, which is illustrated in Figure 4.4. The complete system data at the peak load demand were obtained from [37], and the system parameters are listed in Tables B.3 and B.4. The power supply for this system originates from a single substation with a total peak load of 3.715 MW and 2.30 MVAr. The total power losses at peak demand without RDGs integration were found to be 212.95 kW. In accordance with the IEEE-standard [38], the lower and upper voltage limits, V^{min} and V^{max}, at the kth bus were set to 0.95 pu and 1.05 pu, respectively. Additionally, the power generating limits of RDGs were set to be equal to the total power demand. The use of this test system allowed for the rigorous evaluation of the proposed methodology in a realistic and challenging scenario.

4.9.1 Simulation 1: Optimal location and size of RDGs

Location and size of 1 RDG

In order to determine the optimal location for a single RDG installation, Algorithm 1 was employed, and the results are illustrated in Figure 4.8. This figure shows the variation of QSVS for each bus and for different peak load factors. The radius of the figure represents the value of QSVS, while the sector represents the individual bus from which the load is disconnected. Based on the analysis of the maximum increment of QSVS for peak load factors of 80%, 100%, and 120%, bus number 15 was identified as the most vulnerable bus for voltage collapse and was subsequently selected as the optimal location for a single RDG installation. The maximum increment of QSVS achieved by disconnecting the load from bus 15 is presented in Table 4.4. These results demonstrate the effectiveness of the proposed methodology in identifying the optimal location for a single RDG installation, which can significantly enhance the stability and efficiency of power systems.

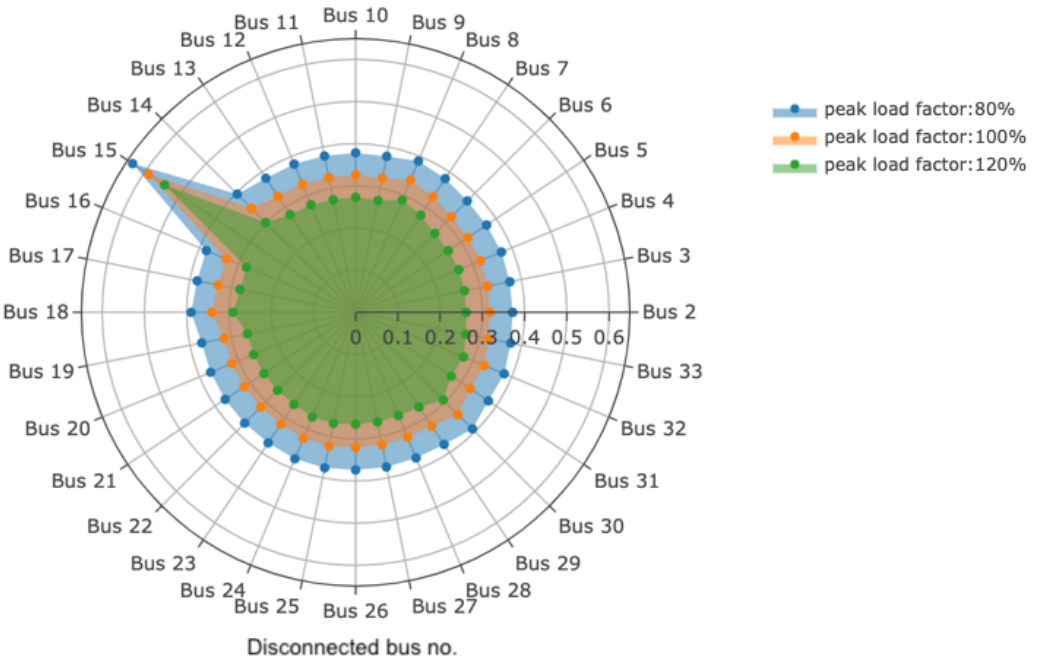

Figure 4.8: Variation of QSVS for load removal from each bus and for each peak load factor on IEEE33-bus test distribution system

Table 4.4: The candidate location of a single RDG installation for each peak load factor of EEE33-bus test distribution system using Algorithm 1

Peak load factor	The disconnected bus	Maximum increment of QSVS (%)
80%	15	70.98%
100%	15	85.59%
120%	15	108.31%

Algorithm 2 was employed to determine the optimal size of the RDG located at bus 15. The optimization process was based on minimizing power losses, and the results are presented in Figure 4.9 and Table 4.5. The optimal size was determined to be 1040.20 kW, and as a result, the power losses were reduced to 134.71 kW. This corresponds to a loss reduction of 0.0752 per 1kW generated power of the RDG. Furthermore, to ensure that the optimized solution did not negatively affect the system's supply ability to support demand, the minimum loading margin was also evaluated. The proposed methodology was compared with several other methodologies [11, 13, 18, 26, 27, 29, 31, 39], and the results are presented in Table 4.6. The comparison showed that the proposed methodology achieved the best power loss reduction per 1 kW generated power of the single RDG with improved voltage stability. These findings demonstrate the effectiveness and reliability of the proposed methodology for optimizing the size and location of RDGs in power systems.

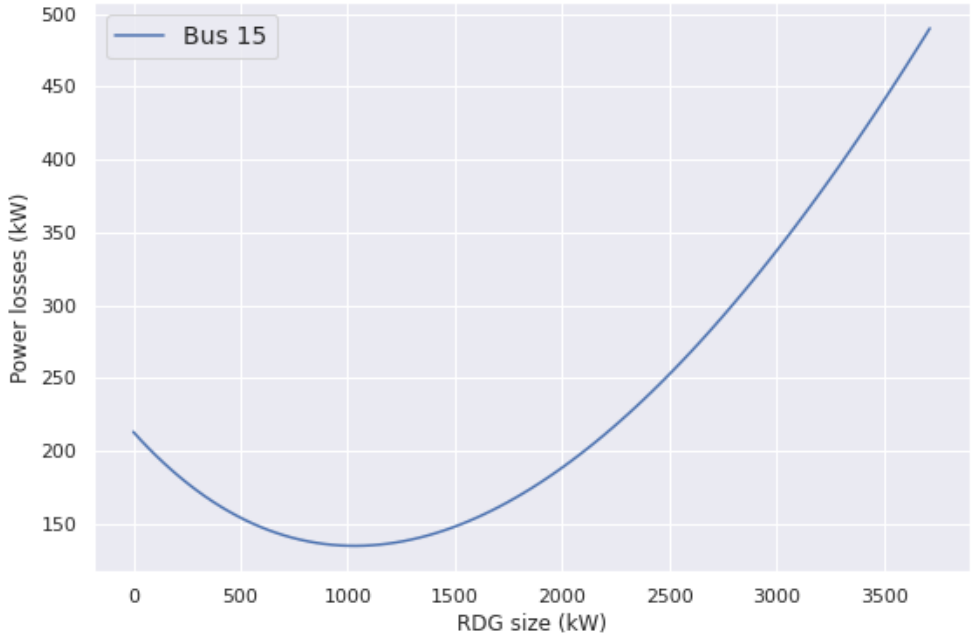

Figure 4.9: Variation of power losses with a single RDG for the IEEE33-bus test distribution system

Table 4.5: Results for installing a single RDG on IEEE33-bus test distribution systems

Optimal location (Bus no.)	Optimal size (kW)	RCR	Power losses (kW)	
			without	with 1 RDG
15	1040.20	0	212.95	134.71

Table 4.6: Comparison results of optimal locations and sizes for installing one RDG of IEEE33-bus distribution test system (↑:improvement of voltage stability; ↓ degradation of voltage stability; red. : power loss reduction)

Technique	RDG location	RDG size	losses		VS
	(Bus no.)	(kW)	(kW)	LRE	
Without	-	-	212.95	-	0.0698
GA [26]	6	2580	112.68	0.0389	0.0728 ↓
BSOA [29]	8	1857.50	119.81	0.0501	0.0683 ↑
PSO [27]	6	3150	116.89	0.0305	0.0752 ↓
Analytical [11, 13]	6	2490	112.83	0.0402	0.0725 ↓
ALOA [18]	6	2450	112.97	0.0408	0.0724 ↓
WOA [31]	30	1542.67	126.92	0.0558	0.0655 ↑
MLPSO [39]	6	2420	113.10	0.0413	0.0723 ↓
LDNA-QSVS	**15**	**1040.20**	**134.71**	**0.0752**	**0.0691** ↑

VS: Voltage stability evaluated with the maximum of L-index

Locations and sizes of 2 RDGs

In order to determine the optimal locations for two RDG installations, Algorithm 1 was employed, and the results are presented in Figure 4.10. This figure illustrates the variation of QSVS for load removal from pairs of buses for different peak load factors. The colors in the figure represent the values of QSVS. Based on the analysis of the maximum increment of QSVS for peak load factors of 80%, 100%, and 120%, buses 15th and 17th were identified as the most vulnerable buses for voltage collapse and were subsequently selected as the optimal locations for two RDG installations. This approach demonstrates the effectiveness of the proposed methodology in identifying the optimal locations for multiple RDG installations, which can significantly enhance the stability and efficiency of power systems.

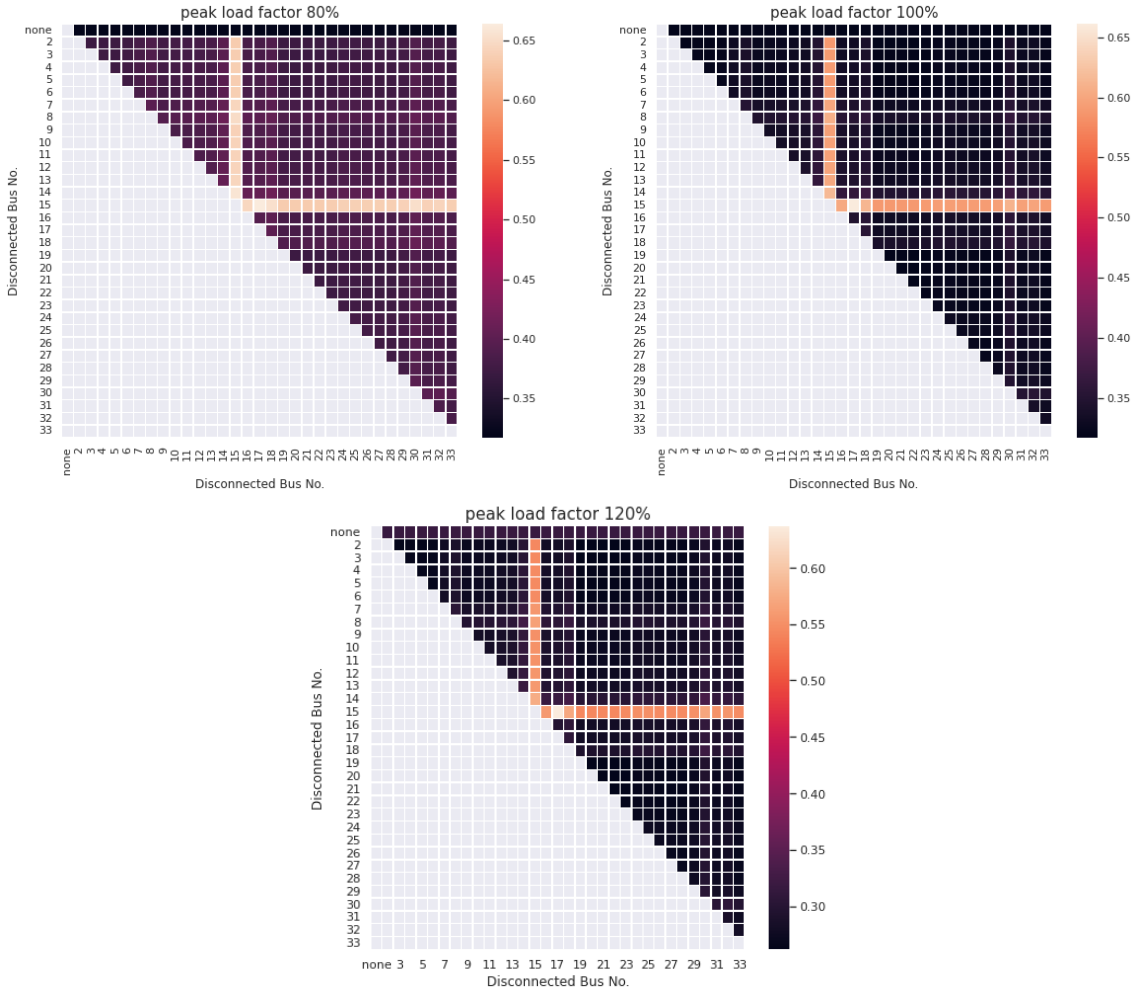

Figure 4.10: Variation of QSVS at each removal loads and for each peak load factors on IEEE33-bus test distribution system

Table 4.7: The candidate locations of two RDGs installation for each peak load factor of IEEE33-bus test distribution system using Algorithm 1

Peak load factor	The disconnected bus	Maximum increment of QSVS
80%	15, 17	109.22%
100%	15, 17	108.31%
120%	15, 17	100.71%

Algorithm 2 was employed to determine the optimal sizes of the two RDGs located at buses 15 and 17. The optimization process was based on minimizing power losses, and the results are presented in Figure 4.11 and Table 4.8. The sizes of the RDGs were determined to be 866.83 kW and 123.83 kW for buses 15 and 17, respectively. As a result, the power losses were reduced from 212.95 kW to 134.42 kW, which corresponds to a loss reduction of 0.0793 per 1kW generated power of the two RDGs. The proposed methodology was compared with several other methodologies [13,18,26,27,29,39], and the results are presented in Table 4.9. The comparison showed that the proposed methodology achieved the best power loss reduction per 1 kW generated power of the two RDGs with improved voltage stability. These findings demonstrate the effectiveness and reliability of the proposed methodology for optimizing the size and location of multiple RDGs in power systems.

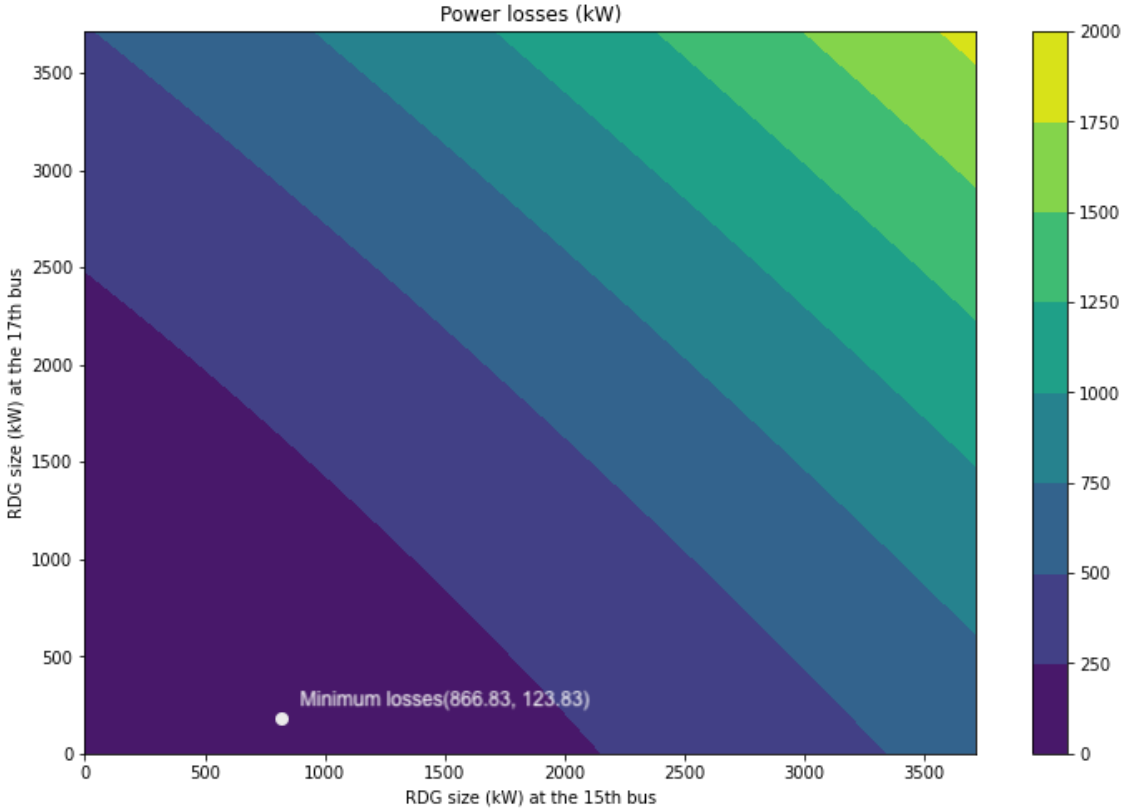

Figure 4.11: Variation of power losses with two RDGs for the IEEE33-bus test distribution system

Table 4.8: Result for installing two RDGs of IEEE33-bus distribution test system

Optimal location (Bus no.)	Optimal size (kW)	RCR	losses (kW)	
			without	with 2 RDGs
15, 17	866.83, 123.83	0	212.95	134.42

Table 4.9: Comparison results of optimal locations and sizes for installing two RDGs of IEEE 33-bus distribution test system (↑:improvement of voltage stability; ↓ degradation of voltage stability; red. power loss reduction)

Technique	RDG location	RDG size	losses		VS
	(Bus no.)	(kW)	(kW)	LRE	
-	without	-	212.95	-	0.06981
GA [26]	13	837.5	88.00	0.0610	0.0687↑
	29	1212.2			
BOSA [29]	13	880	90.05	0.0681	0.0676↑
	31	924			
PSO [27,39]	11	2420	171.53	0.0123	0.0733↓
	31	960			
ALOA [18]	13	850	87.80	0.0613	0.0655↑
	30	1191.1			
MLPSO [39]	13	820	87.76	0.0635	0.0654↑
	30	1150			
LDNA-QSVS	**15**	**866.83**	**134.42**	**0.0793**	**0.0681↑**
	17	**123.83**			

VS: Voltage stability evaluated with the maximum of L-index

4.9.2 Simulation 2: Reactive power compensation test

In order to investigate the hypothetical effect of uncontrollable reactive power compensation of RDGs on voltage stability degradation, the RCR was introduced with different sample values. Specifically, for DP-RDGs, RCR was set to 0, while for NDP-RDGs, RCR was set to ±0.25 and ±0.5. The maximum L-index was then compared for different RDG installation configurations with different RCR values. The results of the comparison are presented in Table 4.10 and Figure 4.12 for the case of one RDG installation, and in Table 4.11 and Figure 4.13 for the case of two RDGs installation.

These results illustrate the importance of considering the reactive power compensation of RDGs in the optimization process, as it can have a significant impact on the voltage stability of power systems. The proposed methodology provides a comprehensive approach for optimizing the location, size, and reactive power compensation of RDGs, which can lead to improved efficiency and stability of power systems.

Table 4.10: Result for installing one RDG of IEEE33-bus distribution test system with the different reactive compensation (↑:improvement of voltage stability; ↓: degradation of voltage stability)

Technique	RDG location	RDG size	VS				
	(Bus no.)	(kW)	RCR = -0.5	RCR = -0.25	RCR = 0.0	RCR = 0.25	RCR = 0.5
Without	-	-			0.0698		
GA [26]	6	2580	0.0852↓	0.0784↓	0.0728↓	0.0689↑	0.0666↑
BSOA [29]	8	1857.5	0.0775↓	0.0724↓	0.0683↑	0.0656↑	0.0642↑
PSO [27]	6	3150	0.0822 ↓	0.0823↓	0.0752 ↓	0.0698↓	0.0663↑
Analytical [11, 13]	6	2490	0.0861↓	0.0784↓	0.0725 ↓	0.0680↑	0.0655↑
ALOA [18]	6	2450	0.0840↓	0.0776↓	0.0724↓	0.0687↑	0.0667↑
WOA [31]	30	1542.67	0.0746↓	0.0697↑	0.0655↑	0.0623↑	0.0601↑
MLPSO [39]	6	2420	0.0838↓	0.0774↓	0.0723 ↓	0.0687↑	0.0667↑
LDNA-QSVS	**15**	**1040.20**	**0.0727↓**	**0.0707↑**	**0.0691↑**	**0.0680↑**	**0.0673↑**

VS: Voltage stability evaluated with the maximum of L-index

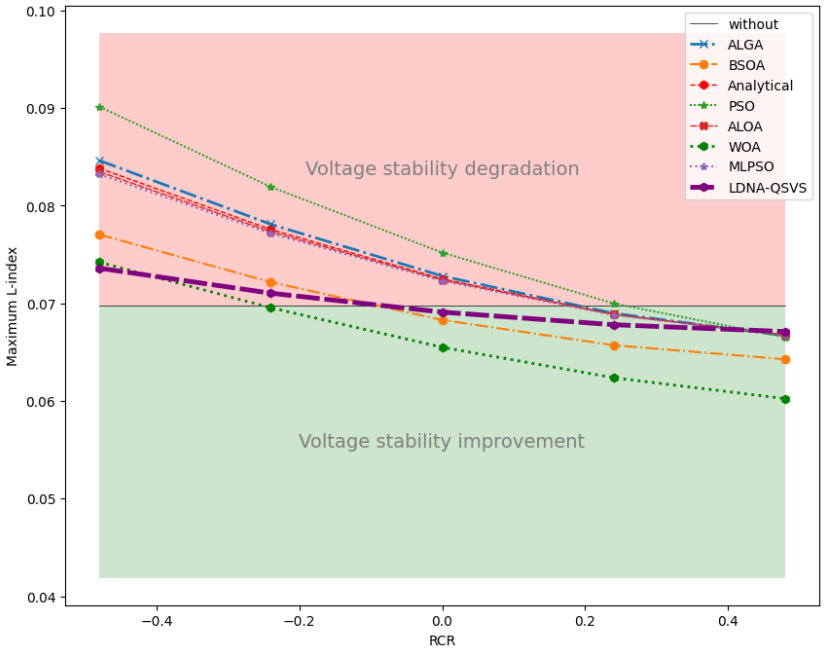

Figure 4.12: Variation of voltage stability with reactive compensations of 1 RDG using maximum L-index

After analyzing the results presented in Table 4.10 and Figure 4.12, it was observed that the proposed methodology achieved the best voltage stability compared to other methodologies. These findings demonstrate the effectiveness and reliability of the proposed methodology in optimizing the location, size, and reactive power compensation of RDGs in power systems. The comprehensive approach provided by the proposed methodology can contribute to the improved efficiency and stability of power systems.

Table 4.11: Result for installing two RDGs of IEEE33-bus distribution test system with 3 different RCRs (↑:improvement of voltage stability; ↓: degradation of voltage stability)

Technique	RDG location	RDG size	VS				
	(Bus no.)	(kW)	RCR = -0.5	RCR = -0.25	RCR = 0.0	RCR = 0.25	RCR = 0.5
Without	-	-			0.0698		
GA [26]	13 29	837.5 1212.2	0.0792↓	0.0733↓	0.0687↑	0.0655↑	0.0637↑
BOSA [29]	13 31	880 924	0.0792↓	0.0717↓	0.0676↑	0.0649↑	0.0634↑
PSO [27, 39]	11 31	2420 960	0.0768↓	0.0818↓	0.0733↓	0.0669↑	0.0626↑
ALOA [18]	13 30	850 1191.1	0.0775↓	0.0710↓	0.0655↑	0.0613↑	0.0585↑
MLPSO [39]	13 15	820 1114.5	0.0782↓	0.0725↓	0.0680↑	0.0649↑	0.0633↑
LDNA-QSVS	**15** **17**	**866.83** **123.83**	**0.0717↓**	**0.0697↑**	**0.0681↑**	**0.0671↑**	**0.0664↑**

VS: Voltage stability evaluated with the maximum of L-index

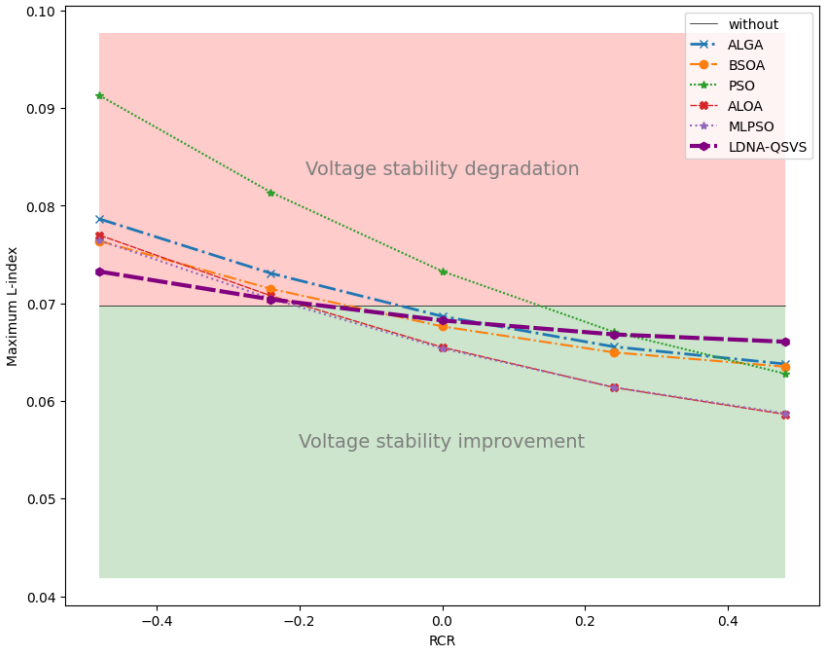

Figure 4.13: Variation of voltage stability with reactive compensations of 2 RDGs using maximum L-index

The analysis of the results presented in Table 4.11 and Figure 4.13 demonstrated that the proposed methodology provided the most robust voltage stability against uncontrollable reactive compensation when compared to other methodologies. This further confirms the effectiveness and reliability of the proposed methodology for optimizing the location, size, and reactive power compensation of RDGs in power systems, and highlights the potential for improving the efficiency and stability of power systems through the adoption of this comprehensive approach.

4.9.3 Observations

In the analysis, it was observed that maximum reduction in power losses does not necessarily result in maximum voltage stability, particularly when reactive compensations are involved. The simulations conducted in this study revealed that maximizing the increment of QSVS, which estimates the voltage collapse margin, provided the best results in improving voltage stability. It was evident from the results that the voltage stability of a distribution system is highly dependent on its voltage collapse margin. However, identifying the most vulnerable bus of voltage collapse cannot be accomplished directly using voltage stability indicators, such as the L-index.

Moreover, the results obtained from the simulations clearly indicate that reactive compensation has a significant impact on the voltage stability of distribution systems. Therefore, it is essential to account for the generators' uncontrollable reactive compensation and reactive support's ability while considering voltage stability. Additionally, the analysis demonstrated that identifying the vulnerable bus of voltage collapse in peak load situations is more apparent than during lower peak demand conditions.

4.9.4 Summary results

Based on the objectives in the optimization of location and sizing of RDGs, the performances of LRE and voltage stability are compared in the previous section. In order to make the comparison more simple and straightforward, a new metric $Nsum$ which is the sum of individually normalized metrics is introduced. With respect to LRE and VS (voltage stability evaluated with the maximum of L-Index), $Nsum$ is defined as follows.

$$Nsum = \frac{LRE - LRE^{min}}{LRE^{max} - LRE^{min}} + \frac{VS^{max} - VS}{VS^{max} - VS^{min}} \tag{4.29}$$

where

$$\begin{aligned} LRE^{max} &= \underset{\text{over all samples}}{\text{MAX}} \{LRE\} \\ LRE^{max} &= \underset{\text{over all samples}}{\text{MAX}} \{LRE\} \\ VS^{max} &= \underset{\text{over all samples}}{\text{MAX}} \{VS\} \\ VS^{min} &= \underset{\text{over all samples}}{\text{MIN}} \{VS\} \end{aligned}$$

Note that, for each normalized metric, 1 is the best performance and 0 is the worst performance. Table 4.12 shows the comparison of different methods in normalized LRE, normalized VS (the worst case with RCR=-0.5), and their sum $Nsum$.

Table 4.12 presents the normalized results for LRE and voltage stability at RCR $= -0.5$. The proposed LDNA-QSVS method achieves the top position in 1 out of 2 categories for LRE and in 2 out of 2 categories for voltage stability. Furthermore, when considering the specific normalizations of LRE and voltage stability at RCR $= -0.5$, the LDNA-QSVS model outperforms other solutions.

It is important to note that the computation times for other solutions were not provided, which limits the comparison in terms of computational efficiency. However, it can be included the computation time of LDNA-QSVS for future reference and comparison.

Table 4.12: Comparison results with respect to LRE and VS at RCR = 0 and RCR = −0.5.

Technique	Computation time (second)	norm. LRE	norm. VS RCR = -0.5	$Nsum$
Without	-	-	0.0698	
Case 1: 1RDG - IEEE33				
GA [26]	-	0.1879	0.0672	0.2551
BSOA [29]	-	0.4385	0.6418	1.0803
PSO [27]	-	0.0000	0.2910	0.2910
Analytical [11, 13]	-	0.2170	0.0000	0.2170
ALOA [18]	-	0.2304	0.1567	0.3871
WOA [31]	-	0.5660	0.8582	1.4242
MLPSO [39]	-	0.2416	0.1716	0.4133
LDNA-QSVS	**109**[a]	**1.0000**	**1.0000**	**2.0000**
Case 2: 2RDG - IEEE33				
GA [26]	-	0.7269	0.0000	0.7269
BOSA [29]	-	0.8328	0.0000	0.8328
PSO [27, 39]	-	0.0000	0.2526	0.2526
ALOA [18]	-	0.7313	0.1789	0.9103
MLPSO [39]	-	0.7642	0.1053	0.8694
LDNA-QSVS	**3267**[a]	**1.0000**	**1.0000**	**2.0000**

Computation specification [a] : Google Colab using an Intel Xeon CPU @2.20 GHz, 13 GB RAM, and Python programming language.
VS: Voltage stability evaluated with the maximum of L-index,
norm. : Normalization

The differences in results obtained from the LDNA-QSVS method and other approaches can be attributed to various factors:

1. Methodology: The LDNA-QSVS method employs a unique and innovative approach that focuses on location determination by considering load disabling to analyze and optimize power systems. This differs from traditional or conventional methods used by others. The specific techniques, algorithms, or models utilized in the LDNA-QSVS method may lead to distinct outcomes.

2. Implementation and Algorithmic Differences: Variation in the implementation strategies and algorithms used by the LDNA-QSVS method and other approaches can result in diverse results. Differences in the order of finding locations, determining sizes, or simultaneously optimizing various parameters can contribute to contrasting outcomes.

3. Optimization Objectives: The optimization objectives pursued by the LDNA-QSVS method may differ from those of other approaches. While other methods mainly focus on power loss minimization, the LDNA-QSVS methodology considers a mathematical key function that controls the power loss. This difference in objectives can lead to variations in the obtained results.

Considering these factors is crucial when comparing the results obtained from the LDNA-QSVS method with other approaches, as they provide insights into the underlying reasons for the observed differences.

4.10 Concluding Remarks

This study presents a methodology that combines the voltage-reactive power margin (Γ) and optimal RDG placement to enhance voltage stability and mitigate the risks of voltage collapse. The methodology incorporates the ability to optimize the objective function by disabling the power load, offering several advantages and benefits. By utilizing this method, significant improvements are achieved in the determination of optimal RDG placement, surpassing alternative approaches and providing superior solutions. The effectiveness of the proposed approach is demonstrated by applying different ratios of RCR to the IEEE33-bus test distribution system. In addition, a comparative analysis is conducted to evaluate the performance of the methodology in terms of reducing power losses, improving voltage stability, and maintaining robust voltage stability under varying reactive power compensation conditions.

Acknowledging the limitations of the proposed method is crucial, including the substantial computation time required, the assumption of predetermined installation quantities, the focus on steady-state conditions, and the neglect of unbalanced load and compensation of active and reactive power. Addressing these limitations in future research will contribute to improving the method's computational efficiency, flexibility in RDG placement, and consideration of dynamic system behavior, thereby advancing the development of more comprehensive and robust optimization techniques for RDGs. Additionally, one notable drawback to consider is the inherent challenge of reducing computation time in the initial stage of the proposed method, given the complex nature of observing the non-linear characteristic.

Chapter 5

Optimal Location and Sizing of Renewable Distributed Generators for Improving Robust Voltage Stability against Uncontrollable Reactive Compensation

5.1 Introduction

In this chapter, Section 4.2 presents a comprehensive review of the voltage product function and its significance in formulating the objective function for the determination of optimal RDG locations. Furthermore, various case studies will be conducted using simulations to analyze the correlation between the voltage product function, voltage stability, and power loss reduction. The goal of examining these case studies is to gain a deeper understanding of the voltage product function's impact and significance in optimizing the location of RDGs to achieve enhanced voltage stability and reduced power losses.

5.2 Exploring the Contributions of the Voltage Production Function

In this section, the derivation of the voltage production (v-p) function is revisited to formulate the key terms required for describing the subsequent contributions. For any kth bus, the conjugate complex power $\overline{S}^*$ is given as

$$\begin{aligned}\overline{S}_k^* &= \overline{V}_k^* \overline{I}_k \\ &= \overline{V}_k^* \sum_{n=1}^{N} \overline{Y}_{kn} \overline{V}_n\end{aligned}$$

which can be converted to

$$\frac{\overline{S}_k^*}{\overline{Y}_{kk}} = \left(\sum_{n=1, n\neq k}^{N} \frac{\overline{Y}_{kn} \overline{V}_n}{\overline{Y}_{kk}} \right) \cdot \overline{V}_k^* + V_k^2 \tag{5.1}$$

The voltage product (v-p) function ($\overline{\psi}_k$) at the kth bus is defined as

$$\overline{\psi}_k \triangleq \frac{\sum_{n=1,n\neq k}^{N} \overline{Y}_{kn}\overline{V}_n}{\overline{Y}_{kk}} \tag{5.2}$$

Next, Equation (5.1) is inserted into $\overline{\psi}_k$, as shown below.

$$\frac{\overline{S}_k^*}{\overline{Y}_{kk}} = \overline{\psi}_k \overline{V}_k^* + V_k^2 \tag{5.3}$$

$$= \psi_k V_k \cos(\zeta_k - \delta_k) + j\psi_k V_k \sin(\zeta_k - \delta_k) + V_k^2 \tag{5.4}$$

where ψ_k and ζ_k are the v-p magnitude and the v-p angle at the kth bus, respectively.

With the aid of a complex transformation, Equation (5.3) can be expressed in a different form.

$$\frac{\overline{S}_k^*}{\overline{Y}_{kk}V_k^2} = \frac{\overline{\psi}_k}{\overline{V}_k} + 1 \tag{5.5}$$

5.2.1 Voltage stability improvement

Voltage stability refers to the capability of maintaining the voltage level within an acceptable range for each bus under normal operating conditions and after any contingency events [33]. However, incorporating the nonlinear relationship between the power injection of RDGs and voltage stability, as expressed in the L-index formulation, poses challenges when addressing the problem of RDG placement and sizing. Voltage stability is influenced not only by the voltage levels and power injection at individual nodes but also by neighboring buses and various system variables. In this study, the significance of the voltage product function (Equation (5.2)) is explored in addressing the issue of voltage stability. To illustrate this, a 3-bus system, as shown in Figure 5.1, will be utilized to emphasize the relationship between the function and the enhancement of voltage stability.

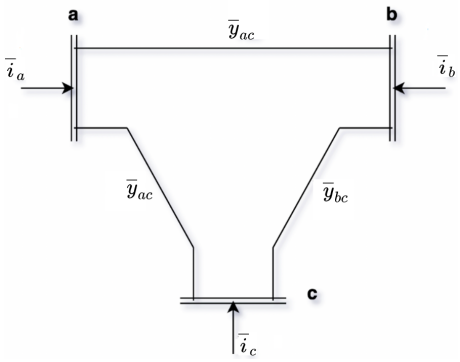

Figure 5.1: Single line diagram of the 3-bus system.

Under different choices of reference bus in the 3-bus system, three different network models can be obtained, as shown in Figure 5.1. Specifically, Case I, Case II, and Case III correspond to the selection of bus c, bus b, and bus a as the reference node, respectively.

Then, the hybrid parameters of the three cases are obtained as following equations.

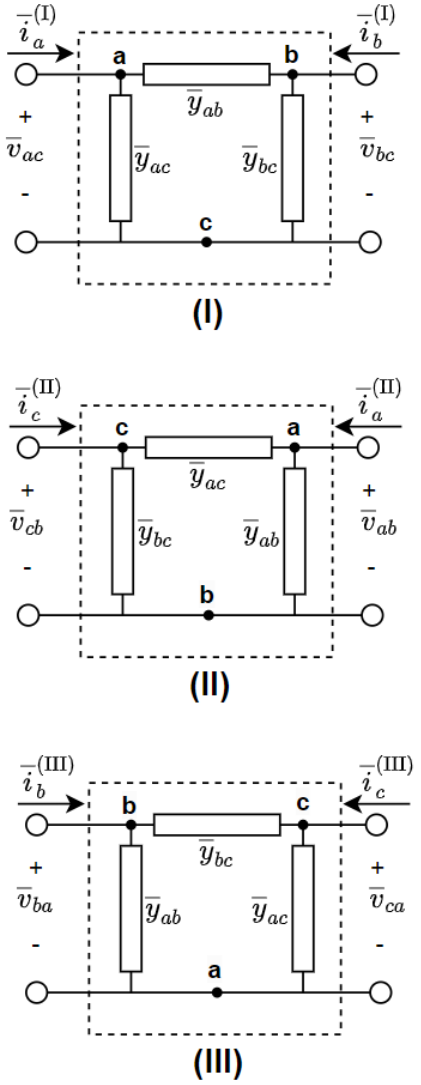

Figure 5.2: Three different cases regarding referent buses

Case (I)

$$\bar{v}_{ac} = h_{11}^{(I)} \cdot \bar{i}_a^{(I)} + h_{12}^{(I)} \cdot \bar{v}_{bc} \tag{5.6}$$

$$\bar{i}_b^{(I)} = h_{21}^{(I)} \cdot \bar{i}_a^{(I)} + h_{22}^{(I)} \cdot \bar{v}_{bc} \tag{5.7}$$

Then, $h_{11}^{(I)}, h_{12}^{(I)}, h_{21}^{(I)}$ and $h_{22}^{(I)}$ can be computed,

$$
\begin{aligned}
h_{11}^{(\mathrm{I})} &= \left.\frac{\overline{v}_{ac}}{\overline{i}_a^{(\mathrm{I})}}\right|_{v_{bc}=0} \\
&= \frac{\overline{v}_{ac}}{v_{ac}\cdot\overline{y}_{ac}+\overline{v}_{ac}\cdot\overline{y}_{ab}} = \frac{1}{\overline{y}_{ac}+\overline{y}_{ab}} \\
h_{12}^{(\mathrm{I})} &= \left.\frac{\overline{v}_{ac}}{\overline{v}_{bc}}\right|_{i_a^{(\mathrm{I})}=0} \\
&= \frac{\overline{y}_{ab}}{\overline{y}_{ab}+\overline{y}_{ac}} \\
h_{21}^{(\mathrm{I})} &= \left.\frac{\overline{i}_b^{(\mathrm{I})}}{\overline{i}_a^{(\mathrm{I})}}\right|_{v_{bc}^{(\mathrm{I})}=0} \\
&= -\frac{\overline{y}_{ab}}{\overline{y}_{ac}+\overline{y}_{ab}} \\
h_{22}^{(\mathrm{I})} &= \left.\frac{\overline{i}_b^{(\mathrm{I})}}{\overline{v}_{bc}}\right|_{i_a^{(\mathrm{I})}=0} \\
&= \overline{y}_{bc}+(\frac{\overline{y}_{ab}\cdot\overline{y}_{bc}}{\overline{y}_{ab}+\overline{y}_{bc}})
\end{aligned}
$$

Then,the matrix of hybrid parameters of the Case (I) can be obtained,

$$
\begin{bmatrix} h_{11}^{(\mathrm{I})} & h_{12}^{(\mathrm{I})} \\ h_{21}^{(\mathrm{I})} & h_{22}^{(\mathrm{I})} \end{bmatrix} = \begin{bmatrix} \frac{1}{\overline{y}_{ab}+\overline{y}_{ac}} & \frac{\overline{y}_{ab}}{\overline{y}_{ab}+\overline{y}_{ac}} \\ -\frac{\overline{y}_{ab}}{\overline{y}_{ab}+\overline{y}_{ac}} & \overline{y}_{bc}+(\frac{\overline{y}_{ab}\cdot\overline{y}_{ac}}{\overline{y}_{ab}+\overline{y}_{ac}}) \end{bmatrix}
$$

Case (II)

$$
\overline{v}_{cb} = h_{11}^{(\mathrm{II})}\cdot\overline{i}_c^{(\mathrm{II})} + h_{12}^{(\mathrm{II})}\cdot\overline{v}_{ab} \tag{5.8}
$$

$$
\overline{i}_a^{(\mathrm{II})} = h_{21}^{(\mathrm{II})}\cdot\overline{i}_c^{(\mathrm{II})} + h_{22}^{(\mathrm{II})}\cdot\overline{v}_{ab} \tag{5.9}
$$

Then, the matrix of hybrid parameters of the Case (II) can be obtained,

$$
\begin{bmatrix} h_{11}^{(\mathrm{II})} & h_{12}^{(\mathrm{II})} \\ h_{21}^{(\mathrm{II})} & h_{22}^{(\mathrm{II})} \end{bmatrix} = \begin{bmatrix} \frac{1}{\overline{y}_{ac}+\overline{y}_{bc}} & \frac{\overline{y}_{ac}}{\overline{y}_{ac}+\overline{y}_{bc}} \\ -\frac{\overline{y}_{ac}}{\overline{y}_{ac}+\overline{y}_{bc}} & \overline{y}_{ab}+(\frac{\overline{y}_{ac}\cdot\overline{y}_{bc}}{\overline{y}_{ac}+\overline{y}_{bc}}) \end{bmatrix}
$$

Case (III)

$$
\overline{v}_{ba} = h_{11}^{(\mathrm{III})}\cdot\overline{i}_b^{(\mathrm{III})} + h_{12}^{(\mathrm{III})}\cdot\overline{v}_{ca} \tag{5.10}
$$

$$
\overline{i}_c^{(\mathrm{III})} = h_{21}^{(\mathrm{III})}\cdot\overline{i}_b^{(\mathrm{III})} + h_{22}^{(\mathrm{III})}\cdot\overline{v}_{ca} \tag{5.11}
$$

Then, the matrix of hybrid parameters of the Case (III) can be obtained,

$$
\begin{bmatrix} h_{11}^{(\mathrm{III})} & h_{12}^{(\mathrm{III})} \\ h_{21}^{(\mathrm{III})} & h_{22}^{(\mathrm{III})} \end{bmatrix} = \begin{bmatrix} \frac{1}{\overline{y}_{ab}+\overline{y}_{bc}} & \frac{\overline{y}_{bc}}{\overline{y}_{ab}+\overline{y}_{bc}} \\ -\frac{\overline{y}_{bc}}{\overline{y}_{ab}+\overline{y}_{bc}} & \overline{y}_{ac}+(\frac{\overline{y}_{bc}\cdot\overline{y}_{ab}}{\overline{y}_{ab}+\overline{y}_{bc}}) \end{bmatrix}
$$

When $h_{12}^{(\mathrm{I})}, h_{12}^{(\mathrm{II})}$, and $h_{12}^{(\mathrm{III})}$ are obtained, L-index of the three cases can be expressed,

$$L_{ac}^{(\mathrm{I})} = |1 - \frac{h_{12}^{(\mathrm{I})} \cdot \overline{v}_{bc}}{\overline{v}_{ac}}| = |1 - \frac{\left(\frac{\overline{y}_{ab}}{\overline{y}_{ab}+\overline{y}_{ac}}\right) \cdot \overline{v}_{bc}}{\overline{v}_{ac}}| \tag{5.12}$$

$$L_{cb}^{(\mathrm{II})} = |1 - \frac{h_{12}^{(\mathrm{II})} \cdot \overline{v}_{ab}}{\overline{v}_{cb}}| = |1 - \frac{\left(\frac{\overline{y}_{ac}}{\overline{y}_{ac}+\overline{y}_{bc}}\right) \cdot \overline{v}_{ab}}{\overline{v}_{cb}}| \tag{5.13}$$

$$L_{ba}^{(\mathrm{III})} = |1 - \frac{h_{12}^{(\mathrm{III})} \cdot \overline{v}_{ca}}{\overline{v}_{ba}}| = |1 - \frac{\left(\frac{\overline{y}_{bc}}{\overline{y}_{ab}+\overline{y}_{ab}}\right) \cdot \overline{v}_{ca}}{\overline{v}_{ba}}| \tag{5.14}$$

On the other hand, by applying Equation (5.2) to each case, the v-p functions $\overline{\psi}_{ac}^{(\mathrm{I})}$, $\overline{\psi}_{cb}^{(\mathrm{II})}$, and $\overline{\psi}_{ba}^{(\mathrm{III})}$ are given as follows

$$\overline{\psi}_{ac}^{(\mathrm{I})} = \left(\frac{-\overline{y}_{ab}}{\overline{y}_{ab} + \overline{y}_{ac}}\right) \cdot \overline{v}_{bc} \tag{5.15}$$

$$\overline{\psi}_{cb}^{(\mathrm{II})} = \left(\frac{-\overline{y}_{ac}}{\overline{y}_{ac} + \overline{y}_{bc}}\right) \cdot \overline{v}_{ab} \tag{5.16}$$

$$\overline{\psi}_{ba}^{(\mathrm{III})} = \left(\frac{-\overline{y}_{bc}}{\overline{y}_{ab} + \overline{y}_{bc}}\right) \cdot \overline{v}_{ca} \tag{5.17}$$

Hence, L-index and v-p function are related in the following forms.

$$L_{ac}^{(\mathrm{I})} = \left|1 + \frac{\overline{\psi}_{ac}^{(\mathrm{I})}}{\overline{v}_{ac}}\right| \tag{5.18}$$

$$L_{cb}^{(\mathrm{II})} = \left|1 + \frac{\overline{\psi}_{cb}^{(\mathrm{II})}}{\overline{v}_{cb}}\right| \tag{5.19}$$

$$L_{ba}^{(\mathrm{III})} = \left|1 + \frac{\overline{\psi}_{ba}^{(\mathrm{III})}}{\overline{v}_{ba}}\right| \tag{5.20}$$

From the above observation as well as the similarity between L-index defined with the so-called "equivalent-voltage" [1] and its variant having v-p function

Next, the relationship between the L-index and the v-p function in the general case is established. For a given system, nodes are initially divided into the set α_G, which includes generator nodes, and the set α_L, encompassing consumer nodes. Following this separation, a system equation in terms of a hybrid matrix is formulated as follows.

$$\begin{pmatrix} V^L \\ I^G \end{pmatrix} = \begin{pmatrix} Z^{LL} & F^{LG} \\ K^{GL} & Y^{GG} \end{pmatrix} \begin{pmatrix} I^L \\ V^G \end{pmatrix} \tag{5.21}$$

where V^L and I^L are vectors of voltages and currents, respectively, at consumer nodes, V^G and I^G are vectors of voltages and currents, respectively, at generator nodes, and Z^{LL}, F^{LG}, K^{GL} and Y^{GG} are submatrices of the hybrid matrix. Then, for any consumer node k, $k \in \alpha_L$, its voltage $\overline{V}_k$ is represented as follows.

$$\overline{V}_k = \sum_{n \in \alpha_L} \overline{Z}_{kn} \cdot \overline{I}_n + \sum_{n \in \alpha_G} \overline{F}_{kn} \cdot \overline{V}_n \tag{5.22}$$

By performing a multiplication of $\overline{V}_k^*$ on both sides of the equation, the result is as follows,

$$\begin{aligned} V_k^2 &= \left(\sum_{n\in\alpha_L} \overline{Z}_{kn}\cdot\overline{I}_n\right)\overline{V}_k^* + \left(\sum_{n\in\alpha_G} \overline{F}_{kn}\cdot\overline{V}_n\right)\overline{V}_k^* \\ &= \overline{Z}_{kk}\left(\sum_{\substack{n\in\alpha_L \\ n\neq k}} \frac{\overline{Z}_{kn}}{\overline{Z}_{kk}}\cdot\frac{\overline{S}_n^*}{\overline{V}_n^*}\right)\overline{V}_k^* + \overline{Z}_{kk}\cdot\overline{I}_k\cdot\overline{V}_k^* \\ &\quad -\left(-\sum_{n\in\alpha_G}\overline{F}_{kn}\cdot\overline{V}_n\right)\overline{V}_k^* \\ &= \frac{\left(\overline{S}_k^{corr}+\overline{S}_k\right)^*}{\overline{Y}_{kk}} - \overline{V}_{0k}\cdot\overline{V}_k^* \end{aligned} \tag{5.23}$$

where

$$\overline{S}_k^{corr} = \left(\sum_{\substack{n\in\alpha_L \\ n\neq k}} \frac{\overline{Z}_{kn}^*}{\overline{Z}_{kk}^*}\cdot\frac{\overline{S}_n}{\overline{V}_n}\right)\overline{V}_k \tag{5.24}$$

$$\overline{Y}_{kk} = \frac{1}{\overline{Z}_{kk}} \tag{5.25}$$

$$\overline{V}_{0k} = -\sum_{n\in\alpha_G}\overline{F}_{kn}\cdot\overline{V}_n \tag{5.26}$$

From Equation (5.23), the following equation is derived:

$$1+\frac{\overline{V}_{0k}}{\overline{V}_k} = \frac{\left(\overline{S}_k^{corr}+\overline{S}_k\right)^*}{\overline{Y}_{kk}\cdot V_k^2} \tag{5.27}$$

Finally, L-index has been defined as follows.

$$L_k = \left|1-\frac{\sum_{n\in\alpha_G}\overline{F}_{kn}\cdot\overline{V}_n}{\overline{V}_k}\right| \tag{5.28}$$

$$= \left|1+\frac{\overline{V}_{0k}}{\overline{V}_k}\right| \tag{5.29}$$

$$= \left|\frac{\left(\overline{S}_k^{corr}+\overline{S}_k\right)^*}{\overline{Y}_{kk}\cdot V_k^2}\right| \tag{5.30}$$

Recalling that a power system is a linear time-invariant circuit, let us now focus on a system excited by a single generator with a voltage of $\overline{V}_G$. Due to the linearity of the circuit, every current $\overline{I}_n$ can be represented as the product of $\overline{T}_n$, the transfer conductance from the generator to the nth bus current, and $\overline{V}_G$. Accordingly, the following is observed.

$$\overline{I}_n = \overline{T}_n\cdot\overline{V}_G = \frac{\overline{T}_n}{\overline{T}_k}\cdot\overline{T}_k\cdot\overline{V}_G = \frac{\overline{T}_n}{\overline{T}_k}\cdot\overline{I}_k \tag{5.31}$$

Consequently, $\overline{S}_k^{corr}$ can be related to $\overline{S}_k$ in the following form.

$$\begin{aligned}
\overline{S}_k^{corr} &= \left(\sum_{\substack{n \in \alpha_L \\ n \neq k}} \frac{\overline{Z}_{kn}^*}{\overline{Z}_{kk}^*} \cdot \frac{\overline{S}_n}{\overline{V}_n} \right) \overline{V}_k \\
&= \left(\sum_{\substack{n \in \alpha_L \\ n \neq k}} \frac{\overline{Z}_{kn}^*}{\overline{Z}_{kk}^*} \cdot \overline{I}_n^* \right) \overline{V}_k \\
&= \left(\sum_{\substack{n \in \alpha_L \\ n \neq k}} \frac{\overline{Z}_{kn}^*}{\overline{Z}_{kk}^*} \cdot \frac{\overline{T}_n^*}{\overline{T}_k^*} \cdot \overline{I}_k^* \right) \overline{V}_k \\
&= \left(\sum_{\substack{n \in \alpha_L \\ n \neq k}} \frac{\overline{Z}_{kn}^*}{\overline{Z}_{kk}^*} \cdot \frac{\overline{T}_n^*}{\overline{T}_k^*} \right) \overline{S}_k
\end{aligned} \tag{5.32}$$

$$\begin{aligned}
1 + \frac{\overline{V}_{0k}}{\overline{V}_k} &= \frac{\left(\overline{S}_k^{corr} + \overline{S}_k\right)^*}{\overline{Y}_{kk} \cdot V_k^2} \\
&= \frac{(W_{kn} + 1)^* \cdot \overline{S}_k^*}{\overline{Y}_{kk} \cdot V_k^2}
\end{aligned} \tag{5.33}$$

where

$$W_{kn} = \sum_{\substack{n \in \alpha_L \\ n \neq k}} \frac{\overline{Z}_{kn}^*}{\overline{Z}_{kk}^*} \cdot \frac{\overline{T}_n^*}{\overline{T}_k^*} \tag{5.34}$$

Finally,

$$\begin{aligned}
L_k &= \left| \frac{\left(\overline{S}_k^{corr} + \overline{S}_k\right)^*}{\overline{Y}_{kk} \cdot V_k^2} \right| \\
&= |W_{kn} + 1| \cdot \left| \frac{\overline{S}_k^*}{\overline{Y}_{kk} \cdot V_k^2} \right| \\
&= |W_{kn} + 1| \cdot \left| 1 + \frac{\overline{\psi}_k}{\overline{V}_k} \right|
\end{aligned} \tag{5.35}$$

As a result, it can be assumed that the following relation.

$$L_k \propto \left| 1 + \frac{\psi_k}{V_k} \right| \tag{5.36}$$

Let γ be a proportional coefficient, and using Equation (5.5), then,

$$L_k^2 = \frac{\gamma^2 S_k^2}{Y_{kk}^2 V_k^4} \tag{5.37}$$

Considering that the power load is constant and hence $\frac{\partial S_k}{\partial \psi_k} = 0$, the derivative of L_k^2 with respect to ψ_k can be given as follow.

$$2L_k \frac{\partial L_k}{\partial \psi_k} = -\frac{4\gamma^2 S_k^2}{Y_{kk}^2 V_k^5} \cdot \frac{\partial V_k}{\partial \psi_k} \tag{5.38}$$

On the other hand, using another arranged form of Equation(5.5);

$$\frac{S_k^2}{Y_{kk}^2} = V_k^4 + 2\psi_k V_k^3 \cos(\Delta_k) + \psi_k^2 V_k^2 \tag{5.39}$$

$\frac{\partial V_k}{\partial \psi_k}$ is given as the following formula.

$$\frac{\partial V_k}{\partial \psi_k} = -\frac{V_k \left(V_k \cos(\Delta_k) + \psi_k\right)}{(2V_k + \psi_k)(V_k + \psi_k)} \tag{5.40}$$

Finally, by substituting Equation (5.40) into Equation (5.38), it becomes,

$$\frac{\partial L_k}{\partial \psi_k} = \frac{2\gamma^2 S_k^2 \left(V_k \cos(\Delta_k) + \psi_k\right)}{L_k Y_{kk}^2 V_k^4 (2V_k + \psi_k)(V_k + \psi_k)} \tag{5.41}$$

From this formula, it is found that L_k decreases when ψ_k increases if the following condition holds.

$$\cos(\Delta_k) < -\frac{\psi_k}{V_k} \tag{5.42}$$

5.2.2 Power loss reduction

The power loss in a wire is influenced by the voltage difference between its two ends. Increasing the lower terminal voltage can effectively reduce the power loss. Furthermore, a higher voltage allows for the transmission of the same power with a smaller current, thereby contributing to power loss reduction. Equation (5.40) indicates that as ψ_k increases, V_k also increases, given that condition (5.42) is satisfied.

5.2.3 Normalized voltage stability Index

The previous section showcased several demonstrations that highlighted the correlation between the voltage production (v-p) function and two vital parameters of power systems: the L-index for measuring voltage stability and power loss. These relationships serve as motivation to employ the v-p function as a reliable indicator for identifying RDG locations that address both voltage stability and power loss. In terms of the L-index and power loss, maximizing the lowest v-p function value across all buses is desirable. Conversely, when considering the relationship between the v-p function and bus voltage, minimizing the gap between the maximum and minimum v-p function values across all buses becomes important as it indicates reduced voltage deviation.

Based on these observations, the magnitude of the v-p function normalized by the gap between the maximum and the minimum of v-p function value, which is denoted by λ_k, is proposed as an indicator of voltage stability and power loss for the kth bus.

$$\lambda_k = \frac{\psi_k}{\psi^{\max} - \psi^{\min}} \tag{5.43}$$

where

$$\psi^{\max} = \max\{\psi_1, \psi_2, \ldots, \psi_N\} \tag{5.44}$$

$$\psi^{\min} = \min\{\psi_1, \psi_2, \ldots, \psi_N\} \tag{5.45}$$

For assessing the voltage stability of overall system, the minimum magnitude of the normalized voltage product functions over all buses is utilized and named "Normalized Voltage Stability index (Λ)," as follows.

$$\Lambda = \min\{\lambda_1, \lambda_2 \cdots, \lambda_N\} \tag{5.46}$$

5.3 LDNA-RVS: The Methodology for Optimal Location and Size of RDGs

The proposed method LDNA-RVS is applied to IEEE33- and IEEE69-bus test distribution systems which are provided by [37] and [40]. For the IEEE33-bus system, Figure 4.4 shows the system diagram, which has a total load of 3720 kW and 2300 kVAr at a voltage level of 12.66 kV. Figure 5.3 shows the system diagram, which has a total load of 3800 kW and 2690 kVAr at 12.6 kV for the IEEE69-bus system. The information on the maximum levels of power consumption of loads is required when maximum power losses and voltage stability are evaluated. All simulations were carried out using Python programming with a library called PYPSA [36].

One RDG installation and two RDGs installation for both IEEE33- and IEEE69-bus systems are examined. After the results are obtained, the variations of voltage stability with non-reactive compensation (RCR = 0) and maximum reactive compensation (RCR = -0.48) are evaluated. Finally, a summary of the simulation results is provided with the two performance indexes, i.e., the loss reduction efficiency (LRE) and voltage stability (VS).

5.3.1 Optimal location determination

In order to improve the voltage stability after RDG installation, Normalized Voltage Stability index (Λ) is used as the objective function in LDNA along with RCR= -0.48 and lf= 100%.

$$\underset{(c_1,c_2,\cdots,c_N)\in\mathcal{C}}{\arg\max} \{\Lambda((c_1, c_2, \cdots, c_N), lf, RCR)\} \tag{5.47}$$

The optimization problem given in Equation (5.47) should be solved with being subjected to Equations (4.17), (4.18) and (4.21).

Locating of RDGs using the Normalized Voltage Stability index as the objective function to be maximized is called Load-Disabling Nodal Analysis for Robust Voltage Stability (LDNA-RVS).

5.3.2 Optimal size determination

After finding the locations $\mathcal{X} = \{G_1, \cdots, G_{|\mathcal{X}|}\}$ of RDGs, the optimal sizes of RDGs are determined so as to minimize the power losses ($P_{loss}^{\mathcal{X}}$), which can be calculated using Equation (2.3) along with RCR = -0.48.

$$(P_{G_1}^{RE}, \ldots, P_{G_{|\mathcal{X}|}}^{RE}) = \underset{(x_{G_1},\ldots,x_{G_{|\mathcal{X}|}})\in\mathbb{R}^{|\mathcal{X}|}}{\arg\min} \left\{ P_{loss}^{\mathcal{X}}((x_{G_1}, \ldots, x_{G_{|\mathcal{X}|}})) \right\} \tag{5.48}$$

Equation (5.48) should be solved with being subjected to Equations (4.17), (4.18), (4.19) and (4.23).

5.4 LDNA-RVS: Simulations

The proposed method LDNA-RVS is applied to IEEE33- and IEEE69-bus test distribution systems which are provided by [37] and [40]. For the IEEE33-bus system, Figure 4.4 shows the system diagram, which has a total load of 3720 kW and 2300 kVAr at a voltage level of 12.66 kV. Figure 5.3 shows the system diagram, which has a total load of 3800 kW and 2690 kVAr at 12.6 kV for the IEEE69-bus system. The information on the maximum levels of power consumption of loads is required when maximum power losses and voltage stability are evaluated. All simulations were carried out using Python programming with a library called PYPSA [36].

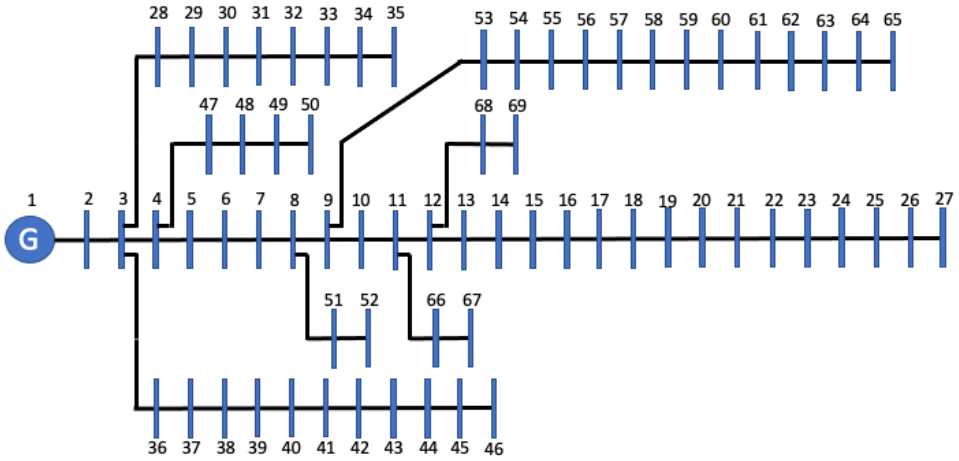

Figure 5.3: Single line diagram of the 69-bus test distribution system

One RDG installation and two RDGs installation for both IEEE33- and IEEE69-bus systems are examined. After the results are obtained, the variations of voltage stability with non-reactive compensation (RCR = 0) and maximum reactive compensation (RCR = −0.48) are evaluated. Finally, a summary of the simulation results is provided with the two performance indexes, i.e., the loss reduction efficiency (LRE) and voltage stability (VS).

5.4.1 Simulation 1: Optimal locations and sizing

One RDG installation

For one RDG installation, the optimal location and size are obtained via LDNA-RVS. Figure 5.4 and 5.5 show the variation of Λ for different choices of load disconnecting nodes with a peak load factors 80%, 100%, and 120%. From Figure5.4, it can be found

that disconnecting the 14th bus achieves the maximum Λ, and hence there is the best location for one RDG installation for IEEE33-bus system. Similarly, Figure5.5 indicates that the 61st bus is the best location for one RDG installation in IEEE69-bus system.

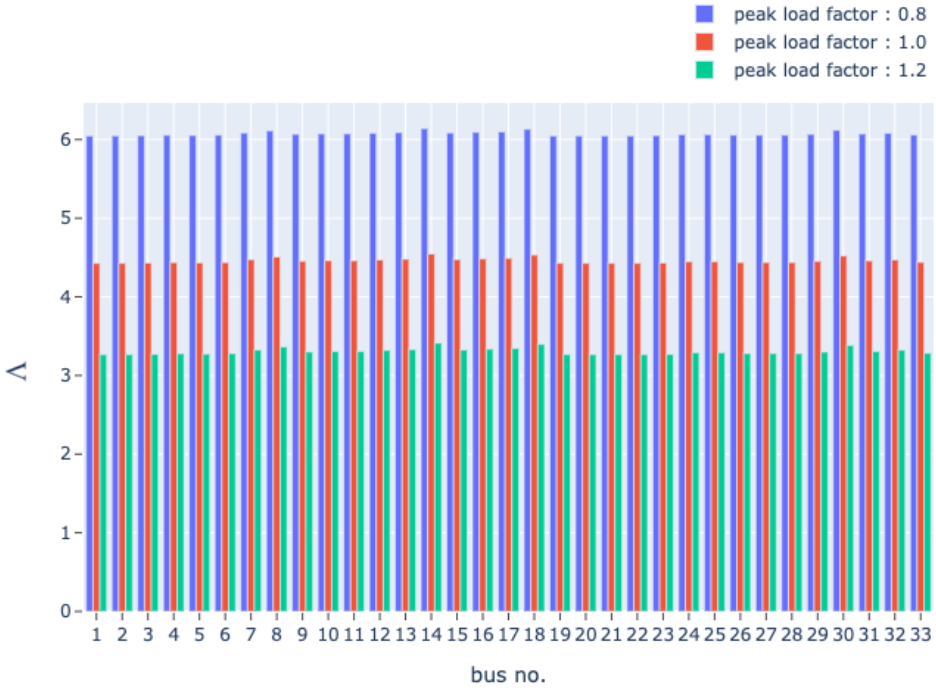

Figure 5.4: Variation of Λ at each removal loads and for each peak load factors on IEEE33-bus test distribution system.

By considering the system power losses minimization, the size of RDG installing at the 14th bus is determined at 1151.65kW for IEEE33-bus system as Figure 5.6 shows, and the one at the 61st bus for IEEE69-bus system is fixed at 1023.81kW as Figure 5.7 shows. As a result, in IEEE33-bus system, the system power loss is decreased from 212.95kW to 178.24kW, which corresponds to power loss reduction efficiency LRE =0.1082. Similarly, for the IEEE69-bus system, the system power loss is decreased from 244.16kW to 183.35kW, which corresponds to LRE = 0.1241.

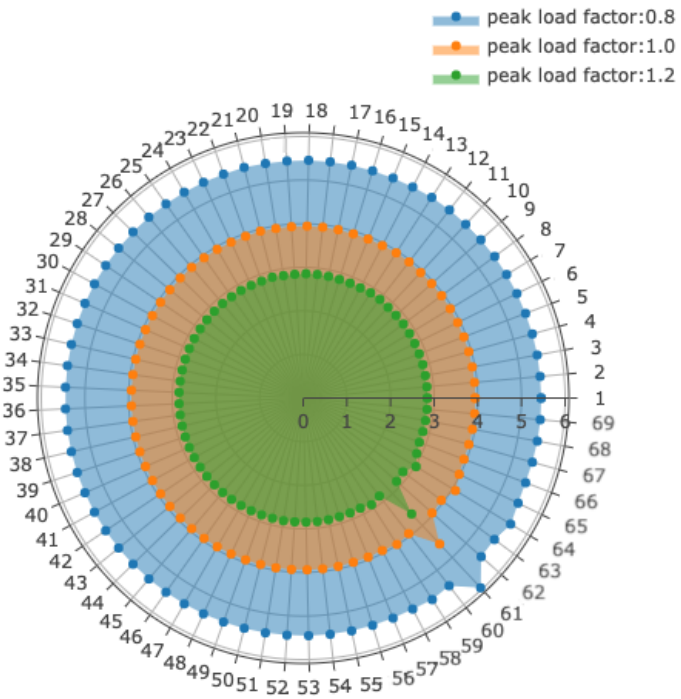

Figure 5.5: Variation of Λ at each removal loads and for each peak load factors on IEEE69-bus test distribution system.

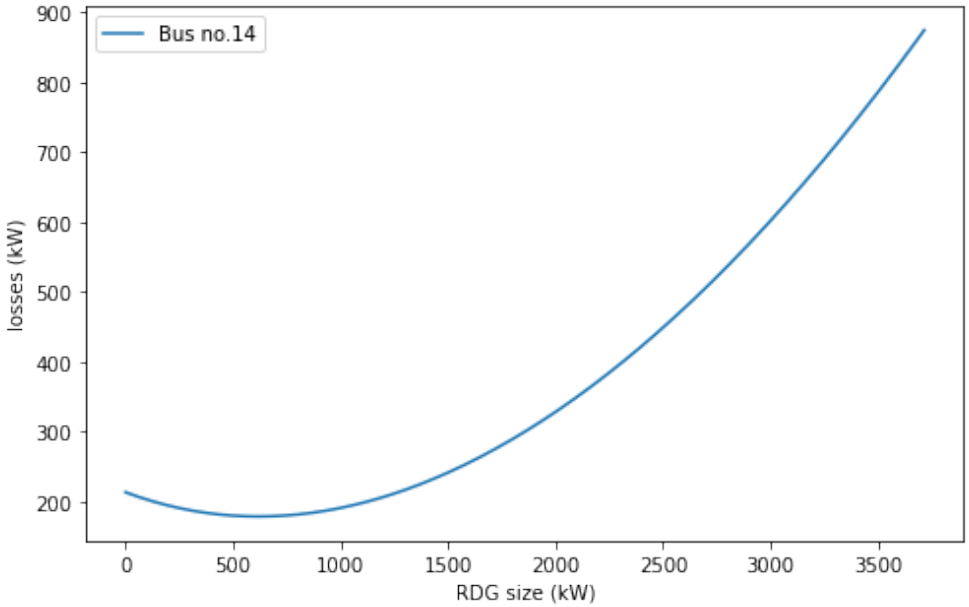

Figure 5.6: Variation of total power losses with a single RDG for the IEEE33-bus test distribution system.

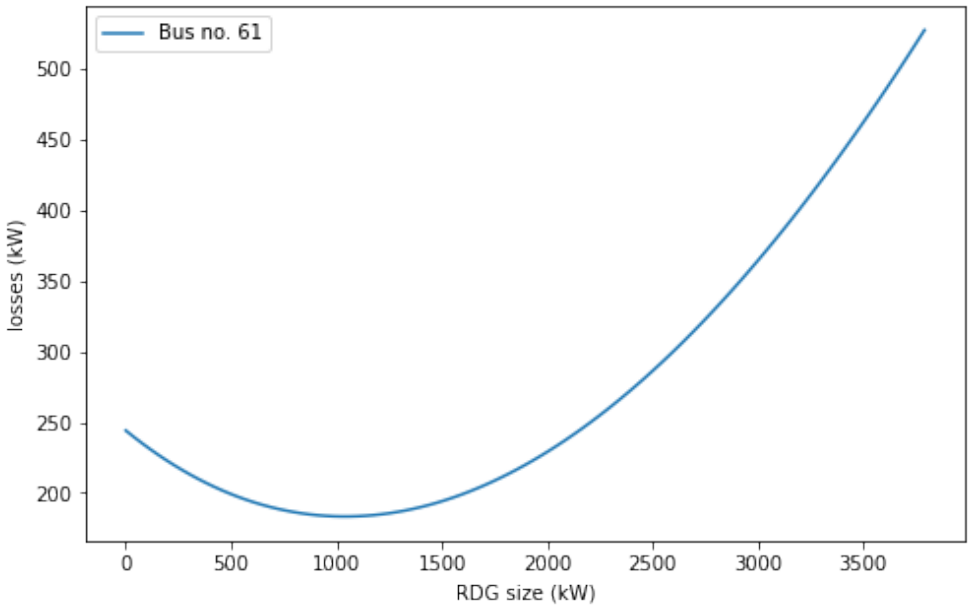

Figure 5.7: Variation of total power losses with a single RDG for the IEEE69-bus test distribution system.

Tables 5.1 and 5.2 organize the numerical results of the proposed method of LDNA-RVS which are compared with [11, 26–31] in terms of LRE and voltage stability. For the one RDG installation on IEEE33-bus test system, it is found that LDNA-RVS performs the best in LRE and voltage stability when RCR = 0. For the one RDG installation on IEEE69-bus test system, it is found that LDNA-RVS performs the best in LRE while GA [14] and LDNA-QSVS perform the best in voltage stability when RCR = 0. By considering the results at RCR = −0.48, it is found that LDNA-RVS performs the best in both LRE and voltage stability.

Table 5.1: One RDG integration results for IEEE33-bus test distribution system

Technique	RDG location (Bus no.)	RDG size (kW)	losses (kW)	RCR = 0 (PF = 1)		RCR = -0.48 (PF = -0.9)	
				LRE	VS	LRE	VS
without	-	-	212.94	-	0.0698	-	0.0698
ALGA [26]	6	2580	112.68	0.0389	0.0846	0.0059	0.0846
BSOA [29]	8	1857.5	119.81	0.0501	0.0771	0.0069	0.0771
PSO [27]	6	3150	116.88	0.0305	0.0901	−0.0041	0.0901
Analytical [11]	6	2490	112.82	0.0402	0.0838	0.0075	0.0838
ALOA [30]	6	2450	112.96	0.0408	0.0832	0.0082	0.0835
WOA [31]	30	1542.67	126.92	0.0558	0.0742	−0.0006	0.0742
MLPSO [28]	6	2420	113.09	0.0413	0.0832	0.0087	0.0832
LDNA-QSVS (Chapter 4)	**15**	**1040.2**	**134.71**	**0.0752**	**0.0736**	**0.0152**	**0.0736**
LDNA-RVS (Chapter 5)	**14**	**1151.65**	**178.24**	**0.1082**	**0.0677**	**0.0922**	**0.0706**

VS: Voltage stability evaluated with the maximum of L-index

Table 5.2: One RDG integration results for IEEE69-bus test distribution system

Technique	RDG location (Bus no.)	RDG size (kW)	losses (kW)	RCR=0 (PF=1)		RCR=-0.48 (PF=-0.9)	
				LRE	VS	LRE	VS
without	-	-	244.16	-	0.0960	-	0.0960
ABC [12]	61	1900.00	88.37	0.0819	0.0748	0.0126	0.0923
ALGA [26]	61	1872.00	88.32	0.0832	0.0748	0.0140	0.0921
Analytical [11]	61	1820.00	88.43	0.0860	0.0749	0.0172	0.0917
Grid search [13]	61	1807.80	88.32	0.0831	0.0748	0.0138	0.0921
GA [14]	61	1794.00	88.50	0.0868	0.0748	0.0180	0.0916
MTLBO [16]	61	1819.69	88.39	0.0856	0.0748	0.0167	0.0917
BB-BC [17]	61	1872.50	88.32	0.0832	0.0748	0.0140	0.0921
ALOA [30]	61	1800.00	88.47	0.0865	0.0749	0.0177	0.0916
LDNA-QSVS (Chapter 4)	**61**	**1794.00**	**88.50**	**0.0868**	**0.0748**	**0.0180**	**0.0916**
LDNA-RVS (Chapter 5)	**61**	**1023.81**	**183.35**	**0.1241**	**0.0794**	**0.0594**	**0.0889**

VS: Voltage stability evaluated with the maximum of L-index

Two RDG locations

Next, two RDGs installation are examined. By considering the maximum increment of Λ after disconnecting loads from candidate node pairs, the 14th and 30th buses are selected as the best locations of two RDGs installation for IEEE33-bus system. Similarly, the 12th and 61st buses are selected for IEEE69-bus system.

By considering the system power losses minimization for IEEE33-bus system, the size at the 14th and 30th buses determined at 520.10kW and 520.10kW (see Figure 5.6). As a result, the system power losses are decreased from 212.95kW to 165.91kW, which corresponds to LRE = 0.0959.

For the IEEE69-bus system, the sizes of RDGs installing at the 12th and 61st buses are respectively determined at 403.60kW and 941.74kW (see Figure 5.7). As a result, the system power losses are decreased from 244.16kW to 110.53kW, which corresponds to LRE = 0.0993.

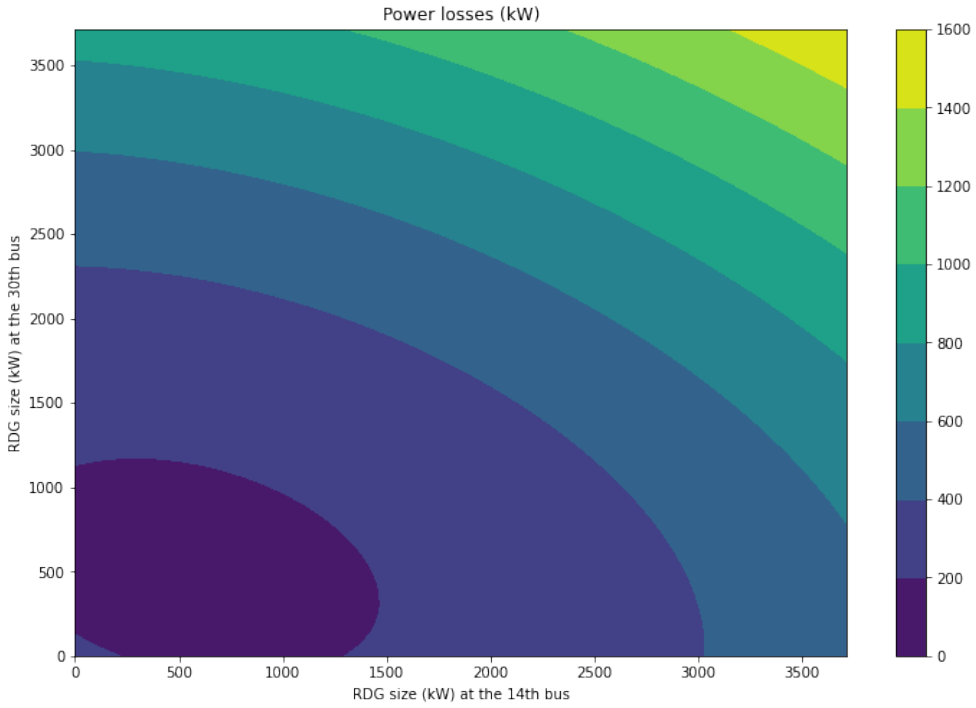

Figure 5.8: Variation of total power losses with two RDGs installation for the IEEE33-bus test distribution system.

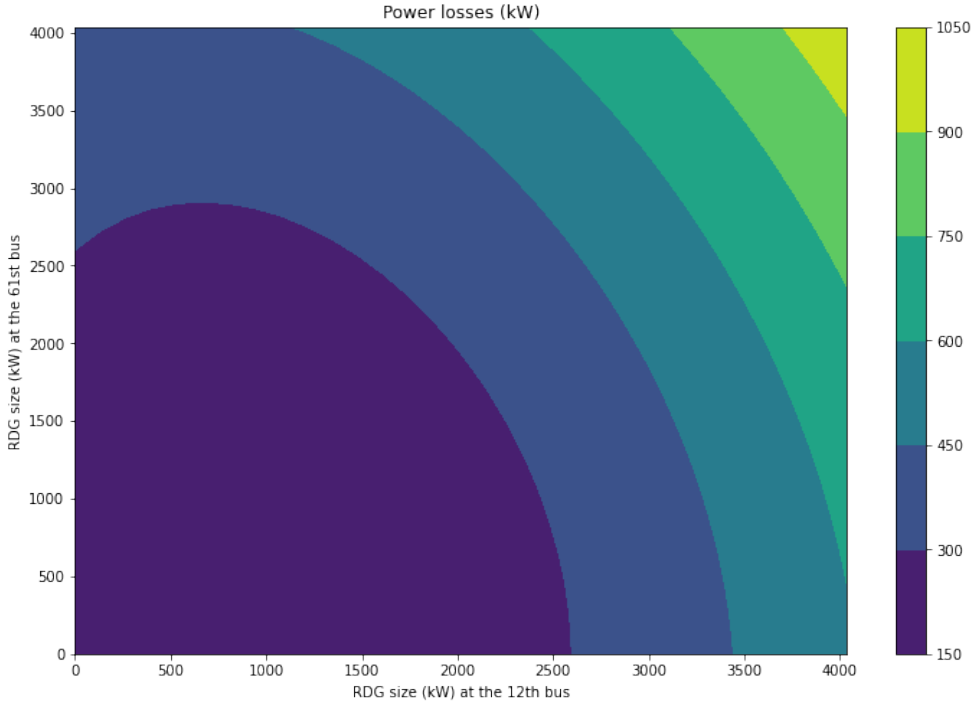

Figure 5.9: Variation of total power losses with two RDGs installation for the IEEE69-bus test distribution system.

Table 3 shows the comparison of LDNA-RVS with [26–29] and [30] for IEEE33-bus system in terms of RDG size, total power losses , LRE and voltage stability, and it is found that LDNA-RVS performs the best in LRE and VS when RCR = 0.

Table 5.3: Two RDGs integration results for IEEE33-bus test distribution system

Technique	RDG location (Bus no.)	RDG size (kW)	losses (kW)	RCR=0 (PF=1.0) LRE	RCR=0 (PF=1.0) VS	RCR=-0.48 (PF=-0.9) LRE	RCR=-0.48 (PF=-0.9) VS
Without	-	-	212.94	-	0.0698	-	0.0698
ALGA [26]	13 29	837.5 1212.2	87.99	0.0610	0.0687	0.0082	0.0787
BSOA [29]	13 31	880 924	90.04	0.0681	0.0676	0.0123	0.0764
PSO [27]	11 31	2420 960	171.52	0.0123	0.0733	−0.0532	0.0913
ALOA [30]	13 30	850 1191.1	87.79	0.0613	0.0655	0.0063	0.0770
MLPSO [28]	13 30	820 1150	87.76	0.0635	0.0654	0.0089	0.0765
LDNA-QSVS (Chapter 4)	**15** **17**	**928.75** **185.75**	**134.71**	**0.0702**	**0.0683**	**0.0086**	**0.0733**
LDNA-RVS (Chapter 5)	**14** **30**	**520.10** **520.10**	**165.91**	**0.0959**	**0.0644**	**0.0452**	**0.0703**

VS: Voltage stability evaluated with the maximum of L-index

Similarly, for the two RDGs installation on the IEEE69-bus test system, compared with [16, 25, 26, 30, 41] in Table 5.4, LDNA-RVS performs the best result in LRE, while MTLBO [16] performs the best result in VS when RCR = 0. By considering the results at RCR = −0.48, it is found that LDNA-RVS performs the best in both LRE and voltage stability.

Table 5.4: Two RDGs integration results for IEEE69-bus test distribution system

Technique	RDG location (Bus no.)	RDG size (kW)	losses (kW)	RCR=0 (PF=1.0) LRE	RCR=0 (PF=1.0) VS	RCR=-0.48 (PF=-0.9) LRE	RCR=-0.48 (PF=-0.9) VS
Without	-	-	244.15	-	0.0960	-	0.0960
GA [25]	61 11	1777 555	79.93	0.0704	0.0741	0.0135	0.0950
ALGA [26]	1 62	6 1794	89.92	0.0857	0.0969	0.0166	0.1082
PSO [41]	14 62	700 2100	101.14	0.0841	0.0972	0.0349	0.1073
MTLBO [16]	17 61	519.705 1732.004	76.58	0.0744	0.0757	0.0149	0.0956
ALOA [30]	17 61	538.777 1700	76.74	0.0748	0.0758	0.0158	0.0956
LDNA-QSVS (Chapter 4)	**60** **61**	**201.8** **1614.42**	**76.73**	**0.0859**	**0.0759**	**0.0178**	**0.0925**
LDNA-RVS (Chapter 5)	**12** **61**	**403.60** **941.74**	**110.53**	**0.0993**	**0.0783**	**0.0483**	**0.0899**

VS: Voltage stability evaluated with the maximum of L-index

5.4.2 Simulation 2: Loss reduction considering reactive compensation

The minimization of power losses is one major aspect of determining RDGs' optimal placements and can be affected by the uncontrollable reactive compensation of RDGs. The following simulations show the LRE variation of the one and two RDGs installation cases.

Loss reduction of one RDG integration

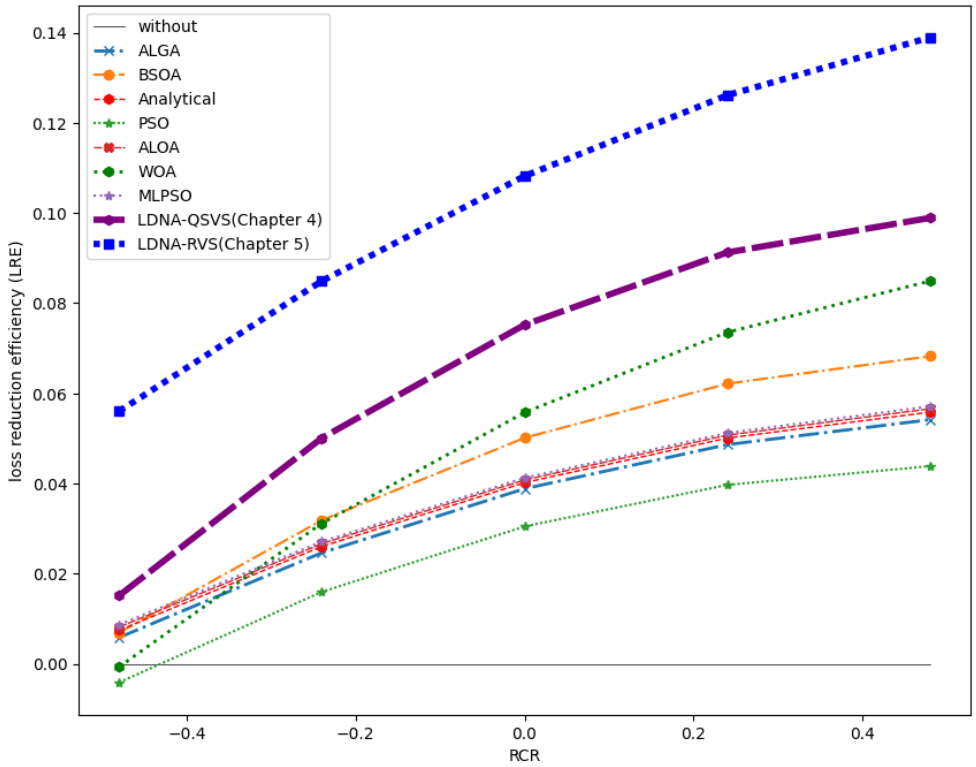

Figure 5.10: Variation of LRE of the IEEE33-bus system with reactive compensations of 1 RDG.

Figs. 5.10 and 5.11 show the variation of LRE versus RCR for several different locations and sizes of one RDG installation in IEEE33-bus system and IEEE69-bus system, respectively. Based on these results, the variation of function LRE appears to be decreased directly proportional to the capacity of reactive compensation of RDGs. Another point is that, even if the location of RDG installation is identical, different size of RDG may yield different LRE.

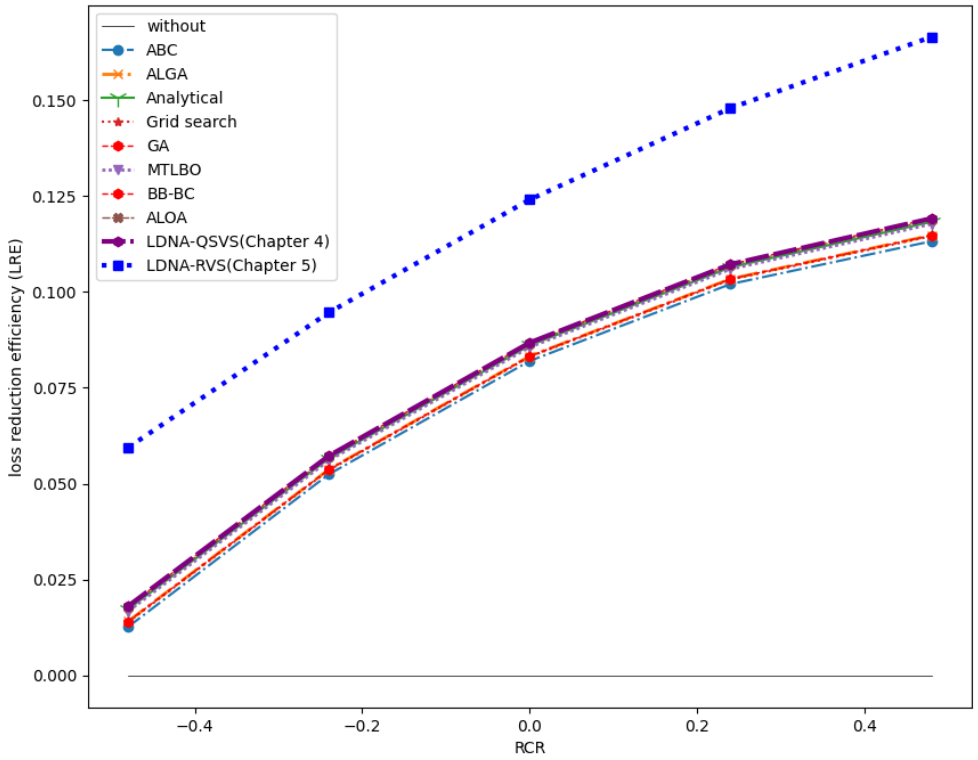

Figure 5.11: Variation of LRE of the IEEE69-bus system with reactive compensations of 1 RDG.

Loss reduction of 2 RDGs integration

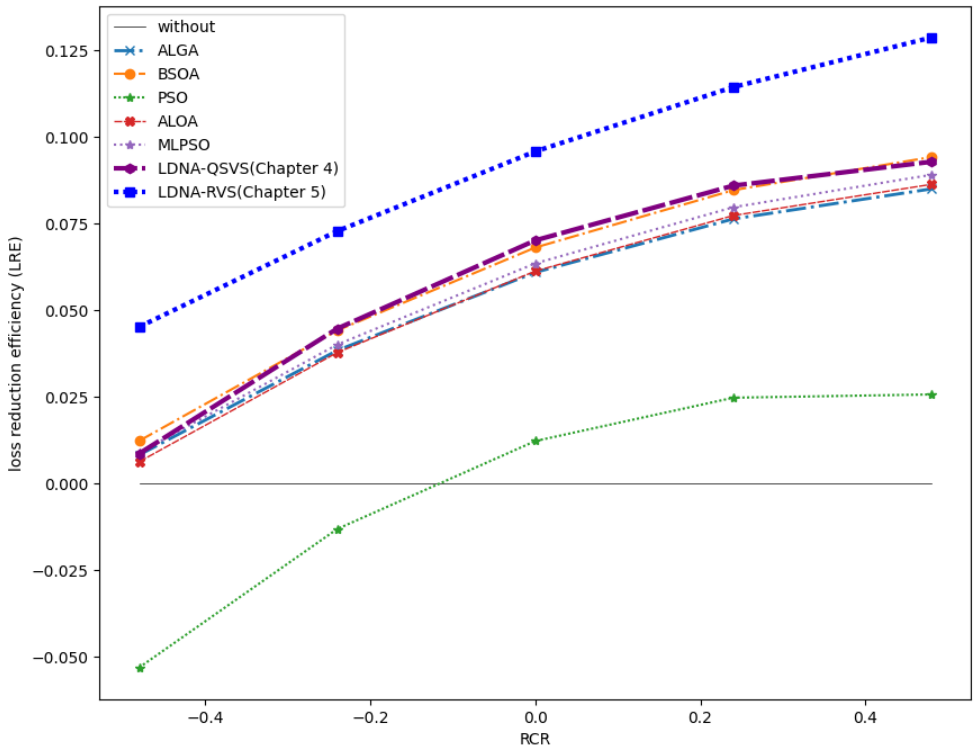

Figure 5.12: Variation of LRE of the IEEE33-bus system with reactive compensations of 2 RDG.

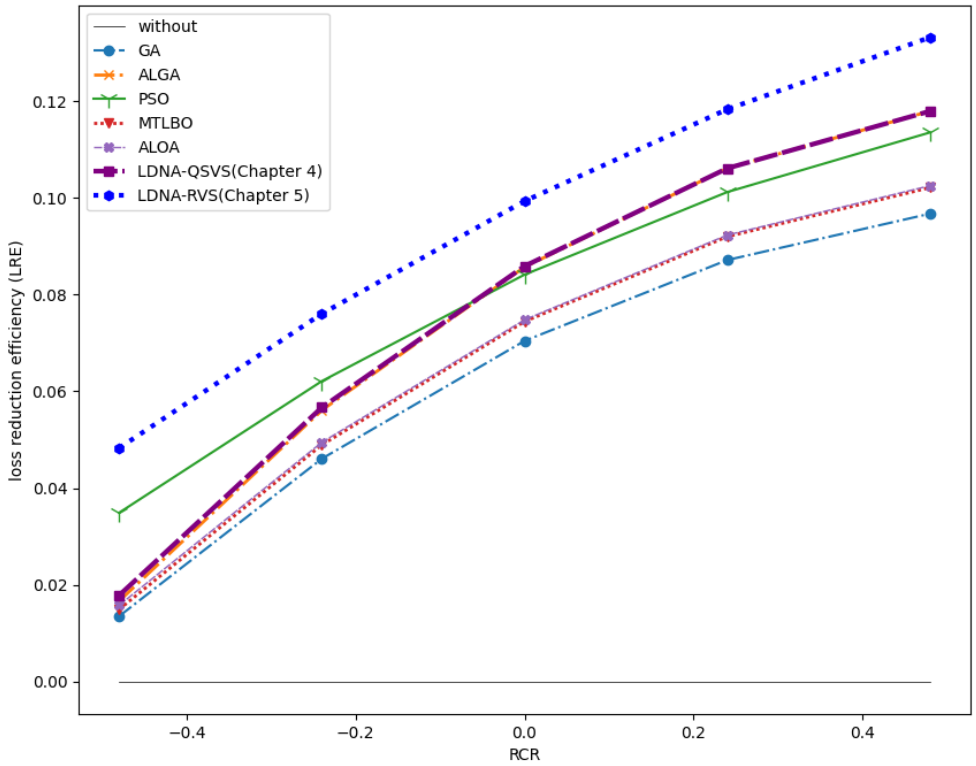

Figure 5.13: Variation of LRE of the IEEE69-bus system with reactive compensations of 2 RDG.

Figures 5.12 and 5.13 show the variation of LRE for different locations and sizes of RDGs installation. Here the similar characteristics on LRE with those in the case of one RDG installation can be observed.

While RDGs compensate for the reactive power to maintain the voltage level at the operating point, their LRE is reduced and the power losses may increase. This can be seen in examples PSO [27] and WOA [31] illustrated in Figures 5.10 and 5.12. Therefore, to avoid increasing losses against the fluctuation of RDGs, LRE of them needs to be considered within the target range of reactive compensation.

5.4.3 Simulation 3: Voltage stability considering reactive compensation

Figures 5.14 and 5.15 show the variations of voltage stability measured by L-index versus RCR for different solutions of RDG installation. Similar to LRE characteristics, L-index is monotonic with respect to RCR, and the worst voltage stability happens at RCR $= -0.48$, the smallest end of RCR under consideration. Most solutions of one RDG installation stay in the region of voltage stability improvement for RCR larger than 0 in IEEE33-bus system and for all range of RCR in IEEE69-bus system. It can be found that the solution by the proposed LDNA-RVS performs the best in the voltage stability at RCR $= -0.48$, and it goes across the border between stability degradation and improvement at the smallest RCR compared with other solutions.

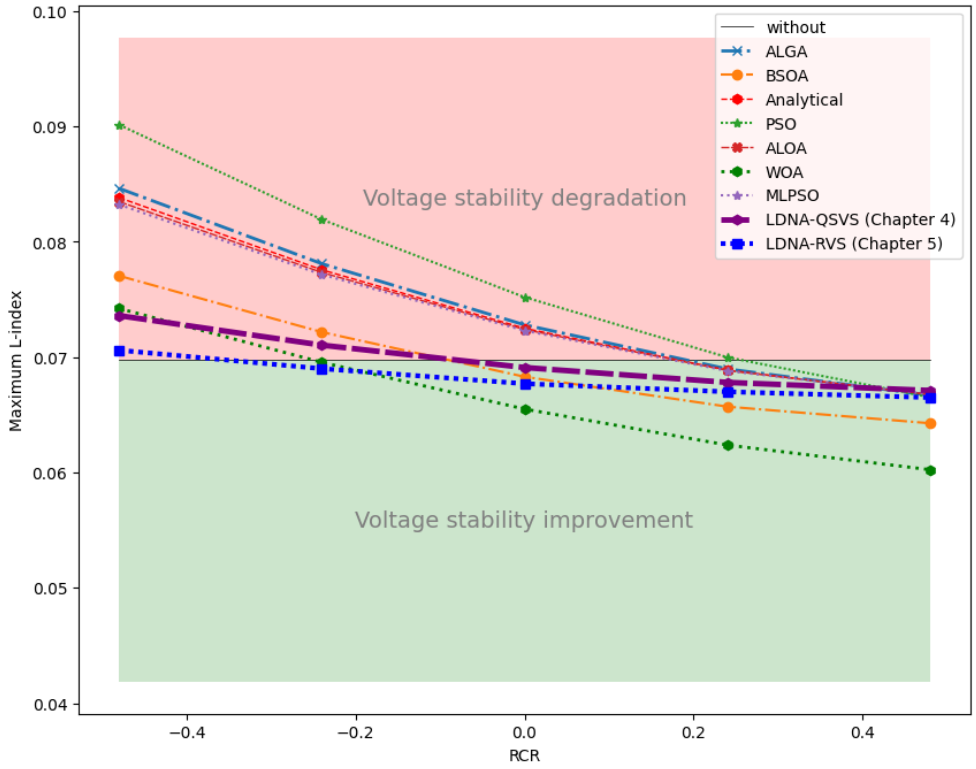

Figure 5.14: Variation of voltage stability of the IEEE33-bus system with reactive compensations of 1 RDG using maximum L-index.

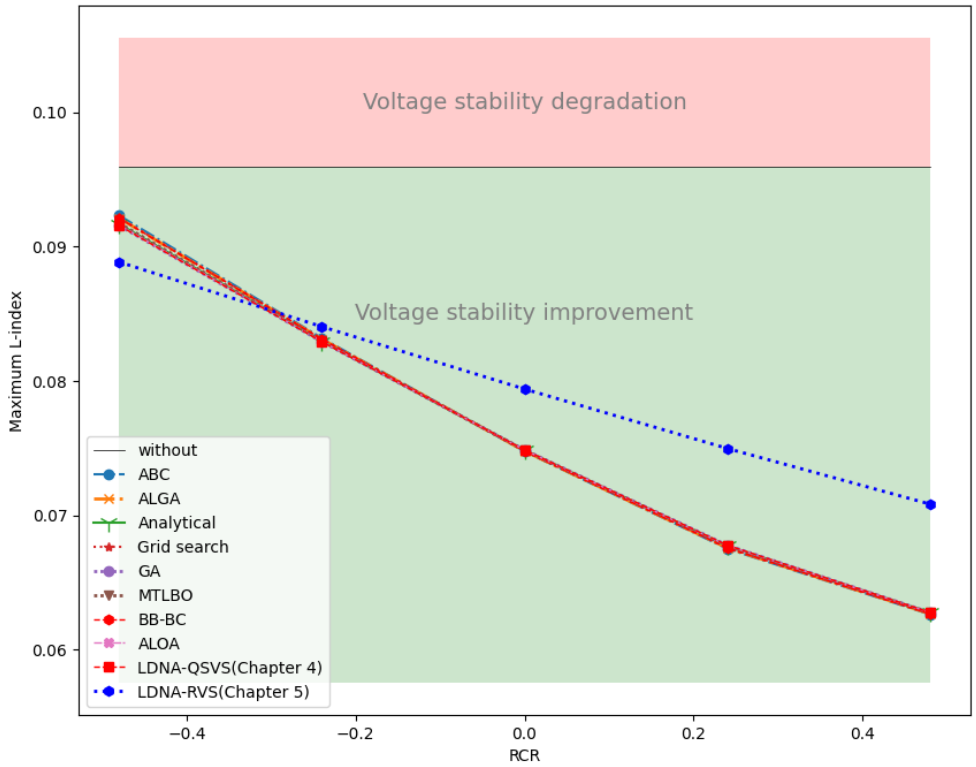

Figure 5.15: Variation of voltage stability of the IEEE69-bus system with reactive compensations of 1 RDG using maximum L-index.

Figures 5.16 and 5.17 show voltage stability characteristics versus RCR achieved by solutions of two RDGs installation, and the similar tendency with one RDG installation case can be found. Here the superiority of the solution by the proposed LDNA-RVS in voltage stability is demonstrated.

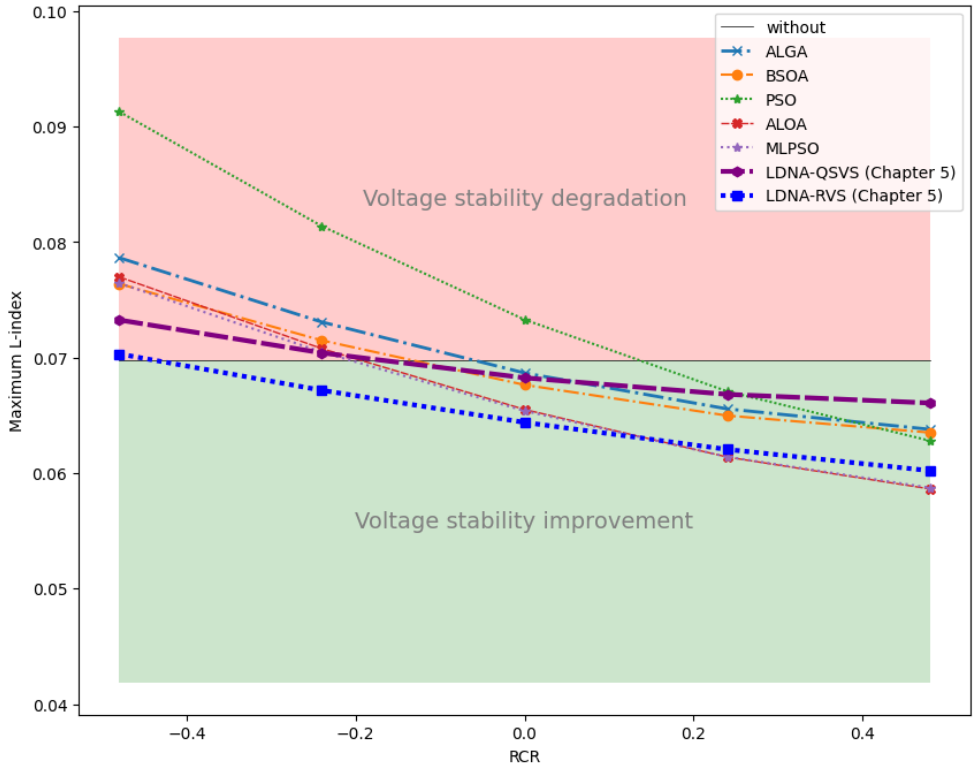

Figure 5.16: Variation of voltage stability of the IEEE33-bus system with reactive compensations of 2 RDGs using maximum L-index.

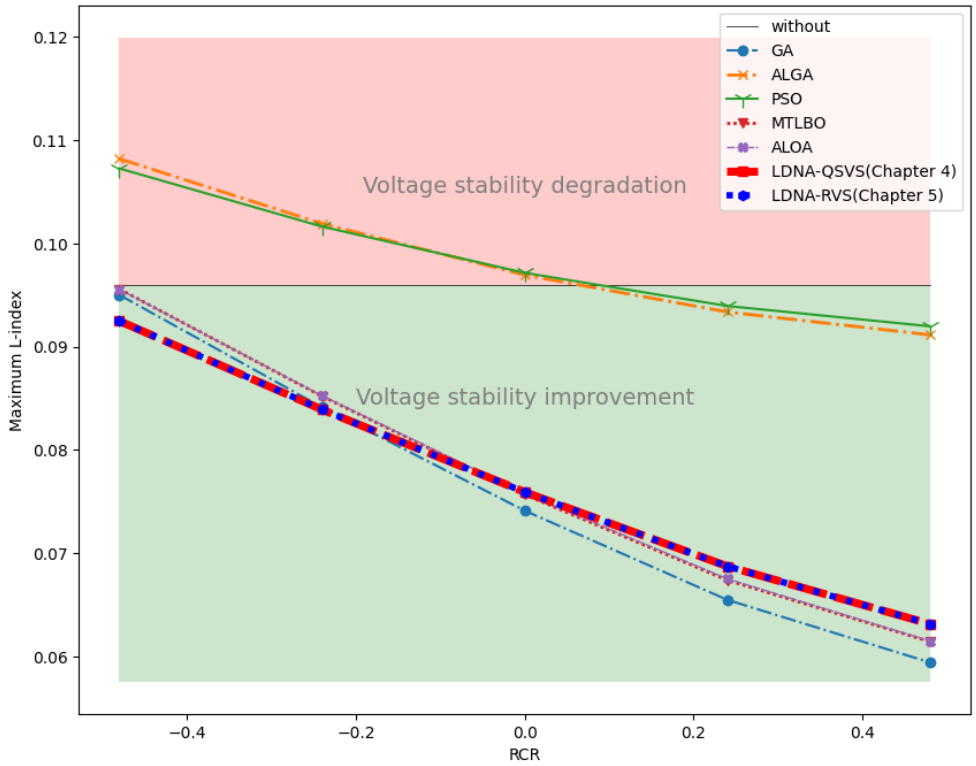

Figure 5.17: Variation of voltage stability of the IEEE69-bus system with reactive compensations of 2 RDGs using maximum L-index.

5.4.4 Summary results

Table 5.5 shows the list of best solutions with respect to LRE and voltage stability at RCR = 0 and RCR = −0.48. The proposed LDNA-RVS takes the first place at 8 categories out of 8 categories in LRE, and at 6 categories out of 8 categories in voltage stability. On the other hand, LDNA-QSVS, GA [14] and MTLBO [16] take the first place at an only one category in voltage stability. Finally, the proposed LDNA-RVS performs the best in LRE and supports the robustness of voltage stability overall in the reactive compensation.

Table 5.5: List of best solutions with respect to LRE and voltage stability at RCR = 0 and RCR = −0.48.

Case	LRE		VS		Increase loss	
	RCR = 0	RCR=-0.48	RCR = 0	RCR=-0.48	RCR = 0	RCR=-0.48
IEEE33 (1 RDG)	**LDNA-RVS** (Chapter 5)	**LDNA-RVS** (Chapter 5)	**LDNA-RVS** (Chapter 5)	**LDNA-RVS** (Chapter 5)	-	PSO [27], WOA [31]
IEEE69 (1 RDG)	**LDNA-RVS** (Chapter 5)	**LDNA-RVS** (Chapter 5)	GA [14], **LDNA-QSVS** (Chapter 4)	**LDNA-RVS** (Chapter 5)	-	PSO [27]
IEEE33 (2 RDGs)	**LDNA-RVS** (Chapter 5)	**LDNA-RVS** (Chapter 5)	**LDNA-RVS** (Chapter 5)	**LDNA-RVS** (Chapter 5)	-	-
IEEE69 (2 RDGs)	**LDNA-RVS** (Chapter 5)	**LDNA-RVS** (Chapter 5)	MTLBO [16]	**LDNA-RVS** (Chapter 5)	-	-

VS: Voltage stability evaluated with the maximum of L-index

The differences in results obtained from the LDNA-RVS methods and other approaches can be attributed to various factors:

1. The LDNA-RVS and LDNA-QSVS methods utilize a distinctive and innovative approach that centers on determining locations by incorporating load disabling for power system analysis and optimization. This sets them apart from conventional or traditional methods employed by other approaches. The specific techniques, algorithms, or models employed in the LDNA-RVS method may yield different results due to its unique methodology.

2. Variations in Operating Point Implementation Choices: Differences in the operating point employed by the LDNA-RVS method and other approaches can result in varying outcomes. These discrepancies in implementation and algorithmic choices have a significant impact on the results obtained from the LDNA-QSVS method compared to other approaches.

3. Objective Differences in Optimization: The LDNA-RVS method may have different optimization objectives compared to other approaches. While other methods primarily prioritize power loss minimization, the LDNA-RVS methodology incorporates the proposed indicator that controls both power loss and voltage stability. These differing objectives can contribute to variations in the results obtained.

Similar to the previous chapter, the analysis utilizes normalized LRE and normalized voltage stability as tools to scale the LRE and voltage stability measurements on an equalized basis. Table 5.6 presents the normalized results for LRE and voltage stability at RCR $= -0.48$. When considering the specific normalizations of LRE and voltage stability at RCR $= -0.48$, the LDNA-RVS model demonstrates superior performance compared to other solutions. However, it should be noted that the computation times for each method are still not provided, which limits the comparison in terms of computational efficiency. The LDNA-RVS method's drawback is its computation time, and improvements in this aspect are necessary for future reference.

Table 5.6: Comparison results with respect to LRE and VS at RCR = 0 and RCR = −0.48.

Technique	Computation time	norm.LRE	norm.VS	$Nsum$
	(second)	RCR = -0.48	RCR = -0.48	
Case 1: 1RDG - IEEE33				
Without	-	-	-	-
ALGA [26]	-	0.1038	0.2821	0.3859
BSOA [29]	-	0.1142	0.6667	0.7809
PSO [27]	-	0.0000	0.0000	0.0000
Analytical [11, 13]	-	0.8214	0.3231	1.1445
ALOA [18]	-	0.1277	0.3385	0.4662
WOA [31]	-	0.0363	0.8154	0.8517
MLPSO [39]		0.1329	0.3538	0.4868
LDNA-QSVS	**109**	**0.2004**	**0.8462**	**1.0466**
LDNA-RVS	**108.5**	**1.0000**	**1.0000**	**2.0000**
Case 2: 1RDG - IEEE69				
Without	-	-	-	-
ABC [12]	-	0.2121	0.5211	0.7332
ALGA [26]	-	0.2357	0.5493	0.7850
Analytical [11]	4.109	0.2896	0.6056	0.8952
Grid search [13]	0.078	0.2323	0.5493	0.7816
GA [14]	-	0.3030	0.6197	0.9227
MTLBO [16]	0.3	0.2811	0.6056	0.8868
BB-BC [17]	-	0.2357	0.5493	0.7850
ALOA [30]	-	0.2980	0.6197	0.9177
LDNA-QSVS	**304.20**	**0.3030**	**0.6197**	**0.9227**
LDNA-RVS	**304.20**	**1.0000**	**1.0000**	**2.0000**
Case 3: 2RDG - IEEE33				
Without	-	-	-	-
ALGA [26]	-	0.6240	0.6000	1.2240
BSOA [29]	-	0.6657	0.7095	1.3752
PSO [27]	-	0.0000	0.0000	0.0000
ALOA [18]	-	0.6047	0.6810	1.2856
MLPSO [39]	-	0.6311	0.7048	1.3359
LDNA-QSVS	**149**	**0.6280**	**0.8571**	**1.4852**
LDNA-RVS	**149**	**1.0000**	**1.0000**	**2.0000**
Case 4: 2RDG - IEEE69				
Without	-	-	-	-
GA [25]	-	0.2795	0.1639	0.4434
ALGA [26]	-	0.3437	-2.0000	-1.6563
PSO [41]	-	0.7226	-1.8525	-1.1299
MTLBO [16]	0.7	0.3085	0.0656	0.3741
ALOA [30]	-	0.3271	0.0656	0.3927
LDNA-QSVS	**4980.6**[a]	**0.3685**	**0.5738**	**0.9423**
LDNA-RVS	**4980.6**[a]	**1.0000**	**1.0000**	**2.0000**

Computation specification [a]: Google Colab using an Intel Xeon CPU @2.20 GHz, 13 GB RAM, and Python programming language.

Computation specification [11]: The commercial software MATLAB-7

Computation specification [13]: The power flow program MATPOWER

Computation specification [16]: The commercial software MATLAB has been used on a 3.4-GHz PC with 4 GB RAM.

VS: Voltage stability evaluated with the maximum of L-index,

norm. : Normalization

5.5 Concluding Remarks

The discussions and simulations in this paper confirm the effectiveness of the proposed voltage stability index (Λ) in identifying optimal locations for RDG installation for both voltage stability enhancement and efficient power loss reduction. Even though this paper primarily tackles the placement of RDGs, the proposed LDNA-RVS can also be applied to DG placement and a mix of DGs and RDGs, provided their reactive power compensation ratios are explicitly specified.

The study places emphasis on three key aspects: the methodology employed for determining optimal locations, the proposed objective function, and the determination of the reactive compensation level in sizing RDGs. These elements play a crucial role in achieving acceptable solutions.

Upon application to the test system, the proposed method exhibits significant improvements compared to alternative approaches, delivering superior outcomes. Furthermore, the methodology allows for the updating of the objective function and addresses increased power loss by compensating for reactive power.

It is important to acknowledge the limitations of the proposed method, which include the extensive computation time required, the assumption of predetermined installation quantities, the emphasis on steady-state conditions, and the neglect of unbalanced load and compensation of active and reactive power. Recognizing these limitations and addressing them in future research will contribute to enhancing the method's computational efficiency, flexibility in RDG placement, and consideration of dynamic system behavior, thereby advancing the development of more comprehensive and robust optimization techniques for RDGs. Furthermore, one potential drawback to consider is the computation time, which is challenging to avoid in the initial stage of the proposed method due to the inherent complexity of observing the non-linear characteristic.

Chapter 6

Allocation Design of Hybrid Renewable Energy Systems considering Robustness Against Fluctuations

6.1 Introduction

The use of Renewable Energy Source (RES) as alternative energy sources is on the rise, driven by the need to conserve natural resources and reduce carbon dioxide emissions. However, the allocation of RESs in hybrid renewable energy systems (HRESs) can be a complex problem due to their reliance on fluctuating sources like wind and solar, particularly with high penetration levels.

To address this challenge, this chapter presents a novel system design method for optimizing the size and allocation of sources and loads in HRES design. The method considers the robustness against power fluctuations of RESs and loads as a mandatory requirement for the sizing and allocation of power sources. Specifically, the author aims to design an HRES that is capable of handling unexpected variations in power generation and consumption, ensuring a reliable and sustainable power supply. Then, the author incorporates the concept of perfect matching from Graph Theory, which identifies the optimal matching of power sources to loads in a network. This helps to ensure a balanced and efficient distribution of power, minimizing wastage and maximizing the use of renewable energy.

To validate the proposed approach, the effectiveness is demonstrated using a simplified model of a real power system. The results indicate that the proposed system design method yields a more reliable and efficient HRES, with the potential for significant cost savings and environmental benefits. Overall, the method offers a practical and effective solution for the design and optimization of HRESs, helping to promote the adoption of renewable energy sources and contribute to a more sustainable future.

This chapter describes a novel approach for determining the size and location of power devices (sources and loads). Notably, the proposed model considers both the minimum and maximum power levels of devices for sizing calculations instead of a single value. Moreover, to counter energy shortages, a concept termed "robustness conditions" is introduced to ensure design reliability against power fluctuations. This condition is deemed a crucial safety requirement. The proposed method also incorporates the principle

of the perfect matching in Graph Theory. The effectiveness of the method is demonstrated using a simplified model of a real power system.

6.2 System Model in This Chapter

6.2.1 System description

In this chapter, a power system comprising a set $\mathcal{PS}$ of power sources, a set $\mathcal{PL}$, of power loads, and a set of power connections $\mathcal{X} \subseteq PS \times PL$ is investigated. The sources and loads are divided into two categories: controllable and fluctuating. Controllable devices have adjustable power levels, whereas fluctuating devices have power levels that cannot be controlled due to factors such as environmental conditions or uncontrollable user behavior. For a given set S of devices, $\mathcal{C}(S)$ denotes the set of controllable devices in S, and $\mathcal{F}(S)$ denotes the set of fluctuating devices in S. Each source $PS_m \in \mathcal{PS}$ has a minimum and maximum generating power level, denoted by ps_m^{min} and ps_m^{max}, respectively, and the actual generating power level of the mth bus (ps_m) of PS_m is bounded as follows:

$$ps_m^{min} \leq ps_m \leq ps_m^{max}$$

Similarly, each load PL_n has a minimum and maximum consuming power level, denoted by pl_n^{min} and pl_n^{max}, respectively, and the actual consuming power level of the nth bus (pl_n) of PL_n is bounded as follows:

$$pl_n^{min} \leq pl_n \leq pl_n^{max}$$

A connection, denoted by (PS_m, PL_n), is a power transmission line through which power can flow from PS_m to PL_n. If $(PS_m, PL_n) \in \mathcal{X}$, then PL_n is considered a neighbor of PS_m, and vice versa. The set of neighbors of PS_m is denoted by $N(PS_m)$. For a set S of devices, $N(S)$ denotes the union of neighbor sets of elements in S, i.e., $N(S) = \bigcup_{PD \in S} N(PD)$. Let $x : \mathcal{X} \to \mathbb{R}_+$ be a power flow assignment to connections, where $x(PS_m, PL_n)$ denotes the amount of power flow on a connection (PS_m, PL_n) in the direction from PS_m towards PL_n.

To simplify notation, the following expressions are introduced:

$$O_x(PS_m) \triangleq \sum_{PL_n \in N(PS_m)} x(PS_m, PL_n)$$

$$I_x(PL_n) \triangleq \sum_{PS_m \in N(PL_n)} x(PS_m, PL_n)$$

$O_x(PS_m)$ denotes the total power flow going out from source PS_m, and $I_x(PL_n)$ denotes the total power flow coming into load PL_n.

6.2.2 Power flow control in electrical systems

To maintain stable operation in electrical power systems, it is crucial to maintain a balance between power generation and consumption. However, fluctuations in power generation and consumption can lead to the power flow control problem, as discussed in [42]. The objective of the power flow control problem is to identify the power flows in each connection of the system that satisfy certain constraints.

The power levels of fluctuating sources and loads are denoted as ps_j^f and pl_l^f for $PS_j^f \in \mathcal{F}(\mathcal{PS})$ and $PL_l^f \in \mathcal{F}(\mathcal{PL})$, respectively. The power flow on each connection, $x(PS_m, PL_n)$ for $(PS_m, PL_n) \in \mathcal{X}$, needs to be determined such that the following constraints are satisfied:

$$ps_i^{c.min} \leq O_x(PS_i^c) \leq ps_i^{c.max}, \qquad \forall PS_i^c \in \mathcal{C}(\mathcal{PS}) \tag{6.1}$$

$$ps_j^f = O_x(PS_j^f), \qquad \forall PS_j^f \in \mathcal{F}(\mathcal{PS}) \tag{6.2}$$

$$pl_k^{c.min} \leq I_x(PL_k^c) \leq pl_k^{c.max}, \qquad \forall PL_k^c \in \mathcal{C}(\mathcal{PL}) \tag{6.3}$$

$$pl_l^f = I_x(PL_l^f), \qquad \forall PL_l^f \in \mathcal{F}(\mathcal{PL}) \tag{6.4}$$

Here, $ps_i^{c.min}$ and $ps_i^{c.max}$ represent the lower and upper bounds on the power level of controllable source $PS_i^c \in \mathcal{C}(\mathcal{PS})$, and $pl_k^{c.min}$ and $pl_k^{c.max}$ represent the lower and upper bounds on the power level of controllable load $PL_k^c \in \mathcal{C}(\mathcal{PL})$, respectively. The power levels of controllable sources and loads are denoted as ps_i^c and pl_k^c, respectively.

It is important to note that the power levels of controllable sources and loads can be automatically determined from the power flows on connections, as shown below:

$$ps_i^c := O_x(PS_i^c) \tag{6.5}$$

$$pl_k^c := I_x(PL_k^c) \tag{6.6}$$

Therefore, the power flow control problem is equivalent to the power flow assignment problem, which aims to decide $x : \mathcal{X} \to \mathbb{R}$. The power flow assignment problem can be solved using various optimization techniques, such as linear programming, non-linear programming, and heuristic algorithms.

6.2.3 Controllability

A power system is considered robust if it can provide a workable solution for any fluctuating power levels of sources and loads, while staying within the constraints of $ps_j^{f.max}$ or $pl_l^{f.max}$. For given power levels ps_j^f for $PS_j^f \in \mathcal{F}(\mathcal{PS})$ and pl_l^f for $PL_l^f \in \mathcal{F}(\mathcal{PL})$ of fluctuating sources and loads, the power flow assignment problem has a feasible solution if and only if the following two types of conditions hold [42].

$\forall \mathcal{S} \subseteq \mathcal{PS}$,

$$\sum_{PS_i^c \in \mathcal{C}(\mathcal{S})} ps_i^{c.min} + \sum_{PS_j^f \in \mathcal{F}(\mathcal{S})} ps_j^f \leq \sum_{PL_k^c \in \mathcal{C}(\mathcal{N}(\mathcal{S}))} pl_k^{c.max} + \sum_{PL_l^f \in \mathcal{F}(\mathcal{N}(\mathcal{S}))} pl_l^f \tag{6.7}$$

$\forall \mathcal{T} \subseteq \mathcal{PL}$,

$$\sum_{PS_i^c \in \mathcal{C}(\mathcal{N}(\mathcal{T}))} ps_i^{c.max} + \sum_{PS_j^f \in \mathcal{F}(\mathcal{N}(\mathcal{T}))} ps_j^f \geq \sum_{PL_k^c \in \mathcal{C}(\mathcal{T})} pl_k^{c.min} + \sum_{PL_l^f \in \mathcal{F}(\mathcal{T})} pl_l^f \tag{6.8}$$

In order for a power system to have the robustness, the above two types of constraints must be satisfied for any power levels of fluctuating sources and loads. Fortunately, the worst case situation for each type of condition provides the condition for system robustness [42].

Theorem 1

A power system has the robustness, i.e., the power flow assignment problem has always a feasible solution for any power levels of fluctuating sources and loads, if and only if the following two types of constraints hold.

$\forall \mathcal{S} \subseteq \mathcal{PS}$,

$$\sum_{\mathcal{C}(\mathcal{S})} ps^{c.min} + \sum_{\mathcal{F}(\mathcal{S})} ps^{f.max} \leq \sum_{\mathcal{C}(\mathcal{N}(\mathcal{S}))} pl^{c.max} + \sum_{\mathcal{F}(\mathcal{N}(\mathcal{S}))} pl^{f.min} \tag{6.9}$$

$\forall \mathcal{T} \subseteq \mathcal{PL}$,

$$\sum_{\mathcal{C}(\mathcal{N}(\mathcal{T}))} ps^{c.max} + \sum_{\mathcal{F}(\mathcal{N}(\mathcal{T}))} ps^{f.min} \geq \sum_{\mathcal{C}(\mathcal{T})} pl^{c.min} + \sum_{\mathcal{F}(\mathcal{T})} pl^{f.max} \tag{6.10}$$

6.2.4 System transformation

In order to describe the rest of the calculations, the network of power systems needs to be transformed into a bipartite graph of Graph theory, as shown in Figure 6.1. In the bipartite graph, the line or the connection of each device (source(s) and load(s)) means the available status of power flowing between the connected devices.

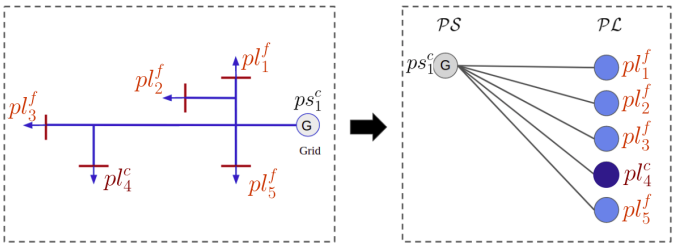

Figure 6.1: A sample of the transforming a power system to a bipartite graph

6.2.5 Allocation design problem and the robustness condition

To identify the load zone in a power system, it is necessary to evaluate the sufficiency of power sources to meet the loads. The power flow control can be analyzed and transformed into mathematical expressions to formulate a problem for determining the load zone. By applying these mathematical expressions and constraints, it becomes possible to determine the power flow on each connection and ensure that the power levels of controllable sources and loads are within acceptable limits. This analysis and formulation of the load zone problem is a critical step in designing robust power systems that can withstand fluctuations in power sources and loads.

Allocation Design Problem-I (Alloc-I)

Given a set $\mathcal{PS}$ of controllable and fluctuating sources with their minimum and maximum generating power levels (ps^{min} and ps^{max}) and a set $\mathcal{PL}$ of controllable and fluctuating loads with their minimum and maximum consuming power levels (pl^{min} and pl^{max}), find a

set $\mathcal{X} \subseteq \mathcal{PS} \times \mathcal{PL}$ *of connection between sources and loads which satisfies the conditions* (6.9) *and* (6.10) *for a robust system.*

Whether the allocation design problem has a feasible solution or not depends on the given set of sources and loads.

Theorem 2

Allocation Design Problem-I has a feasible solution, i.e., a set of connections which makes the whole system robust against fluctuation of generated power levels of fluctuating power sources and fluctuation of power demands of fluctuating power loads, if and only if the following conditions are satisfied.

$$\sum_{\mathcal{C}(\mathcal{PS})} ps^{c.min} + \sum_{\mathcal{F}(\mathcal{PS})} ps^{f.max} \leq \sum_{\mathcal{C}(\mathcal{PL})} pl^{c.max} + \sum_{\mathcal{F}(\mathcal{PL})} pl^{f.min} \tag{6.11}$$

$$\sum_{\mathcal{C}(\mathcal{PS})} ps^{c.max} + \sum_{\mathcal{F}(\mathcal{PS})} ps^{f.min} \geq \sum_{\mathcal{C}(\mathcal{PL})} pl^{c.min} + \sum_{\mathcal{F}(\mathcal{PL})} pl^{f.max} \tag{6.12}$$

Proof of Theorem 2

Necessity: If (6.11) fails, then (6.9) fails with $\mathcal{S} = \mathcal{PS}$. Similarly, if (6.12) fails, then (6.10) fails with $\mathcal{T} = \mathcal{PL}$. Then, in order to fulfill (6.9) and (6.10), (6.11) and (6.12) are necessary

Sufficiency: If (6.11) is fulfilled, $\mathcal{X} = \mathcal{PS} \times \mathcal{PL}$ satisfies (6.9), since for any subset $\mathcal{S}$ of $\mathcal{PS}$,

$$\sum_{\mathcal{C}(\mathcal{S})} ps^{c.min} + \sum_{\mathcal{F}(\mathcal{S})} ps^{f.max} \leq \sum_{\mathcal{C}(\mathcal{PS})} ps^{c.min} + \sum_{\mathcal{F}(\mathcal{PS})} ps^{f.max}$$

and $N(\mathcal{S}) = \mathcal{PL}$ under $\mathcal{X} = \mathcal{PS} \times \mathcal{PL}$, which shows

$$\sum_{\mathcal{C}(\mathcal{N}(\mathcal{S}))} pl^{c.max} + \sum_{\mathcal{F}(\mathcal{N}(\mathcal{S}))} pl^{f.min} = \sum_{\mathcal{C}(\mathcal{PL})} pl^{c.max} + \sum_{\mathcal{F}(\mathcal{PL})} pl^{f.min}$$

Combining (6.11) with the above two equations, (6.9) is shown to be fulfilled. Similar argument applies to the second condition, and (6.12) is also satisfied with $\mathcal{X} = \mathcal{PS} \times \mathcal{PL}$, if (6.12) is fulfilled.

6.3 Design Optimization

It has been discovered that if (6.11) and (6.12) are fulfilled, a trivial solution $\mathcal{X} = \mathcal{PS} \times \mathcal{PL}$ exists. Nevertheless, a system's complexity, controller complexity, among other factors, are influenced by the number of connections, hence a smaller number of connections is generally preferred.

6.3.1 Optimization problem

The following optimization problem is considered.

Allocation Design Problem-II (Alloc-II)

Given a set $\mathcal{PS}$ of controllable and fluctuating sources, each with their minimum and maximum generating power levels denoted by ps^{min} and ps^{max}, respectively, and a set $\mathcal{PL}$ of controllable and fluctuating loads, each with their respective minimum and maximum consuming power levels denoted by pl^{min} and pl^{max}, the task is to identify a set $\mathcal{X} \subseteq \mathcal{PS} \times \mathcal{PL}$ of connections between power sources and loads such that the conditions expressed in (6.9) *and* (6.10) *are met, ensuring that the system is robust, while also minimizing the number of connections relative to other feasible solutions. The sets $\mathcal{PS}$ and $\mathcal{PL}$ must satisfy the constraints given in* (6.11) *and* (6.12)*.*

6.3.2 Transformation

Directly applying the constraints (6.9) and (6.10) to check the feasibility of a solution in the design process may not be a suitable approach since the computation time required is exponential in terms of the number of sources and loads. The power flow assignment $x : \mathcal{X} \to \mathbb{R}_+$ can be utilized to explore the relationship between its solution and the constraints, thereby avoiding the direct use of the constraints in their original forms.

Lemma 1

For given power flow system $(\mathcal{PS}, \mathcal{PL}, \mathcal{X})$, generating power of each sources, ps_m for $PS_m \in \mathcal{PS}$, and power demand of each load, pl_n for $PL_n \in \mathcal{PL}$, there exists a power flow assignment $x : \mathcal{X} \to \mathbb{R}_+$ which satisfies

$$ps_m = O_x(PS_m), \qquad \forall PS_m \in \mathcal{PS}$$
$$I_x(PL_n) \leq pl_n, \qquad \forall PL_n \in \mathcal{PL}$$

if and only if the following condition is satisfied.

$$\forall \mathcal{S} \subseteq \mathcal{PS}, \sum_{PS_m \in \mathcal{S}} ps_m \leq \sum_{PL_n \in N(\mathcal{S})} pl_n$$

Similarly, there exists a power flow assignment $y : \mathcal{X} \to \mathbb{R}_+$ which satisfies

$$ps_m \geq O_y(PS_m), \qquad \forall PS_m \in \mathcal{PS}$$
$$I_y(PL_n) = pl_n, \qquad \forall PL_n \in \mathcal{PL}$$

if and only if the following condition is satisfied.

$$\forall \mathcal{T} \subseteq \mathcal{PL}, \sum_{PS_m \in N(\mathcal{T})} ps_m \geq \sum_{PL_n \in \mathcal{T}} pl_n$$

(Note that the former type of power flow assignment is said to saturate all power sources, and the latter is said to saturate all power loads.)

Based on this lemma, Allocation Design Problem-II (Optimization problem) can be transformed into the following form.

Allocation Design Problem-II' (Alloc-II')

A set $\mathcal{X} \subseteq \mathcal{PS} \times \mathcal{PL}$ of connections between controllable and fluctuating power sources $\mathcal{PS}$ and controllable and fluctuating power loads $\mathcal{PL}$, each with their respective minimum and maximum generating or consuming power levels, can be determined given that the conditions in equations (6.11) *and* (6.12) *are satisfied.*

> *Allocation Design Problem-II'-1 (Alloc-II'-1): the system with $ps_i^{c.min}$ for $PS_i^c \in \mathcal{C}(\mathcal{PS})$, $ps_j^{f.max}$ for $PS_j^f \in \mathcal{F}(\mathcal{PS})$, $pl_k^{c.max}$ for $PL_k^c \in \mathcal{C}(\mathcal{PL})$, and $pl_l^{f.min}$ for $PL_l^f \in \mathcal{F}(\mathcal{PL})$ has a power flow assignment x which satisfies the following requirements.*

$$\left.\begin{array}{ll} ps_i^{c.min} = O_x(PS_i^c), & \forall PS_i^c \in \mathcal{C}(\mathcal{PS}) \\ ps_j^{f.max} = O_x(PS_j^f), & \forall PS_j^f \in \mathcal{F}(\mathcal{PS}) \\ I_x(PL_k^c) \leq pl_k^{c.max}, & \forall PL_k^c \in \mathcal{C}(\mathcal{PL}) \\ I_x(PL_l^f) \leq pl_l^{f.min} & \forall PL_l^f \in \mathcal{F}(\mathcal{PL}) \end{array}\right\} \tag{6.13}$$

> *Allocation Design Problem-II'-2 (Alloc-II'-2.): the system with $ps_i^{c.max}$ for $PS_i^c \in \mathcal{C}(\mathcal{PS})$, $ps_j^{f.min}$ for $PS_j^f \in \mathcal{F}(\mathcal{PS})$, $pl_k^{c.min}$ for $PL_k^c \in \mathcal{C}(\mathcal{PL})$, and $pl_l^{f.max}$ for $PL_l^f \in \mathcal{F}(\mathcal{PL})$ has a power flow assignment y which satisfies the following requirements.*

$$\left.\begin{array}{ll} ps_i^{c.max} \geq O_y(PS_i^c), & \forall PS_i^c \in \mathcal{C}(\mathcal{PS}) \\ ps_j^{f.min} \geq O_y(PS_j^f), & \forall PS_j^f \in \mathcal{F}(\mathcal{PS}) \\ I_y(PL_k^c) = pl_k^{c.min}, & \forall PL_k^c \in \mathcal{C}(\mathcal{PL}) \\ I_y(PL_l^f) = pl_l^{f.max}, & \forall PL_l^f \in \mathcal{F}(\mathcal{PL}) \end{array}\right\} \tag{6.14}$$

and the number of connections is minimum among all feasible solutions.

6.4 MILP Solution of Design Optimization

The design optimization problem takes as input a set of controllable sources and fluctuating sources, a set of controllable loads and fluctuating power loads, as well as their corresponding minimum and maximum power levels. Specifically, $ps_i^{c.min}, ps_i^{c.max}$ are defined for $PS_i^c \in \mathcal{C}(\mathcal{PS})$, $ps_j^{f.min}$, $ps_j^{f.max}$ for $PS_i^c \in \mathcal{F}(\mathcal{PS})$, $pl_k^{c.min}$, $pl_k^{c.max}$ for $PL_k^c \in \mathcal{C}(\mathcal{PL})$, and $pl_l^{f.min}$, $pl_l^{f.max}$ for $PL_l^f \in \mathcal{F}(\mathcal{PL})$.

In order to formulate MILP problem instance from the Allocation Design Problem-II', the following variables are introduced.

$x(p, q)$: Power flow assignment x for representing the solution for Alloc-II'-1. p for all controllable and fluctuating sources, and q for all controllable and fluctuating loads.

$y(p, q)$: Power flow assignment y for representing the solution for Alloc-II'-2. p for all controllable and fluctuating sources, and q for all controllable and fluctuating loads.

$C(p,q)$: Binary variable representing presence ($C(p,q)=1$) or absence ($C(p,q)=0$) of a connection between PS_p and PL_q.

Then, constrains are formulated as follows.

Representing a solution for Alloc-II'-1:

$$ps_i^{c.min} = \sum_{q=1}^{K+L} x(i,q), \qquad PS_i^c \in \mathcal{C}(\mathcal{PS}) \tag{6.15}$$

$$ps_j^{f.max} = \sum_{q=1}^{K+L} x(I+j,q), \qquad PS_j^f \in \mathcal{F}(\mathcal{PS}) \tag{6.16}$$

$$\sum_{p=1}^{I+J} x(p,k) \leq pl_k^{c.max}, \qquad PL_k^c \in \mathcal{C}(\mathcal{PL}) \tag{6.17}$$

$$\sum_{p=1}^{I+J} x(p,K+l) \leq pl_l^{f.min}, \qquad PL_l^f \in \mathcal{F}(\mathcal{PL}) \tag{6.18}$$

Representing a solution for Alloc-II'-2:

$$ps_i^{c.min} \geq \sum_{q=1}^{K+L} y(i,q), \qquad PS_i^c \in \mathcal{C}(\mathcal{PS}) \tag{6.19}$$

$$ps_j^{f.max} \geq \sum_{q=1}^{K+L} y(I+j,q), \qquad PS_j^f \in \mathcal{F}(\mathcal{PS}) \tag{6.20}$$

$$\sum_{p=1}^{I+J} y(p,k) = pl_k^{c.min}, \qquad PL_k^c \in \mathcal{C}(\mathcal{PL}) \tag{6.21}$$

$$\sum_{p=1}^{I+J} y(p,K+l) = pl_l^{f.max}, \qquad PL_l^f \in \mathcal{F}(\mathcal{PL}) \tag{6.22}$$

In order to solve Alloc-II'-2, a distinct power flow problem from Alloc-II'-1 needs to be addressed. As a result, power flow variables $y(p,q)$ that differ from $x(p,q)$ are necessary.

Checking presence/absence of individual connection:

$$x(p,q) - H \cdot C(p,q) \leq 0, \quad \begin{array}{l} p \in \{1,...,I+J\}, \\ q \in \{1,...,K+L\} \end{array} \tag{6.23}$$

$$y(p,q) - H \cdot C(p,q) \leq 0, \quad \begin{array}{l} p \in \{1,...,I+J\}, \\ q \in \{1,...,K+L\} \end{array} \tag{6.24}$$

where H is a sufficiently large constant.

$$H = \max\{ps_1^{c.max},...,ps_I^{c.max},ps_i^{f.max},...,ps_J^{f.max}\}$$

is one possible choice for H.

The constraints above indicate that if $x(p,q)$ is greater than 0, then $C(p,q)$ must have a value of 1 to satisfy the constraint, which corresponds to the existence of a connection. As the connections are identical for Alloc-II'-1 and Alloc-II'-2, a single variable $C(p,q)$ is used. Specifically, $C(p,q)$ must be 1 when either $x(p,q)$ or $y(p,q)$ has a positive (non-zero) value. When $x(p,q) = y(p,q) = 0$, the constraints allow $C(p,q)$ to be either 0 or 1. However, to minimize the cost function, $C(p,q)$ must have a value of 0.

Minimizing the number of connections:

$$\sum_{p=1}^{I+J} \sum_{q=1}^{K+L} C(p,q) \tag{6.25}$$

Equation (6.25) is chosen as the cost function to be minimized. That's all for Mixed Integer Linear Programming (MILP) formulation of Alloc-II'.

6.5 Demonstrations

HRES refers to a hybrid renewable energy system composed of renewable power sources, with or without conventional power sources, that can operate in off-grid or on-grid mode [43]. For the purpose of the demonstrations in this study, two types of HRES are used: HRES without off-grid mode and HRES with on-off-grid mode. To design the HRES using the proposed method, three types of elements are required: the power system or HRES, the given set of device's power level (maximum and minimum), and additional sources. The power system used as a sample in this study is the 22kV power distribution network located in a rural area of Krabi, Thailand, as shown in Figure 6.2, and it is expected to be a HRES in the future [44]. For the given set of devices, one controllable source, one controllable load, and four fluctuating loads with their power levels are considered based on the power consumption characteristics in the Krabi area, as depicted in Figure 6.2. The lower bound of the loads is assumed to be less than 25% of their upper bound, and the upper bound is assumed to be 80% of their power limit, as presented in Table 6.1. Additional sources, which can be controllable or fluctuating or both, need to be installed to the power system.

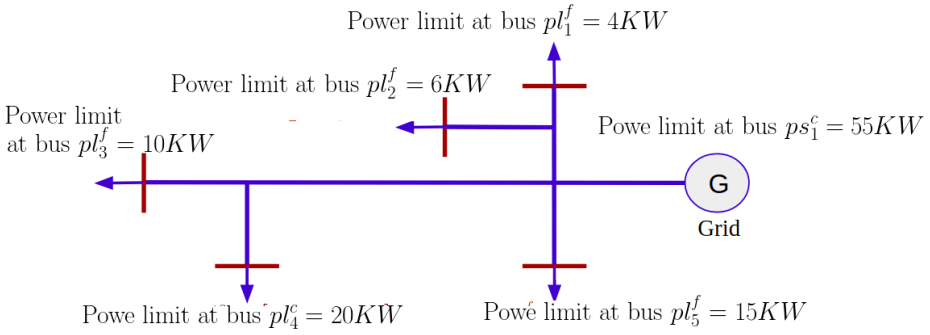

Figure 6.2: The sample of 22kV power distribution network in rural area of Krabi, Thailand.

The goal is to optimize the size and allocation of HRES design in both operation modes: HRES operating on-grid (without off-grid) mode and HRES operating on-off-grid

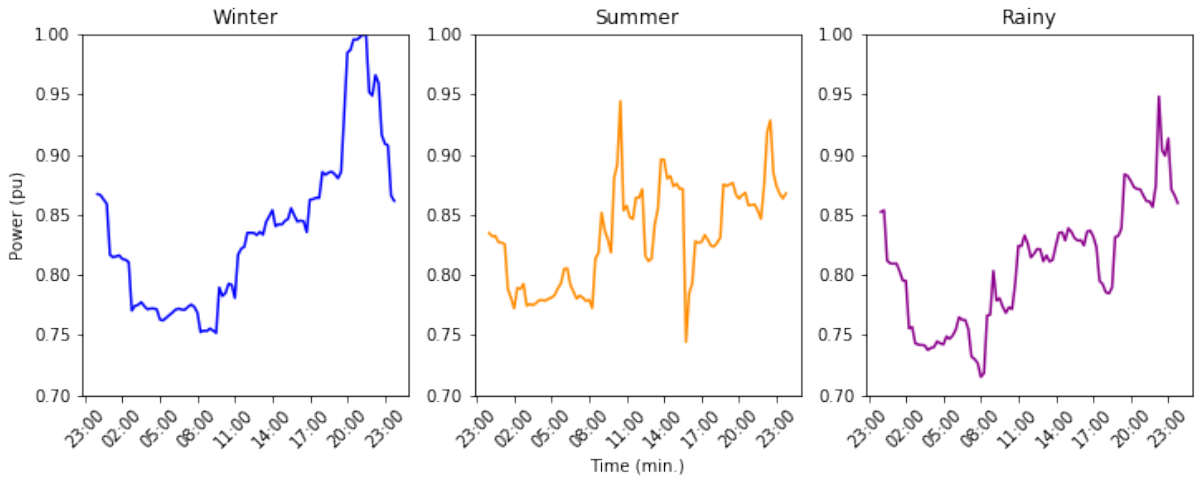

Figure 6.3: Characteristic of Power Consumption in Krabi, Thailand

Table 6.1: Given set of Krabi's power consumption

Item	Minimum (KW)	Maximum (KW)
ps_1^c(grid)	0	44.00
pl_1^f	2.41	3.20
pl_2^f	3.62	4.80
pl_3^f	6.03	8.00
pl_4^c	5.00	16.00
pl_5^f	9.05	12.00

mode, as per the objective. The system design method comprises of two methods, namely sizing and allocation.

To achieve the objective, a two-step approach consisting of sizing and allocation methods for both operation modes of the HRES design, i.e., on-grid mode (without off-grid) and on-off-grid mode is utilized. In the first step, the optimal size of additional power sources and loads which can be installed in the power system, is demonstrated in Demonstration I. Demonstration I is divided into two subsections, namely, Demonstration I (a), which involves sizing additional devices for HRES without off-grid mode, and Demonstration I (b), which involves sizing additional devices for HRES with on-off-grid mode. In the second step, the additional power sources are allocated in the HRES using the proposed method, which is demonstrated in Demonstration II. Demonstration II also consists of two subsections, i.e., Demonstration II (a), which is the allocation of additional sources for HRES without off-grid mode, and Demonstration II (b), which is the allocation of additional sources for HRES with on-off-grid mode.

6.5.1 Demonstration I : Sizing method implementations

Balancing supply energy and consumer demand is a basic concept of the sizing method. For any power system having only controllable sources, though consumers or loads are fluctuating in the limit of the source's capacity, the consumers are supplied energy sufficiently. However, for any power system having just fluctuating sources, though consumers or loads are fluctuating the supply's capacity boundary from the sources, the consumers are supplied energy insufficiently. Therefore, the fluctuation of power sources causes the

problem in the system design. For this reason, conditions (6.11) and (6.12) (the robustness condition as in Theorem 1), which can be used as the requirements for the installation of additional sources, are proposed. Moreover, the conditions is not only the requirement for (controllable and fluctuating) sources but for (controllable and fluctuating) loads.

The aim of this section is to determine the feasible range of additional power sources (PS) for HRES (without off-grid mode) and (PS') for HRES (with on-off-grid mode) that can be installed in the power system. In addition, the renewable energy potential is also considered in the area to calculate the feasible range of fluctuating power sources (PS) and (PS'), specifically wind and solar energy, that can be integrated into the existing power distribution network.

The following demonstrations describes how to implement the proposed conditions for calculating (PS) and (PS').

Demonstration I (a) : Sizing of HRES (without off-grid mode)

To find PS^f of the total additional fluctuating power sources, which consists of their maximum boundary ($PS^{f.max}$) and their minimum boundary ($PS^{f.min}$), with the given sets of the power system as in Table 6.2. The calculation of PS is described as follows:

A rewritten version of the equations can be obtained by manipulating the mathematical expressions in (6.11).

$$\sum_{\mathcal{C}(\mathcal{PS})} ps^{c.min} + PS^{f.max} \leq \sum_{\mathcal{C}(\mathcal{PL})} pl^{c.max} + \sum_{\mathcal{F}(\mathcal{PL})} pl^{f.min} \tag{6.26}$$

$$ps_1^{c.min}(\text{grid}) + PS^{f.max} \leq +pl_4^{c.max} + \sum_{l=1 \text{ and } l\neq 4}^{5} pl_l^{f.min} \tag{6.27}$$

Therefore,

$$PS^{f.max} \leq +pl_4^{c.max} + \sum_{l=1 \text{ and } l\neq 4}^{5} pl_l^{f.min} - ps_1^{c.min}(\text{grid}) \tag{6.28}$$

One can manipulate the mathematical expressions in (6.12) to achieve the rewriting of the equations, which yields

$$\sum_{\mathcal{C}(\mathcal{PS})} ps^{c.max} + PS^{f.min} \leq \sum_{\mathcal{C}(\mathcal{PL})} pl^{c.min} + \sum_{\mathcal{F}(\mathcal{PL})} pl^{f.max} \tag{6.29}$$

$$ps_1^{c.max}(\text{grid}) + PS^{f.min} \geq +pl_4^{c.min} + \sum_{l=1 \text{ and } l\neq 4}^{5} pl_l^{f.max} \tag{6.30}$$

Therefore,

$$PS^{min} \geq +pl_4^{c.min} + \sum_{l=1 \text{ and } l\neq 4}^{5} pl_l^{f.max} - ps_1^{c.max}(\text{grid}) \tag{6.31}$$

As the result, according to the calculation, the total additional fluctuating power sources PS^f is obtained as shown in Table 6.2:

Table 6.2: Result of Demonstration I (a) : Sizing of HRES (without off-grid mode)

Size	Minimum (KW)	Maximum (KW)
PS^f	≥ 0	≤ 37.11

Demonstration I (b) : sizing of HRES (with off-grid mode)

HRES that is capable of operating in the off-grid mode can also be utilized for the on-grid mode. In the off-grid mode, the power distribution network's energy is not provided by the main grid or $ps_1^c(\text{grid}) = 0$. Nevertheless, to satisfy the robustness conditions, as per (6.11) and (6.12), the total sources should contain additional reserve or controllable power sources (PS'^c) to supply energy during the off-grid mode.

The objective of this experiment is to compute the upper and lower limits of additional fluctuating sources (PS'^f) and controllable sources (PS'^c) that can be incorporated into the HRES (with on-off-grid mode) design, given the input parameters provided in Table 6.1. The computation of PS'^f and PS'^c involves utilizing equation (6.11), which can be expressed as follows:

$$PS'^{c.min} + PS'^{f.max} \leq \sum_{\mathcal{C}(\mathcal{PL})} pl^{c.max} + \sum_{\mathcal{F}(\mathcal{PL})} pl^{f.min} \tag{6.32}$$

Therefore,

$$PS'^{c.min} + PS'^{f.max} \leq +pl_4^{c.max} + \sum_{l=1 \text{ and } l\neq 4}^{5} pl_l^{f.min} \tag{6.33}$$

Next, the calculation can be expressed by utilizing equation (6.12) as follows:

$$PS'^{c.max} + PS'^{f.min} \leq \sum_{\mathcal{C}(\mathcal{PL})} pl^{c.min} + \sum_{\mathcal{F}(\mathcal{PL})} pl^{f.max} \tag{6.34}$$

Therefore,

$$PS'^{c.max} + PS'^{f.min} \leq pl_4^{c.min} + \sum_{l=1 \text{ and } l\neq 4}^{5} pl_l^{f.max} \tag{6.35}$$

The computation results in obtaining the total additional fluctuating and controllable power sources, PS'^f and PS'^c, for the HRES (with on-off-grid mode) design, which are presented in Table 6.3.

Table 6.3: Result of Demonstration I (b) : sizing of HRES (with on-off-grid mode)

Size	Minimum (KW)	Maximum (KW)
PS'^f	≥ 21	≤ 37
PS'^c (reserve)	≥ 0	≤ 20

6.5.2 Demonstration II: Allocation method implementations

The proposed allocation method for HRES design is implemented in this section, assuming that the power system, the given set, and the additional sources are already prepared. The goal is to minimize the number of connections using equation (6.25), which was introduced in Section 4.3. However, the additional sources, obtained from Demonstration I (a) and I (b), must be provided beforehand. Once the sizes, i.e., PS'^{f}, PS'^{f}, and PS'^{c} are determined, the power system is converted into a bipartite graph, as illustrated in Figure 6.4.

The objective is to allocate the devices using the minimum number of connections. More important, in order to result in the system design holding the robustness, all sources and loads need to satisfy the robustness condition. In the Demonstration II, two types of HRES, i.e., HRES (without off-grid mode) and HRES (with on-off-grid mode) are considered for implementation.

The following demonstrations explain the implementation of the allocation method for the two types of HRES.

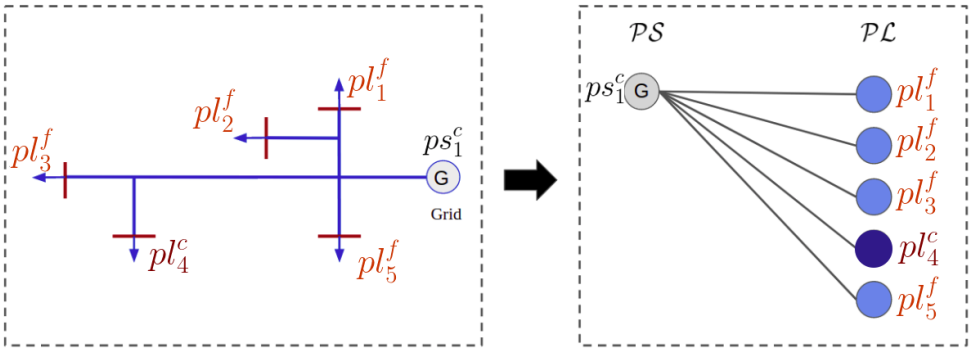

Figure 6.4: Transforming the power system to the bipartite graph of Demonstration II

Demonstration II (a): Allocation Method Implementation for HRES (without off-grid mode) design

In this subsection, the HRES, which is available only for operating in the on-grid mode (without off-grid mode), is studied. The objective of this study is to allocate the additional power sources, of which power levels are assumed under the boundary of PS^f, the result of Demonstration I (a). It is assumed that the additional sources consist of 6 fluctuating sources within the boundary of PS^f. Assuming that the additional power sources to be integrated into the power system consist of 5 fluctuating sources, as shown in Table 6.4.

In addition, the additional sources are described in Table 6.4.

The method proposed to minimize connections can be employed to allocate the additional sources in the HRES (without off-grid mode) design. The result of this allocation is shown in Figure 6.5. Following this, the bipartite graph is converted back into the power system, as illustrated in Figure 6.6.

Table 6.4: Power levels of the additional power sources for Demonstration II (a)

Item	Minimum (kW)	Maximum (kW)
$ps_1'^f$	0	6.19
$ps_2'^f$	0	2.00
$ps_3'^f$	0	10.37
$ps_4'^f$	0	5.00
$ps_5'^f$	0	7.37
$ps_6'^f$	0	6.19

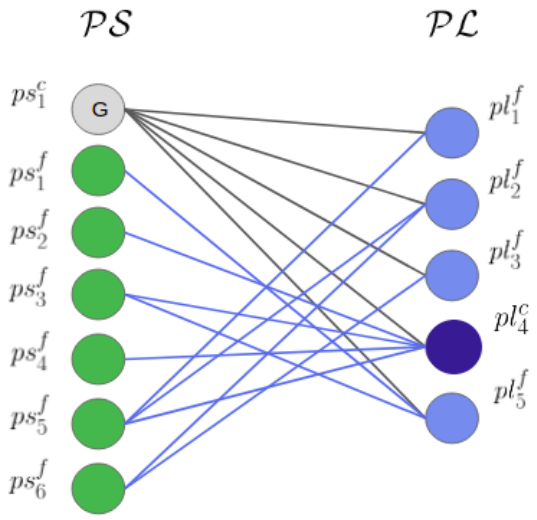

Figure 6.5: Result of Demonstration II (a): the allocation of the additional sources for HRES (without off-grid mode) design demonstrated by the bipartite graph

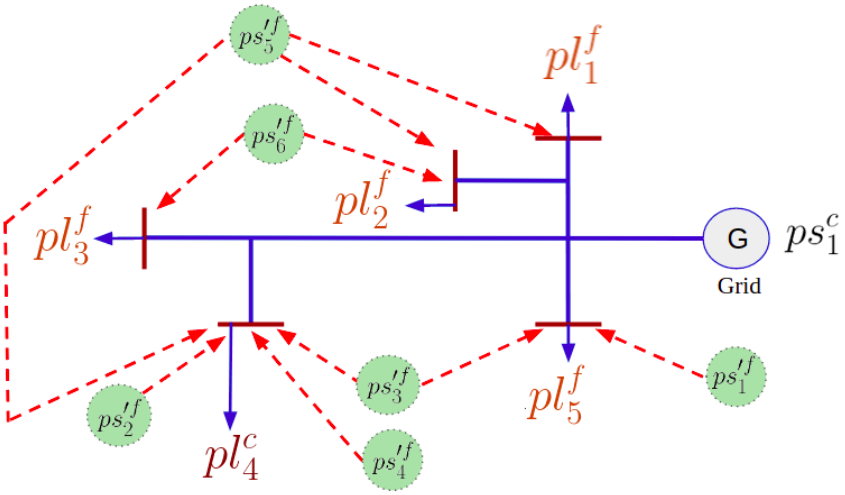

Figure 6.6: Result of Demonstration II (a): the allocation of the additional sources for HRES (without off-grid mode) design demonstrated by the power system

Demonstration II (b): Allocation Method Implementation for HRES (with off-grid mode) design

Demonstration II (b) investigates the HRES operating in both on-grid and off-grid modes. The aim is to match the additional power sources, whose power levels fall within the boundary of PS'^{f} and PS'^{c} obtained in Demonstration I (b). It is assumed that 4 fluctuating sources and 3 controllable sources (reserved power sources or PS'_c) need to be integrated into the power system, as presented in Table 6.5.

Table 6.5: Power levels of the additional power sources for Demonstration II (b)

Item	Minimum (KW)	Maximum (KW)
$ps_1'^{c}$	0	5
$ps_2'^{c}$	0	10
$ps_3'^{c}$	0	5
$ps_1'^{f}$	5	12
$ps_2'^{f}$	6	10
$ps_3'^{f}$	5	7
$ps_4'^{f}$	5	8

Thus, the proposed method of minimizing connections can be utilized to allocate the additional power sources of the HRES (with on-off-grid mode) design, and the result is illustrated in Figure 6.7. Afterward, the bipartite graph is converted back into the power system, as depicted in Figure 6.8.

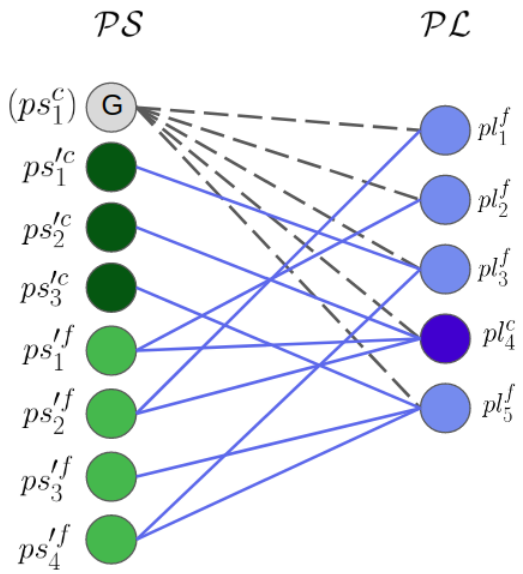

Figure 6.7: Result of Demonstration II (b): the allocation of the additional sources for HRES (with on-off-grid mode) design demonstrated by the bipartite graph

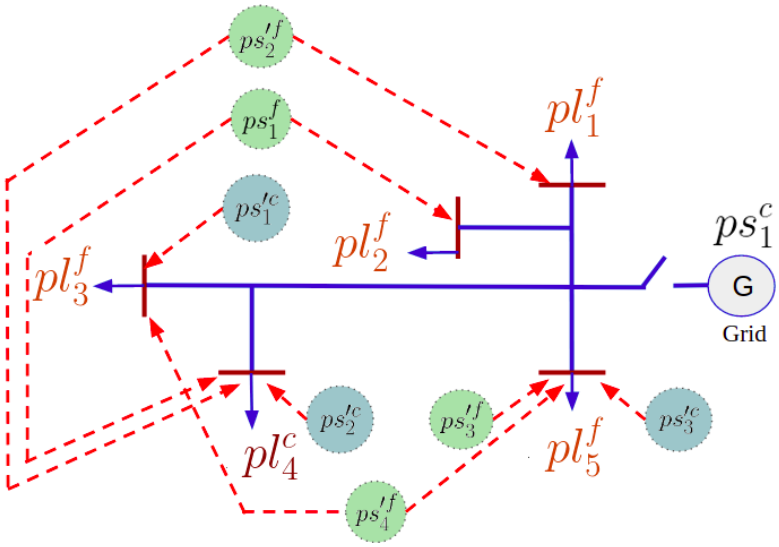

Figure 6.8: Result of Demonstration II (b): the allocation of the additional sources for HRES (with on-off-grid mode) design demonstrated by the power system

6.6 Concluding Remarks

The proposed method presented in this study focuses on optimizing the size and allocation of sources and loads in power systems that incorporate renewable energy sources (RESs), specifically those with fluctuating power. A key emphasis is placed on ensuring robustness against RES fluctuations, which is crucial for the design process. This methodology proves particularly advantageous for designing hybrid renewable energy systems (HRES) that aim to minimize energy costs and ensure reliable operation under varying RES conditions. The approach is expected to contribute to the development of more efficient and reliable HRES design methods in the future.

To apply this system design method, the power system network needs to be transformed into a bipartite graph based on Graph theory. This graph representation facilitates the analysis of fluctuating and controllable sources and loads, considering their power range (maximum and minimum power levels). Section 2.1 provides an overview of the analysis of these elements, while a more detailed discussion is presented in Section 8. Notably, this concept also allows for the utilization of the matching concept in Graph theory for HRES allocation.

When determining the size of power sources and loads, it is generally required that the energy from sources meets the demand of the loads, and the load demand is sufficient to consume the energy from sources. This requirement is expressed through mathematical equations, as demonstrated in Theorem 1. Subsequently, the 'Allocation Design problem-II' is formulated, which has been identified as NP-hard through further examination. Mixed-integer linear programming (MILP) is a potential solution method employed for problem-solving.

Therefore, the proposed method enables the design of HRESs integrated with RESs, particularly fluctuating power sources included in the given set of sources and loads with their power levels (minimum and maximum), while maintaining robustness against fluctuations.

Acknowledging the limitations of the proposed method is necessary, including the

substantial computation time required, the assumption of predetermined installation quantities, the focus on steady-state conditions, and the neglect of unbalanced load and compensation of active and reactive power. Addressing these limitations in future research will contribute to improving the method's computational efficiency, flexibility in RDG placement, and consideration of dynamic system behavior, thereby advancing the development of more comprehensive and robust optimization techniques for RDGs. Additionally, one notable drawback to consider is the inherent challenge of reducing computation time in the initial stage of the proposed method, given the complex nature of observing the non-linear characteristic. However, one potential drawback of this method is the computational time involved. Due to the complexity of the problem and the need to consider fluctuating characteristics, the computation time required may be significant. However, this limitation can be mitigated through optimization techniques and advancements in computational capabilities. Overall, the positive aspects of this method, such as its ability to achieve robustness and optimize HRES design, outweigh the negative aspects, making it a valuable approach for future research and application.

Chapter 7

Conclusion

In summary, this dissertation provides a comprehensive analysis of various aspects concerning the design, allocation, location, and sizing of power devices, with a specific focus on the integration of uncontrollable renewable energy sources into power distribution networks. The research examines the significance of green energy sources, particularly uncontrollable or non-dispatchable energy sources, in meeting the growing demand for sustainable and environmentally friendly energy solutions.

A methodology is proposed to determine the optimal location of renewable distributed generator (RDG) installations based on the voltage-reactive power margin in relation to voltage collapse (Γ). The focus of this approach is to enhance voltage stability in the presence of uncontrollable reactive power compensation. The effectiveness of this methodology is validated through simulations on the IEEE33-bus test distribution system, comparing the results with alternative algorithms. The comparison demonstrates the notable performance of the proposed approach in terms of reducing maximum power losses and maintaining robust voltage stability despite varying levels of reactive power compensation.

Since voltage stability improvement is not only important for power delivery but also for power loss reduction and protection against voltage collapse, it is crucial to consider voltage stability enhancement in addition to minimizing power losses. Previous results have shown that solely minimizing power losses does not always lead to improved voltage stability. Therefore, the methodology's performance is enhanced by incorporating voltage stability improvement. Through extensive discussions and simulations, the effectiveness of the proposed voltage stability index (Λ) in identifying optimal RDG installation locations has been demonstrated. This index takes into account both voltage stability improvement and power loss reduction efficiency. It is worth noting that while this dissertation primarily focuses on the placement of RDGs, the proposed Load-Disabling Nodal Analysis (LDNA) approach can be extended to other types of distributed generators (DGs) and combinations of DGs and RDGs, provided that their reactive power compensation ratios are explicitly specified.

Further, a safety-oriented approach is crucial for designing power distribution networks that incorporate fluctuating power sources. The design methodology takes into account safety margins when allocating (sizing and locating) power devices, including both sources and loads in hybrid renewable energy systems (HRES). By utilizing Graph Theory and transforming the problem into a bipartite graph, this methodology achieves an optimal matching of sources to loads while analyzing power range margins. These design approaches can be adapted for locating power devices in power distribution networks,

particularly in scenarios involving fluctuating power sources.

These findings contribute to the advancement of integrating renewable energy sources into power systems, emphasizing the significance of voltage stability, power loss reduction, and safety considerations. The proposed methodologies provide valuable insights and practical tools for the efficient deployment and utilization of uncontrollable renewable energy sources in power distribution networks.

It is important to acknowledge the limitations of the proposed methods in this research, which encompass extensive computation time, predetermined installation quantities, emphasis on steady-state conditions, and neglect of unbalanced load and compensation of active and reactive power. The computation time presents a potential drawback due to the inherent complexity of observing the non-linear characteristic. However, by addressing this limitation through optimization techniques and advancements in computational capabilities, the proposed methods hold the potential to provide valuable insights and applications in future research.

In conclusion, the research philosophy of this study revolves around acknowledging the impact of power source-load interaction on power delivery efficiency in the distribution system. It highlights the significance of managing voltage stability and minimizing power loss to attain efficient power delivery. Through the analysis of power load disabling scenarios and the decomposition of the problem into smaller components, the research aims to enhance power delivery efficiency and optimize the overall performance of power systems. As a result, this approach leads to advancements in power delivery efficiency and the optimization of power systems' overall performance.

Contributions

The primary contributions of this research include:

- The proposed Load-Disabling Nodal Analysis for Robust Voltage Stability (LDNA-RVS) method is designed to counter the uncontrollable and weather-dependent fluctuations in the dominant reactance within power distribution networks. It does so by enhancing robust voltage stability through the consideration of reactive compensation, and it also improves the efficiency of power loss reduction (LRE) in the integration of Renewable Distributed Generators (RDGs).

- The unpredictable and weather-dependent variations in the dominant reactance within power distribution networks pose significant challenges. These variations can expose the system to the risk of voltage instability, potential collapse, and undesirable total power losses.

- The LDNA-RVS method, when applied to IEEE33-bus and IEEE69-bus test distribution systems, offers robust solutions for voltage stability and LRE in the face of uncontrollable reactive compensation. This has been demonstrated through a comparative analysis with other techniques.

- The relationship between voltage stability, power loss reduction, and the voltage product function has been explored and demonstrated through various case studies.

- The proposed methods not only enhance voltage stability and power loss reduction, but also propose a system voltage stability index, further contributing to the field.

- The effectiveness of the proposed voltage stability index (Λ) has been validated, demonstrating its capability in identifying optimal locations for RDG installations. This approach simultaneously supports both voltage stability improvement and power loss reduction efficiency.

Significance

This dissertation holds significant importance in following aspects:

1. Advancement of Renewable Energy Integration: The thesis addresses key challenges in integrating renewable energy sources, such as solar and wind power, into power distribution networks. By proposing novel methodologies for the design, allocation, location, and sizing of power devices, the thesis aims to enhance the seamless integration of uncontrollable renewable energy sources. This research contributes to the advancement of renewable energy integration, which is crucial for transitioning towards a more sustainable and environmentally friendly power system.

2. Voltage Stability Enhancement: Voltage stability is a critical aspect of power system operation, and the thesis focuses on enhancing voltage stability in the presence of uncontrollable reactive power compensation from RDGs. By developing methodologies that consider the voltage-reactive power margin and optimal RDG locations, the thesis aims to reinforce voltage stability and prevent voltage collapse. This contributes to the reliable and secure operation of power distribution networks with increased renewable energy penetration.

3. Power Loss Reduction: The dissertation also emphasizes the importance of power loss reduction in power distribution networks. By considering both voltage stability and power loss reduction efficiency, the proposed methodologies provide insights into optimizing the allocation and sizing of RDGs. This contributes to minimizing power losses and improving the overall efficiency of the power system, leading to cost savings and reduced environmental impact.

4. Safety and Resilience: The dissertation recognizes the importance of safety and resilience in power system operation. The methodologies developed consider safety margins, robustness against power fluctuations, and controllability conditions to enhance the resilience of power delivery to loads. By integrating these aspects into the design and operation of power systems, the thesis aims to ensure reliable and secure power supply while incorporating renewable energy sources.

5. Practical Implementation: The proposed methodologies in the thesis are validated through simulations using real-world test distribution systems. The comparative analyses demonstrate the effectiveness and superiority of the proposed approaches in terms of voltage stability, power loss reduction, and robustness. These findings provide practical insights and guidance for the implementation of renewable energy integration strategies in real power systems.

Overall, the research's significance lies in its contributions to addressing key challenges in the integration of renewable energy sources, enhancing voltage stability, reducing power losses, ensuring safety and resilience, and providing practical methodologies for the implementation of renewable energy integration strategies. By offering valuable insights

and tools, the thesis contributes to the advancement of sustainable and efficient power systems.

Recommendation of Future work

Several issues need to be addressed in future work to further improve the applicability and performance of the proposed method.

Firstly, it is crucial to reduce the time complexity of the Load Distribution Network Algorithm (LDNA), particularly for large-scale power systems. This is because the time complexity is dependent on the size of the power system and exponentially dependent on the number of RDGs to be installed. One practical solution to this issue could be to the elimination of computations, such as by skipping unpromising candidate locations for RDGs.

Secondly, considering the crucial role that energy storage devices play in absorbing the fluctuations of RDGs, it is essential to extend the proposed method to power systems that incorporate these storage devices. This will help overcome the serious issues associated with uncontrollable reactive compensation and environment-dependent changes. Additionally, exploring the application or extension of the proposed method to the location and sizing of energy storage devices could be a valuable area for future research.

Appendix A

Load-Flow method

A.1 Newton-Raphson method

For solving the non-linear power flow problem, Newton-Raphson method is used for this study. In the simulations and experiments, Python environment is used with the Power System Analysis (PSA) open-source, provided by [36]. If bus 1 is selected as the slack bus, which is the case throughout this paper, the method initially defines the solution set (x), including set the angle (δ) and the magnitude (V) of the voltages,

$$\mathbf{X} = \begin{bmatrix} \delta \\ \mathbf{V} \end{bmatrix} = \begin{bmatrix} \delta_2 \\ \vdots \\ \delta_n \\ V_2 \\ \vdots \\ V_n \end{bmatrix} ; \mathbf{Y} = \begin{bmatrix} \mathbf{P} \\ \mathbf{Q} \end{bmatrix} = \begin{bmatrix} P_2 \\ \vdots \\ P_n \\ Q_2 \\ \vdots \\ Q_n \end{bmatrix} = \begin{bmatrix} P(\mathbf{X}) \\ Q(\mathbf{X}) \end{bmatrix} = \begin{bmatrix} P_2(\mathbf{X}) \\ \vdots \\ P_n(\mathbf{X}) \\ Q_2(\mathbf{X}) \\ \vdots \\ Q_n(\mathbf{X}) \end{bmatrix} \tag{A.1}$$

$$V_k = P_k = P_k(\mathbf{X}) = V_k \sum_{n=1}^{N} Y_{kn} V_n \cos(\delta_k - \delta_n - \theta_{kn}), \quad k = 2, 3, 4, ..., N \tag{A.2}$$

$$V_{k+N} = Q_k = Q_k(\mathbf{X}) = V_k \sum_{n=1}^{N} Y_{kn} V_n \sin(\delta_k - \delta_n - \theta_{kn}) \tag{A.3}$$

where P and Q are the active and reactive power balance equations, respectively.

The Jacobian matrix ($\mathbf{J}$), which is defined by this method, is expressed as,

$$\mathbf{J} = \begin{bmatrix} J_1 & J_2 \\ J_3 & J_4 \end{bmatrix} = \begin{bmatrix} \frac{P_2}{\partial\delta_2} & \cdots & \frac{P_2}{\partial\delta_N} & \frac{P_2}{\partial V_2} & \cdots & \frac{P_2}{\partial V_N} \\ \vdots & \ddots & \vdots & \vdots & \ddots & \vdots \\ \frac{P_N}{\partial\delta_2} & \cdots & \frac{P_N}{\partial\delta_N} & \frac{P_N}{\partial V_2} & \cdots & \frac{P_N}{\partial V_N} \\ \frac{Q_2}{\partial\delta_2} & \cdots & \frac{Q_2}{\partial\delta_N} & \frac{Q_2}{\partial V_2} & \cdots & \frac{Q_2}{\partial V_N} \\ \vdots & \ddots & \vdots & \vdots & \ddots & \vdots \\ \frac{Q_N}{\partial\delta_2} & \cdots & \frac{Q_N}{\partial\delta_N} & \frac{Q_N}{\partial V_2} & \cdots & \frac{Q_N}{\partial V_N} \end{bmatrix} \tag{A.4}$$

$$\Delta\mathbf{Y}^{(i)} = \begin{bmatrix} \Delta P^{(i)} \\ \Delta Q^{(i)} \end{bmatrix} = \begin{bmatrix} \mathbf{P} - P(\mathbf{X}^{(i)}) \\ \mathbf{Q} - Q(\mathbf{X}^{(i)}) \end{bmatrix} \tag{A.5}$$

where $\Delta\mathbf{Y}^{(i)}$ is the mismatch between active and reactive power balance at iteration i-th. After starting with the initial solution set ($\mathbf{X}^{(0)}$), the method continues to satisfy the following convergence:

$$\begin{bmatrix} J_1 & J_2 \\ J_3 & J_4 \end{bmatrix} \begin{bmatrix} \Delta\delta \\ \Delta\mathbf{V} \end{bmatrix} = \begin{bmatrix} \Delta\mathbf{P} \\ \Delta\mathbf{Q} \end{bmatrix} \tag{A.6}$$

$$\mathbf{X}^{(i+1)} = \begin{bmatrix} \delta^{(i+1)} \\ \mathbf{V}^{(i+1)} \end{bmatrix} = \begin{bmatrix} \delta^{(i)} \\ \mathbf{V}^{(i)} \end{bmatrix} + \begin{bmatrix} \Delta\delta \\ \Delta\mathbf{V} \end{bmatrix} \tag{A.7}$$

The method repeats Equations (A.4-A.7) until the power mismatch reaches within a specific value.

Appendix B

The test systems' parameters

B.1 Standard IEEE5-bus test distribution system

The single line diagram of IEEE5-bus test distribution system as shown in Figure 4.3, is presented by [45]. The parameters of transmission line, generation, and loads are given in Table B.1 for the bus and Table B.2 for the transmission line. This test system is used for verifying the proposed voltage stability indicator in the following section. In the calculation, the base quantities of 100MVA and 100kV are defined.

Table B.1: Bus data of the IEEE5-bus test distribution system

Bus no.	Load	
	Active Power (MW)	Reactive Power (MVAr)
2	20	10
3	45	15
4	40	5
5	60	10
2 (Generator)	-40	-30

Table B.2: Transmission line data of the IEEE5-bus test distribution system

Transmission line	Resistance (ohm)	Reactance (ohm)
1-2	0.02	0.06
1-4	0.08	0.24
2-3	0.06	0.18
2-4	0.06	0.18
3-4	0.04	0.12
3-5	0.01	0.03
4-5	0.08	0.24

B.2 Standard IEEE33-bus test distribution system

For demonstrating the proposed methodology, the single line diagram of IEEE33-bus test distribution system as shown in Figure 4.4, which was originally proposed by [37], is

applied. The parameters of transmission line, generation, and loads are given in Table B.3 for the bus and Table B.4 for the transmission line. In the calculation, the base quantities of 100MVA and 12.6kV are redefined.

Table B.3: Bus data of the IEEE33-bus test distribution system

Bus no.	Load	
	Active Power (kW)	Reactive Power (kVAr)
2	100	60
3	90	40
4	120	80
5	60	30
6	60	20
7	200	100
8	200	100
9	60	20
10	60	20
11	45	30
12	60	35
13	60	35
14	120	80
15	60	10
16	60	20
17	60	20
18	90	40
19	90	40
20	90	40
21	90	40
22	90	40
23	90	50
24	420	200
25	420	200
26	60	25
27	60	25
28	60	20
29	120	70
30	200	600
31	150	70
32	210	100
33	60	40

Table B.4: Transmission line data of IEEE33-bus test distribution system

Transmission line	Resistance (ohm)	Reactance (ohm)
1 - 2	0.0922	0.0470
2 - 3	0.4930	0.2511
3 - 4	0.3660	0.1864
4 - 5	0.3811	0.1941
5 - 6	0.8190	0.7070
6 - 7	0.1872	0.6188
7 - 8	1.7114	1.2351
8 - 9	1.0300	0.7400
9 - 10	1.0440	0.7400
10 - 11	0.1966	0.0650
11 -12	0.3744	0.1238
12 - 13	1.4680	1.1550
13 - 14	0.5416	0.7129
14 - 15	0.5910	0.5260
15 - 16	0.7463	0.5450
16 - 17	1.2890	1.7210
17 - 18	0.7320	0.5740
2 - 19	0.1640	0.1565
19 - 20	1.5042	1.3554
20 - 21	0.4095	0.4784
21 - 22	0.7089	0.9373
3 - 23	0.4512	0.3083
23 - 24	0.8980	0.7091
24 - 25	0.8960	0.7011
6 - 26	0.2030	0.1034
26 - 27	0.2842	0.1447
27 - 28	1.0590	0.9337
28 - 29	0.8042	0.7006
29 - 30	0.5075	0.2585
30 - 31	0.9744	0.963
31 - 32	0.3105	0.3619
32 - 33	0.3410	0.5302

B.3 Standard IEEE69-bus test distribution system

The IEEE69-bus test distribution systems, provided in [40], are used for this study. Figure 5.3 presents the system diagram, indicating a total load of 3800kW and 2690kVAr at 12.6kV for the IEEE69-bus system. Information regarding the maximum levels of power consumption by loads is essential when evaluating maximum power losses and voltage stability.

Table B.5: Bus data of the IEEE69-bus test distribution system

Bus no.	Load		Bus no.	Load	
	Active Power (kW)	Reactive Power (kVAr)		Active Power (kW)	Reactive Power (kVAr)
2	0.	0.	36	26.00	18.55
3	0.	0.	37	26.00	18.55
4	0.	0.	38	0.	0.
5	0.	0.	39	24.00	17.00
6	2.60	2.20	40	24.00	17.00
7	40.40	30.00	41	1.20	1.00
8	75.00	54.00	42	0.	0.
9	30.00	22.00	43	6.00	4.30
10	28.00	19.00	44	0.	0.
11	145.00	104.00	45	39.22	26.30
12	145.00	104.00	46	39.22	26.30
13	8.00	5.50	47	0.	0.
14	8.00	5.50	48	79.00	56.40
15	0.	0.	49	384.70	274.50
16	45.50	30.00	50	384.70	274.50
17	60.00	35.00	51	40.50	28.30
18	60.00	35.00	52	3.60	2.70
19	0.	0.	53	4.35	3.50
20	1.0	0.60	54	26.40	19.00
21	114.0	81.00	55	24.00	17.20
22	5.30	3.50	56	0.	0.
23	0.	0.	57	0.	0.
24	28.00	20.00	58	0.	0.
25	0.	0.	59	100.00	72.00
26	14.00	10.00	60	0.	0.
27	14.00	10.00	61	1244.0	888.0
28	26.00	18.60	62	32.00	23.00
29	26.00	18.60	63	0.	0.
30	0.	0.	64	227.00	162.00
31	0.	0.	65	59.00	42.00
32	0.	0.	66	18.00	13.00
33	14.00	10.00	67	18.00	13.00
34	19.50	14.00	68	28.00	20.00
35	6.00	4.00	69	28.00	20.00

Table B.6: Transmission line data of IEEE69-bus test distribution system

Transmission line	Resistance (ohm)	Reactance (ohm)	Transmission line	Resistance (ohm)	Reactance (ohm)
1 - 2	0.0005	0.0012	31 - 32	0.8390	0.2816
2 - 3	0.0015	0.0036	32 - 33	1.7080	0.5646
3 - 4	0.0251	0.0294	33 - 34	1.4740	0.4873
4 - 5	0.3360	0.1864	65 - 66	0.0304	0.0355
5 - 6	0.3811	0.1941	66 - 67	0.0018	0.0021
6 - 7	0.0922	0.0470	67 - 68	0.7283	0.8509
7 - 8	0.0493	0.0251	68 - 69	0.3100	0.3623
8 - 9	0.8190	0.2707	3 - 35	0.0034	0.0084
9 - 10	0.1872	0.0619	35 - 36	0.0851	0.2083
10 - 11	0.7114	0.2351	36 - 37	0.2898	0.7091
11 - 12	1.0300	0.3400	37 - 38	0.0822	0.2011
12 - 13	1.0440	0.3450	7 - 40	0.0928	0.0473
13 - 14	1.0580	0.3496	40 - 41	0.3319	0.1114
14 - 15	0.1966	0.0650	8 - 42	0.1740	0.0886
15 - 16	0.3744	0.1238	42 - 43	0.2030	0.1034
16 - 17	0.0047	0.0016	43 - 44	0.2842	0.1447
17 - 18	0.3276	0.1083	44 - 45	0.2813	0.1433
18 - 19	0.2106	0.0696	45 - 46	1.5900	0.5337
19 - 20	0.3416	0.1129	46 - 47	0.7837	0.2630
20 - 21	0.0140	0.0046	47 - 48	0.3042	0.1006
21 - 22	0.1591	0.0526	48 - 49	0.3861	0.1172
22 - 23	0.3463	0.1145	49 - 50	0.5075	0.2585
23 - 24	0.7488	0.2475	50 - 51	0.0974	0.0496
24 - 25	0.3089	0.1021	51 - 52	0.1450	0.0738
25 - 26	0.1732	0.0572	52 - 53	0.7105	0.3619
2 - 27	0.0044	0.0108	53 - 54	1.0410	0.5302
27 - 28	0.0640	0.1565	10 - 55	0.2012	0.0611
28 - 29	0.3978	0.1315	55 - 56	0.0047	0.0014
29 - 30	0.0702	0.0232	11 - 57	0.7394	0.2444
30 - 31	0.3510	0.1160	57 - 58	0.0047	0.0016

Bibliography

[1] P. Kessel and H. Glavitsch, "Estimating the voltage stability of a power system," *IEEE Transactions on Power Delivery*, vol. 1, no. 3, pp. 346–354, 1986.

[2] D. Q. Hung and N. Mithulananthan, "Multiple distributed generator placement in primary distribution networks for loss reduction," *IEEE Transactions on Industrial Electronics*, vol. 60, no. 4, pp. 1700–1708, 2013.

[3] S. Greene, I. Dobson, and F. Alvarado, "Sensitivity of the loading margin to voltage collapse with respect to arbitrary parameters," *IEEE Transactions on Power Systems*, vol. 12, no. 1, pp. 262–272, 1997.

[4] J. Floyd and K. Zubevich, "Linking foresight and sustainability: An integral approach," *Futures*, vol. 42, no. 1, pp. 59–68, 2010.

[5] R. Luna-Rubio, M. Trejo-Perea, D. Vargas-Vázquez, and G. J. Ríos-Moreno, "Optimal sizing of renewable hybrids energy systems: A review of methodologies," *Solar Energy*, vol. 86, no. 4, pp. 1077–1088, 2012.

[6] F. L. Xu, S. S. Zhao, R. W. Dawson, J. Y. Hao, Y. Zhang, and S. Tao, "A triangle model for evaluating the sustainability status and trends of economic development," *Ecological Modelling*, vol. 195, no. 3-4, pp. 327–337, 2006.

[7] G. Pepermans, J. Driesen, D. Haeseldonckx, R. Belmans, and W. D'haeseleer, "Distributed generation: Definition, benefits and issues," *Energy Policy*, vol. 33, no. 6, pp. 787–798, 2005.

[8] T. Ackermann, G. Andersson, and L. Söder, "Distributed generation: A definition," *Electric Power Systems Research*, vol. 57, no. 3, pp. 195–204, 2001.

[9] G. J. Dalton, D. A. Lockington, and T. E. Baldock, "Case study feasibility analysis of renewable energy supply options for small to medium-sized tourist accommodations," *Renewable Energy*, vol. 34, no. 4, pp. 1134–1144, 2009.

[10] P. Yilmaz, M. Hakan Hocaoglu, and A. E. S. Konukman, "A pre-feasibility case study on integrated resource planning including renewables," *Energy Policy*, vol. 36, no. 3, pp. 1223–1232, 2008.

[11] N. Acharya, P. Mahat, and N. Mithulananthan, "An analytical approach for DG allocation in primary distribution network," *International Journal of Electrical Power and Energy Systems*, vol. 28, pp. 669–678, 12 2006.

[12] L. D. Arya, A. Koshti, and S. C. Choube, "Distributed generation planning using differential evolution accounting voltage stability consideration," *International Journal of Electrical Power and Energy Systems*, vol. 42, pp. 196–207, 11 2012.

[13] T. Gözel and M. H. Hocaoglu, "An analytical method for the sizing and siting of distributed generators in radial systems," *Electric Power Systems Research*, vol. 79, no. 6, pp. 912–918, 2009.

[14] I. Pisica, C. Bulac, and M. Eremia, "Optimal distributed generation location and sizing using genetic algorithms," 12 2009.

[15] D. K. Khatod, V. Pant, and J. Sharma, "Evolutionary programming based optimal placement of renewable distributed generators," *IEEE Transactions on Power Systems*, vol. 28, no. 2, pp. 683–695, 2013.

[16] J. A. M. García and A. J. G. Mena, "Optimal distributed generation location and size using a modified teaching-learning based optimization algorithm," *International Journal of Electrical Power and Energy Systems*, vol. 50, pp. 65–75, 2013.

[17] A. Y. Abdelaziz, Y. G. Hegazy, W. El-Khattam, and M. M. Othman, "A multi-objective optimization for sizing and placement of voltage-controlled distributed generation using supervised big bang-big crunch method," *Electric Power Components and Systems*, vol. 43, pp. 105–117, 1 2015.

[18] E. S. Ali, S. M. Abd Elazim, and A. Y. Abdelaziz, "Optimal allocation and sizing of renewable distributed generation using ant lion optimization algorithm," *Electrical Engineering*, vol. 100, no. 1, pp. 99–109, 2018.

[19] D. Q. Hung, N. Mithulananthan, and K. Y. Lee, "Optimal placement of dispatchable and nondispatchable renewable DG units in distribution networks for minimizing energy loss," *International Journal of Electrical Power and Energy Systems*, vol. 55, pp. 179–186, 2014. [Online]. Available: http://dx.doi.org/10.1016/j.ijepes.2013.09.007

[20] H. HassanzadehFard and A. Jalilian, "Optimal sizing and location of renewable energy based DG units in distribution systems considering load growth," *International Journal of Electrical Power and Energy Systems*, vol. 101, no. January 2017, pp. 356–370, 2018. [Online]. Available: https://doi.org/10.1016/j.ijepes.2018.03.038

[21] R. W. Chang, N. Mithulananthan, and T. K. Saha, "Novel mixed-integer method to optimize distributed generation mix in primary distribution systems," in *AUPEC 2011*, 2011, pp. 1–6.

[22] A. Fazliana Abdul Kadir, A. Mohamed, H. Shareef, A. Asrul Ibrahim, T. Khatib, and W. Elmenreich, "An improved gravitational search algorithm for optimal placement and sizing of renewable distributed generation units in a distribution system for power quality enhancement," *Journal of Renewable and Sustainable Energy*, vol. 6, no. 3, pp. 1–18, 2014.

[23] M. Milovanović, D. Tasić, J. Radosavljević, and B. Perović, "Optimal Placement and Sizing of Inverter-Based Distributed Generation Units and Shunt Capacitors in Distorted Distribution Systems Using a Hybrid Phasor Particle Swarm Optimization and Gravitational Search Algorithm," *Electric Power Components and Systems*, vol. 48, no. 6-7, pp. 543–557, 2020. [Online]. Available: https://doi.org/10.1080/15325008.2020.1797934

[24] F. Yang, C. Song, J. Li, and R. Yuan, "Improved equivalent method for voltage stability margin analysis considering voltage deviation," *IET Generation, Transmission Distribution*, vol. 16, no. 20, pp. 3735–3744, 2022.

[25] T. N. Shukla, S. P. Singh, V. Srinivasarao, and K. B. Naik, "Optimal sizing of distributed generation placed on radial distribution systems," *Electric Power Components and Systems*, vol. 38, pp. 260–274, 1 2010.

[26] A. A. Hassan, F. H. Fahmy, A. E. S. A. Nafeh, and M. A. Abu-elmagd, "Genetic single objective optimisation for sizing and allocation of renewable dg systems," *International Journal of Sustainable Energy*, vol. 36, pp. 545–562, 7 2017.

[27] S. Kansal, V. Kumar, and B. Tyagi, "Optimal placement of different type of DG sources in distribution networks," *International Journal of Electrical Power and Energy Systems*, vol. 53, pp. 752–760, 2013.

[28] E. Karunarathne, J. Pasupuleti, J. Ekanayake, and D. Almeida, "Optimal placement and sizing of DGs in distribution networks using MLPSO algorithm," *Energies*, vol. 13, 12 2020.

[29] A. El-Fergany, "Optimal allocation of multi-type distributed generators using Backtracking Search Optimization Algorithm," *International Journal of Electrical Power Energy Systems*, vol. 64, pp. 1197–1205, 2015.

[30] E. S. Ali, S. M. A. Elazim, and A. Y. Abdelaziz, "Ant lion optimization algorithm for optimal location and sizing of renewable distributed generations," *Renewable Energy*, vol. 101, pp. 1311–1324, 2 2017.

[31] D. P. R. P., V. R. V.C., and G. M. T., "Optimal renewable resources placement in distribution networks by combined power loss index and whale optimization algorithms," *Journal of Electrical Systems and Information Technology*, vol. 5, pp. 175–191, 9 2018.

[32] T. V. Cutsem and C. Vournas, *Voltage Stability of Electric Power Systems*. Springer, Boston, MA, 1998.

[33] N. Hosseinzadeh, A. Aziz, A. Mahmud, A. Gargoom, and M. Rabbani, "Voltage stability of power systems with renewable-energy inverter-based generators: A review," *Electronics (Switzerland)*, vol. 10, no. 2, pp. 1–27, 2021. [Online]. Available: https://doi.org/10.3390/electronics10020115

[34] Z. Shuai, Y. Peng, X. Liu, Z. Li, J. M. Guerrero, and Z. J. Shen, "Parameter stability region analysis of Islanded Microgrid based on Bifurcation theory," *IEEE Transactions on Smart Grid*, vol. 10, no. 6, pp. 6580–6591, 2019.

[35] S. Chakrabarti, "Notes on power system voltage stability," *Dept. of EE, IIT, Kanpur*, 01 2011.

[36] T. Brown, J. Hörsch, and D. Schlachtberger, "PyPSA: Python for Power System Analysis," *Journal of Open Research Software*, vol. 6, no. 4, 2018. [Online]. Available: https://doi.org/10.5334/jors.188

[37] M. Raoofat, "Simultaneous allocation of dgs and remote controllable switches in distribution networks considering multilevel load model," *International Journal of Electrical Power Energy Systems*, vol. 33, no. 8, pp. 1429–1436, 2011. [Online]. Available: https://www.sciencedirect.com/science/article/pii/S0142061511001323

[38] "IEEE Standard requirements, terminology, and test code for step-voltage regulators," *IEEE Std C57.15-1999*, pp. 1–80, 2000.

[39] E. Karunarathne, J. Pasupuleti, J. Ekanayake, and D. Almeida, "Optimal placement and sizing of dgs in distribution networks using MLPSO algorithm," *Energies*, vol. 13, no. 23, 2020. [Online]. Available: https://www.mdpi.com/1996-1073/13/23/6185

[40] M. Kashem, V. Ganapathy, and G. Jasmon, "A geometrical approach for network reconfiguration based loss minimization in distribution systems," *International Journal of Electrical Power Energy Systems*, vol. 23, no. 4, pp. 295–304, 2001. [Online]. Available: https://www.sciencedirect.com/science/article/pii/S0142061500000442

[41] W. S. Tan, M. Y. Hassan, M. S. Majid, and H. A. Rahman, "Allocation and sizing of DG using Cuckoo Search Algorithm," 2012, pp. 133–138.

[42] S. Javaid, M. Kaneko, and Y. Tan, "Structural condition for controllable power flow system containing controllable and fluctuating power devices," *Energies*, vol. 13, no. 7, 2020. [Online]. Available: https://www.mdpi.com/1996-1073/13/7/1627

[43] V. Lazarov, G. Notton, Z. Zarkov, and I. Bochev, "Hybrid power systems with renewable energy sources – types, structures, trends for research and development," in *Proceedings of 11st International Conference on Electrical Machines, Drives and Power Systems.*, ser. ELMA 2005. Sofia, BULGARIA: Paparazzi Press, 2005, pp. 515–520. [Online]. Available: https://www.researchgate.net/publication/236012467

[44] "Krabi goes green: Towards a model town, with more than 100% renewable energy," in *KRABI GOES GREEN Report*, C. Chaaroenlarpnopparut, Ed. Thailand: Greenpeace Southeast Asia, June 2018. [Online]. Available: https://www.greenpeace.or.th/report/Krabi-goes-green-EN.pdf

[45] P. K. Gouda, A. K. Sahoo, and P. K. Hota, "Optimal power flow including unified power flow controller in a deregulated environment," *International Journal of Applied Engineering Research*, vol. 10, no. 1, pp. 505–522, 2015.

Publications

Journal paper

[1] Akanit Kwangkaew, Saher Javaid, Chalie Charoenlarpnopparut, and Mineo Kaneko, "Optimal Location and Sizing of Renewable Distributed Generators for Improving Voltage Stability and Security Considering Reactive Power Compensation," Energies 15, no. 6 : 2126, 2022.

[2] Akanit Kwangkaew, Siriya Skolthanarat, Chalie Charoenlarpnopparut, and Mineo Kaneko, "Optimal Location and Sizing of Renewable Distributed Generators for Improving Robust Voltage Stability against Uncontrollable Reactive Compensation," IEEE Access, 2023 doi: 10.1109/ACCESS.2023.3279716.

International conference

[1] Akanit Kwangkaew, Saher Javaid, Chalie Charoenlarpnopparut, and Mineo Kaneko, "A New Approach to Renewable Energy Sources Allocation considering Robustness against Fluctuations," International Conference on Smart Grids and Energy Systems (SGES), Perth, Australia, pp. 396 − 401, 2020.